Finite element simulation of tensioned membrane structures in deployable systems

Kim Carbonez

Promotoren: prof. dr. ir. Wim Van Paepegem, prof. Marijke Mollaert
Begeleiders: dr. Ali Rezaei, Tien Dung Dinh

Masterproef ingediend tot het behalen van de academische graad van
Master in de ingenieurswetenschappen: architectuur

Vakgroep Toegepaste Materiaalwetenschappen
Voorzitter: prof. dr. ir. Joris Degrieck
Faculteit Ingenieurswetenschappen en Architectuur
Academiejaar 2012-2013

UNIVERSITEIT
GENT

Permission for use of content

The author gives permission to make this master dissertation available for consultation and to copy parts of this master thesis for personal use.
In the case of any other use, the limitations of the copyright have to be respected, in particular with regard to the obligation to state expressly the source when quoting results from this work.

Kim Carbonez, 3 juni 2013

Toelating tot bruikleen

De auteur geeft de toelating deze materproef voor consultatie beschikbaar te stellen en delen van de masterproef te kopiëren voor persoonlijk gebruik.
Elk ander gebruik valt onder de beperkingen van het auteursrecht, in het bijzonder met betrekking tot de verplichting de bron uitdrukkelijk te vermelden bij het aanhalen van resultaten uit dit werk.

Kim Carbonez, 3 juni 2013

Finite element simulation of tensioned membrane structures in deployable systems

Kim Carbonez

Promotoren: prof. dr. ir. Wim Van Paepegem, prof. Marijke Mollaert
Begeleiders: dr. Ali Rezaei, Tien Dung Dinh

Masterproef ingediend tot het behalen van de academische graad van
Master in de ingenieurswetenschappen: architectuur

Vakgroep Toegepaste Materiaalwetenschappen
Voorzitter: prof. dr. ir. Joris Degrieck
Faculteit Ingenieurswetenschappen en Architectuur
Academiejaar 2012-2013

UNIVERSITEIT
GENT

Acknowledgements

"Thesis is only a word for hard work", they told me. But hard work would not have been enough to complete this thesis without the help of several people.

First of all, I would like to thank prof. dr. ir. Wim Van Paepegem, for introducing me in the field of numerical simulation, which was an unknown world for me before. Also prof. dr. ir. Marijke Mollaert, for giving me the chance to work on this interesting subject of membrane architecture.

Furthermore, I am grateful to Silke Puystiens, Maarten Van Craenenbroeck and Lars De Laet, for their advise and experimental data, and the people in room 30 in the Department of Material Sciences, for sharing their work spirit.

My special thanks go to dr. Ali Rezaei, for this patience, belief, guidance and wise advise, also during my Erasmus exchange, which was not always evident. *با تشـــکر از شما*

Endless gratitude to M. Sc. Tien Dűng Dinh, for his spontaneous explanations, critical eye and for making the magic happen in my computer. *Cảm ơn bạn nghịch ngợm Việt*.

Dank u, grazie, ďakujem, Danke, gracias to my friends, who distracted me when I needed it.

And last but not least, my parents, for their unconditional belief, support and smiles through my impetuous five years of study.

Kim Carbonez, 3 juni 2013

Finite element simulation of tensioned membrane structures in deployable systems

by Kim Carbonez
Masterproef ingediend tot het behalen van de academische graad van Master in de ingenieurswetenschappen: Architectuur

Promotoren: prof. dr. ir. Wim Van Paepegem, prof. dr. ir. Marijke Mollaert
Begeleider: dr. ir. Ali Rezaei

Vakgroep Toegepaste materiaalwetenschappen
Voorzitter: prof. dr. ir. Joris Degrieck
Faculteit Ingenieurswetenschappen en Architectuur
Universiteit Gent

Academiejaar 2012-2013

Summary

In the current design of membrane architecture, many assumptions and simplifications are made concerning the structural behavior. The aim of this thesis is focused on the simulation of tensioned membranes on macro scale, with dimensions that are close to the ones in architectural applications as e.g. tents or facade structures, with the goal of predicting the behavior under load. This could enable more accurate design methods in the future.
The simulations are performed by use of the finite element method (FEM) software Abaqus. In order to be relevant for practical use, the envisaged membrane material is a polyvinylchloride coated polyester fabric which is widely used in architectural applications nowadays. This material is implemented in the program as a user material subroutine and is able to map the severely non-linear behavior in each weave direction.
First, the possibilities for simulating a membrane are investigated. An overview of methods used by other researches is then given, based on available literature in this field. The different solutions are compared with each other and verified using the benchmark of a hyper surface.
Apart from this, a numerical model for an in-plane loaded triangular shaped membrane is proposed and extensively discussed.

The sufficiency of FEM software, as well as the applicability of the used material model is validated. At this end, the output of Abaqus is evaluated, based on the load-strain data of an experimental setup that was carried out at the VUB. A description of this experiment is also included in this thesis.
Furthermore, the improvement of the user material is demonstrated by making the comparison with simplified material models.
This work ends with additional studies on the influence of the fiber direction.

Keywords

coated fabric, structural behavior, finite element method (FEM), user material, fiber direction

Eindige elementen simulatie van membraanstructuren in opvouwbare systemen

door Kim Carbonez
Masterproef ingediend tot het behalen van de academische graad van Master in de ingenieurswetenschappen: Architectuur

Promotoren: prof. dr. ir. Wim Van Paepegem, prof. dr. ir. Marijke Mollaert
Begeleider: dr. ir. Ali Rezaei

Vakgroep Toegepaste materiaalwetenschappen
Voorzitter: prof. dr. ir. Joris Degrieck
Faculteit Ingenieurswetenschappen en Architectuur
Universiteit Gent

Academiejaar 2012-2013

Samenvatting

In de berekeningsmethodes die vandaag de dag gehanteerd worden voor het ontwerp van membraanarchitectuur worden vele aannames en vereenvoudigingen gemaakt inzake het structureel gedrag. Met de uiteindelijke ambitie om het gedrag van een membraan onder belasting kunnen voorspellen, is het doel van deze masterproef gericht op de simulatie van gespannen membranen op macro-schaal. De afmetingen komen in de buurt van hun tegenhangers in de architectuur, zoals bv. in tentstructuren of gevelelementen. Dit zou in de toekomst kunnen leiden tot meer nauwkeurige ontwerpmethodes.
De simulaties werden uitgevoerd met behulp van de eindige elementen (EE) software Abaqus. Het beschouwde materiaal is polyvinylgecoat polyesterdoek en werd gekozen met het oog op eventuele latere toepassingen in de realiteit. Dit is namelijk het materiaal bij uitstek in de huidige ontwerpen met membranen. Een speciaal ontwikkeld numeriek materiaalmodel werd gebruikt om het complexe niet-lineaire gedrag, dat daarenboven ook sterk afhangt van de beschouwde weefriching, te kunnen simuleren.
In eerste instantie worden de mogelijkheden om een membraan numeriek te simuleren onderzocht, baserend op relevante literatuur. Er wordt een overzicht gegeven van de methodes die onderzoekers in dit studiedomein gebruiken. Aan de hand van het gekende voorbeeld van de hyperbolische paraboloïde worden de verschillende oplossingen gestaafd.
Daarnaast wordt een numeriek model voorgesteld en bediscussierd: et geval van een driehoekig membraan dat enkel in zijn vlak belast wordt.
Naast de geschiktheid van de EE-software wordt ook de bruikbaarheid van het materiaalmodel onderzocht. Daartoe wordt de output van Abaqus vergeleken en geverifiëerd met de data van een experiment dat werd uitgevoerd aan de VUB. Een beschrijving van dit experiment is ook terug te vinden in deze masterproef.
Voorts worden de voordelen van het gebruikte materiaalmodel ten opzichte van eenvoudigere materiaalmodelen aangetoond d.m.v. vergelijking.
Deze thesis eindigt met een bijkomstig onderzoek naar de invloed van de vezelrichting.

Trefwoorden

gecoat weefsel, structureel gedrag, eindige elementen methode (EEM), user material, vezelrichiting

List of acronyms

FEM	Finite element method
VUB	Vrije Universiteit Brussel - Free University Brussels
UGent	Universiteit Gent - University of Ghent
FWO	Fonds voor wetenschappelijk onderzoek (Fund Scientific Research)
UMAT	User material
KFAS	Kinematic Form Active Structures
PA	Polyamide
PES	Polyester
PVC	Polyvinylchloride
PUR	Polyurethane
UV	Ultra violet
PTFE	Polytetrafluorethylene
ETFE	Ethylenetetrafluorethylene
PE	Polyethylene
IASS	The International Association for Shell and Spatial Structures
ASCE	American Society of Civil Engineers
CPU	Central Processing Unit
AE lab	Architectural engineering Lab (at VUB)
RP	Reference point
DIC	Digital Image Correlation
UMAT	User material Subroutine
DOF	Degree of Freedom
p.	Page
resp.	respectively
Min	Minimum
Max	Maximum
Avg	Average
exp.	Experiment
sim.	Simulation

List of symbols

q_m *[N/m]*	*Force Density*
T_m *[N]*	*Tension in one member of a cabel network*
L [m]	*Length*
P [N]	*External force*
I [N]	*Internal force*
u [m]	*displacement*
K [Pa]	*Tangent stiffness matrix*
c_a *[-]*	*Displacement correction*
R [N]	*Residual force*
λ [-]	*Load magnitude parameter*
F_v *[N]*	*Artificial Viscous Force*
M [kg]	*Artificial Mass*
v [m/s]	*Nodal velocity*
c [-]	*Damping factor*
t [s]	*Time*
K [Pa]	*Transient Stiffness Matrix*
RF [N]	*Reaction force*
$\varepsilon_{\mathrm{Lag}}$ [-]	Lagrangian strain
$\varepsilon_{\log}$ [-]	Logarithmic strain
ε_{11} - E11 [-]	Horizontal strain
ε_{22} - E22 [-]	Vertical strain
ε_{12} - E12 [-]	Shear strain
σ_{11} -S11 [Pa]	Horizontal stress
σ_{22} - S22 [Pa]	Vertical stress
σ_{12} - S12 [Pa]	Shear stress
E [Pa]	Elastic modulus, Young's modulus
E_{warp} [Pa]	Elastic modulus in warp direction
E_{fill} [Pa]	Elastic modulus in fill direction
G [Pa]	Shear modulus
ν [-]	Poisson ratio

Contents

PERMISSION FOR USE OF CONTENT ..... **III**

TOELATING TOT BRUIKLEEN ..... **III**

ACKNOWLEDGEMENTS ..... **VI**

SUMMARY ..... **VII**

SAMENVATTING ..... **VIII**

LIST OF ACRONYMS ..... **IX**

LIST OF SYMBOLS ..... **X**

CONTENTS ..... **XI**

CHAPTER 1 | INTRODUCTION **1**

1.1 OBJECTIVES 2
1.2 THE KFAS-PROJECT 3
1.2.1 Preface *3*
1.2.2 Incentive *3*
1.3 MATERIALIZATION OF MEMBRANES IN ARCHITECTURAL APPLICATIONS 4
1.3.1 Historical overview *4*
1.3.2 Architectural membrane materials *5*
1.3.3 Material considered in this thesis: PVC-coated polyester *8*
1.4 MEMBRANES AND ARCHITECTURE 10
1.4.1 Flexibility exploited *11*
1.4.2 Current design problems for tensile structures *13*
1.5 CONCLUSION 14

CHAPTER 2 | APPROACHES FOR THE SIMULATION OF MEMBRANES **15**

2.1 INTRODUCTION 16
2.2 APPROACHES FOR MEMBRANE SIMULATIONS IN PREVIOUS WORKS 16
2.2.1 The cable network *16*
2.2.2 Continuum surface *17*
2.3 NON-LINEAR PROBLEMS IN ABAQUS 18
2.3.1 Definition of the problem *18*
2.3.2 Global solution method *18*
2.3.3 Solution methods for unstable problems *20*
2.3.4 Application of the solution possibilities *22*
2.4 CONCLUSION 26

CHAPTER 3 | IN-PLANE LOADING OF A TRIANGULAR SHAPED MEMBRANE **27**

3.1 INTRODUTION 28
3.2 EXPERIMENTAL SETUP 28
3.2.1 Geometry and confection of the experimental model *28*
3.2.2 Setup and loading *29*
3.2.3 DIC measurements *31*
3.3 NUMERICAL MODEL 31
3.3.1 Material model *31*
3.3.2 Geometry *32*
3.3.3 Boundary conditions *34*
3.3.4 Efficient discretisation *34*
3.3.5 Damping factor *37*
3.4 COMPARISON OF THE RESULTS 38
3.4.1 Horizontal strain ε11 ..... *40*
3.4.2 Vertical strain ε_{22} *46*
3.4.3 Shear strain ε_{12} *54*
3.4.4 Conclusion of the compared paths *59*

3.5 Conclusion 60

CHAPTER 4 | COMPARISON WITH SIMPLIFIED MATERIAL MODELS 61

4.1 Introduction 62
4.2 Isotropic material 62
4.3 Linear elastic orthotropic material 62
4.4 Comparison 63
4.5 Conclusion 70

CHAPTER 5 | INFLUENCE OF THE FIBER DIRECTION 71

5.1 Introduction 72
5.2 Inversed fiber direction in reinforcement layers 72
5.3 Inversed fiber direction in all membrane parts 73
5.4 Comparison 73
5.4.1 Contour plots inversed fiber direction in the reinforcement layers 74
5.4.2 Contour plots inversed fiber direction in all membrane parts 75
5.4.3 Qualitative comparison 76

CHAPTER 6 | CONCLUSIONS AND RECOMMENDATIONS 83

6.1 General conlusion 84
6.2 Recommendations for future works 85

APPENDIX 86

A. Incorporating gravity 87
B. Kinematic simulation of opening and folding membrane structure 88
B. 1 Experimental setup 88
B.2 Geometry and confection 88
B.3 Setup and loading 89
B.4 Numerical model 90
B.4.2 Recommendations for contact between belt and membrane 90
C Product Sheet T2107 92
D. Product Sheet belts - Load-lok 94

LIST OF TABLES 100

BIBLIOGRAPHY 101

Chapter 1 | Introduction

"I have built little. But, I have built many castles in the air."

Frei Otto, Pioneer in light weight tensile and membrane structures, °1925

Architects are always looking for renewing ideas, touching the borders of what is possible and trying to surpass the conventional themes. After years of static architecture, more and more reconfigurable structures and transformable building parts present themselves, encouraged by the fast evolution in materials and technology [1].
The present thesis takes part in the investigation to convertible lightweight structures of polyester coated fabric. This quite recent material is severely non-linear in its behavior under loading and acts differently in every weaving direction. In current calculation methods it is mostly simplified to a linear elastic material [2], which makes the model rather unreliable when it comes to the prediction of the load behavior. Moreover, assumptions must be made for the manufacturing of the sails for e.g. tents and shelters, resulting in high safety factors and the need for real scale modeling [3]. This last one is often necessary because little is known about the occurring stresses in the membrane, and information must be gained by experimental tests.
This results rarely in constructions that are optimum in weight and use [4,5], which points out clearly the need for more research to achieve appropriate design methodologies and more accurate results.

For the above mentioned reasons, the Free University of Brussels (VUB) and the University of Ghent (UGent) started a 'Fonds voor Wetenschappelijk Onderzoek' (FWO) project in the research to polyester coated fabric, used in architectural constructions. With the aid of experiments performed at the VUB, this particular material itself and the loading behavior of a realistic scale model can be examined. The task of UGent consist of the development of a more realistic material model which can result in a better and more efficient architectural design. The aim of the whole project is to enable the precise modeling of architectural membrane structures through the help of accurate simulations, including transformable constructions with an opening and closing movement.

After the presentation of the intent of this master thesis, this chapter will outline the studied topic in its broader context. In the first section, the contribution of this work in a larger project will be explained together with the description of the previous work of other participants and the ongoing research.
Next, a short overview is given of the typical material used in lightweight architecture. After that, a historical synopsis of architecture with membranes and its developments up till now is outlined, with a closer look on the use of membranes in transformable structures. The chapter ends with information about the current shortcomings in design.

1.1 Objectives

The main objective of this thesis is finite element simulation of the kinematics and mechanical behavior of tension membrane coated fabrics used in foldable architectural structures, by use of the Abaqus-package.
Currently, at University of Ghent an elasto-plastic material model has been developed which incorporates the non-linear behavior of tension membrane fabrics. The developed model can exhibit non-linearity, orthotropy, permanent strains and load dependency of these fabrics. This master thesis intends to highlight the advantages of the proposed model in the study of the mechanical behavior of these fabrics over the simplified isotropic and orthotropic material models, which are mostly used by designers and researchers nowadays.

To achieve the aforementioned goal, the following is to be evaluated and benchmarked:

- The final formation of a fabric
- The effect of proper discretization,
- The stress and strain fields during the loading of a fabric.
- This first phase of the project is essential in order to ascertain the feasibility of the user material for the simulation of an architectural membrane.

Following the verification of the simulations and the development of the kinematic model, the second phase of this work aims to perform a parametric study in which the effect of fibers direction on the stress distribution and deformation of the test membrane is studied.

It must be noted that the project has been planned under the scope of a master thesis and the time limitation does not allow the investigation of all possibilities.

1.2 The KFAS-Project

1.2.1 Preface

This thesis is part of an FWO project about Kinematic Form Active Structures (KFAS) in collaboration between the VUB and the University of Ghent. KFAS are reconfigurable lightweight structures usually covered with technical textiles. When implemented as a building skin these systems can provide controlled daylight entrance and therefore play a role in the heating of the building. This is an example of how KFAS can support in the progression of sustainable buildings.
However, the most difficult and challenging part in the design of these KFAS is the research that investigates the geometric compatibility, pre-tension, curvature and the structural behavior during all phases of deployment. In the limited time-span of four years, the university proposes a study of the structural behavior in 3 positions: initial (0°), intermediate (50°) and final (90°) state (Fig. 1). This is applied on two representative cases: *Folding of a tensioned membrane unit about one axis*, in which this master thesis takes part, and as second case *the shape transformation of a tensioned system composed of several flexible and adaptable parts*, which will be studied in the future.

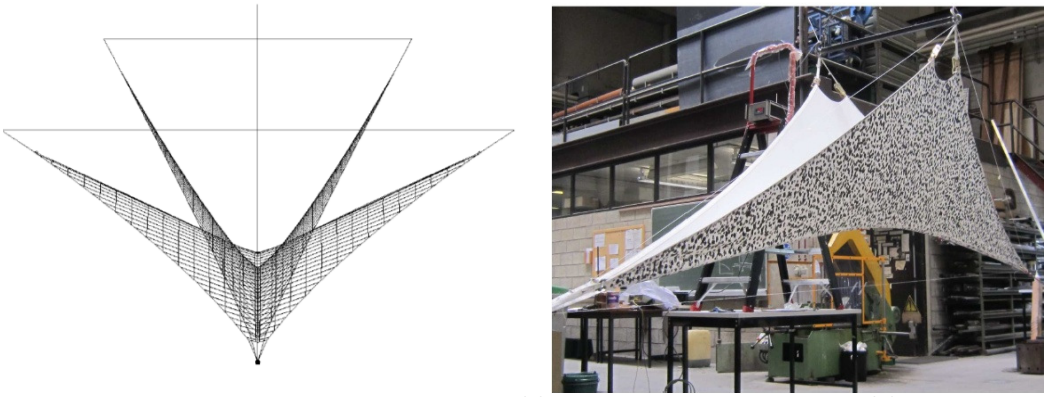

Fig. 1 A tensioned membrane unit folded about 1 axis. (a) The 3 intermediate positions and (b) test setup with opening angle of 50°

The study involves numerical form-finding, as well as the design of a reference configuration and FEM-analysis. To summarize, we can say that the adjustment of the pre-tension will be examined, next to the load and stability analysis. Also optimization of the reconfigurable system in different positions will be investigated. These three main topics will be explored both experimentally and numerically.
In the end, this integrated study should provide the validation of the proposed concept for the opening and closing movement of a membrane. At the same time it will support the design of lightweight KFAS, and encourage to widen the range of these systems [5].

1.2.2 Incentive

Energy-efficiency and sustainable design are the big issues of the century. In this point of view, adaptable building skins could be one of the possibilities to achieve valuable solutions. An adaptable building skin can result in a cheap and easy way to low-energy buildings, since it is able to change the amount of covering for wind and solar radiation. Like this, it can control the temperature and lighting of the building. Recent projects took advantage of this kind of adaptable façades in the sense of foldable concepts and 'retractable' structures, e.g. roofs for sport buildings as is the case for the Wimbledon's Centre Court in the United Kingdom [6].
Reconfigurable systems - this means foldable or transformable into different configurations - are innovative: they are mostly developed in research labs and have some applications in aerospace constructions [7]. But the evolution in technical textiles and sustainable coatings makes the textiles strong and long lasting. Therefore, designers are encouraged to use them also for building applications and they gain importance in architectural projects because of their multi-functionality and light weight [8].

By designing a reconfigurable lightweight frame with a pre-tensioned textile cover, a very versatile system can be obtained. Since flexibility is one of the main characteristics of these technical fabrics, stabilizing a configuration in between an open and a closed state seems to be possible, although not yet applied [9]. In order to increase the applicability and reliability of KFAS in the building industry, various key aspects must be investigated in an integrated manner:

- The study of a technical textile as a building material, with specific characteristics e.g. the stretchability and biaxial behavior.
- The full numerical modeling of a reconfigurable structure, together with the experimental validation of the finite-element results.

This thesis forms a contribution to the second aspect.

1.3 Materialization of membranes in architectural applications

1.3.1 Historical overview

Textile materials in building applications are applied for already thousands of years and are probably one of the first materials which were used by mankind to protect against environmental conditions.
In origin, animal skins were used for tent-like structures during prehistoric times, and step by step the cover developed into woven fabrics. Before the introduction of synthetic fibers, natural fibers from both animals and plants e.g. cotton or flax, were commonly used [10].

The biggest problem with these natural fibers is the fast degradation due to the UV-radiation by the sun. But also moisture can damage the natural fibers, and on top of that, they are also a source of food for mold and microbes. Partly because of these reasons, textiles fell in disuse and formed a minority next to stone, wood and steel in the building industry [11, 12].
It was until the production of synthetic fibers between 1950 and 1960 that a better quality could be obtained and membrane structures started to revive as building material. In this period, people started to experiment with synthetic fibers, supported by new developments in the chemical industry. All kinds of synthetic textiles were introduced, composed out of Polyamide fibers (PA) (e.g. Nylon), Polyester (PES) (e.g. Trevira) or Polyacryl fibers, coated with e.g. Polyvinylchloride (PVC) or Polyurethane (PUR). Synthetic textiles do not only perform better against weather conditions, they also show better achievements under loading [1].

Fig. 2 Musikpavillon Köln, Frei Otto, 1955 [13]

Frei Otto, an icon and a pioneer in the field of membrane structures, did a lot of research and experiments on synthetic fibers. At the first Garden Show in Cologne (1955), he built his first music pavilion (Fig. 2) using the old-fashion cotton fibers. However, he shifted soon to glass fibers with a PUR-coating, e.g. for the erection of the entrance building (Fig. 3) and the famous 'Tanzbrunnen' (a covered area for concerts) (Fig. 4), at the second Garden Show in 1957 [13].

This material, although insensitive for ultra violet light (UV), proved to be damaged easily by water. After one season the cover had degraded completely. Later setups with polyamide-fabric showed easy ruptures already after six weeks. It was a process of trial and error to find a worthy material to substitute the widespread cotton fabric, but with the use of PVC-coated polyester fibers, first applied in the cover for the Freilichttheater in Wunsiedel in 1963, a dignified and even surpassing concurrent was found. After further optimization, this material could break through in 1970 as a standard

material for architectural membrane constructions, thanks to its durability, flexibility and favorable price.

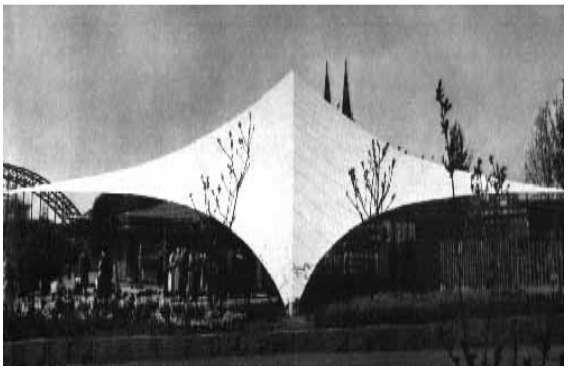

Fig. 3 Eintrittbogen Köln, Frei Otto, 1957

Fig. 4 Tanzbrunnen Köln, Frei Otto

Based on data from 2004, 90 % of the membranes used for applications in buildings or other projects have been made from one of the three materials listed below [1].

- Polytetrafluorethylene (PTFE)-coated glass fiber
- PVC-coated polyester fabric
- ethylenetetrafluorethylene (ETFE)- foil

These materials are highly tested and proved their worth in an increasing number of membrane constructions. Furthermore, the technologies used to handle these material have reached a high level of sophistication. Most of the aspects of their behavior over longer periods is known and documented. But due to the rising demand and increasing interest, the production of the material itself needs optimization as well as further detailed research on the specifications by companies.

By now, a wide range of different material strengths can be produced as standard, offering a differentiated choice for both architects and clients, as well in technical as economical terms. The choice for a material depends on different criteria (e.g. translucency, span, load ...) and should be considered in the initial phase of the project, regarding the technical, architectural and economic requirements and involving all members of the team.
In what follows, the most commonly used fibers and their coatings for architectural membrane will be shortly described, comparing their typical qualities and uses.

1.3.2 Architectural membrane materials [1, 11, 14]

1.3.2.1 Natural fibers

As mentioned before, the first materials used for architectural membranes had an natural origin. Cotton was often used because of its good UV-resistance, but the material exhibits a low strength. The natural descent makes it also more susceptible for mold than synthetics. Nowadays, they form the minority for architectural applications.

1.3.2.2 Glass fibers

Due to their UV-inviolability, glass fibers are found a suitable material for building skins. Moreover, they possess a very high ultimate strength and do not suffer from creep or significant stress relaxation. Many experiments with different coatings took place, e.g. PUR-coating, PVC- and PTFE-coverings were tested and are now often utilized. An example of the last one is the Pontiac Silverdome from Don Davidson (Fig. 5). In this building, the PTFE-coated glass fiber showed to be high-performing concerning structural behavior, besides a satisfying fire resistance.

Fig. 5 Pontiac Silverdome Michigan, Don Davidson [1]

As the name implies, fiberglass is glass that has been heated up and spun into fibers. This is its biggest drawback: the inherent brittleness makes it very sensitivity for foldings and causes abrupt failure once the limits are reached. Therefore only heavy fiberglass fabrics are used and their fabrication, transportation and installation requires more care than other materials.

1.3.2.3 Polyester fibers

Polyester fibers are the most widespread among all others in membrane applications. Their strength and stretch perform the best according to the cost. Moreover, the material shows a good UV and heat resistance, and the fibers are immune for mold. Nevertheless, the natural lifespan is rather short regarding the other materials, but can be elongated with a durable coating. In that aspect they seem to be the least expensive option for long-term fabrications.

1.3.2.4 Coatings

The major purpose of a membrane coating is to protect the fibers against moisture, UV-radiation, fire and infestation of microbes and mold. Their quality is determinative for the lifespan of the fabric. In addition to the influence of the membrane coating to the protection and durability of the textile fabric, it also contributes to the mechanical characteristics and the behavior and improves it significantly. By fixing the geometry of the fibers, the shear stiffness and tear resistance increase. The membrane therefore acts partially as a composite material.
Furthermore, the color can be maintained when pigments are added to the coatings. Another possibility is to print on the canvas afterwards. Also the confection of the membrane can be simplified, e.g. by allowing welding through the use of a thermoplastic coating. In this way, different single membrane strips can be simply be attached just by adding heat.

After preparation of the fabric, coatings are added typically on both sides at the same time. Thermoplastics, such as PVC, PTFE and other fluorpolymers are mostly used for fabrics with synthetic, organic and inorganic fibers (polyester, glass). Exceptions are the so called silicone rubbers, which are elastomers, and silicon resin, which is member of the category of the duroplasts.
There are different methods to coat a scrim and they are depending on the applied resin. Two principles are most common:
- The spreadable process for vinyl coatings (Fig. 6 a)
- The dipping process for PTFE-coatings(Fig. 6 b)

The spreadable process is commonly used for PVC and silicone coatings. The premixed, viscous coating paste for polyester membranes (called Plastisol) is composed of PVC-powder dispersed in a solvent. Additives like heat- and light stabilizers, bacterial and mold killers and pigments are added. The paste is smeared on the fabric surface and the redundant material is wiped away with squeegees. This process is repeated several times, in most cases three. Afterwards, the PVC powder and solvent are joined together in a heating canal, with temperatures around 180 °C.
The total process is repeated for the backside of the membrane, or more efficient, at the same time in a vertical chain. On the other hand, the dipping process is a suitable method for PTFE-coatings, and in some rare cases also for PVC coatings on coarse fabrics. For a glass fiber/PTFE combination, the fabric is immersed in a dispersion of small PTFE-particles. Stepwise, the temperature increases up to 330 °C during the drying and sintering, in order to evaporate the water and moisture-making products. This

process is repeated several times, to reach the aimed quality of coating thickness. Due to the high temperatures during the heating process, this kind of coating is only suitable for fabrics with a high melt temperature.

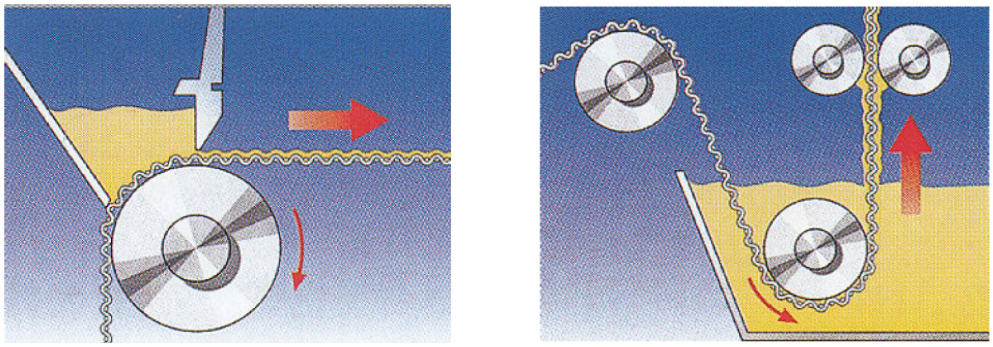

a **b**

Fig. 6 (a) Spreadable process and (b) dipping process [10]

As a conclusion, we can state that resins in general have an influence on the following properties, regulated by additives to the coating:

- strain- / shear stiffness
- weld possibility
- UV-protection of the fibers
- water tightness
- light transmission
- light reflection
- light scatter
- color
- sensitivity for dirt
- heat radiation

Since membranes are composed out of a fabric and a coating, they are also named after both of them. General combinations are (1) Polyester fabric with PVC-coating, (2) glass fiber with PTFE- or silicone coating or PTFE-foil lamination and (3) PTFE-fabric with Fluor polymer coatings.
It is out of the scope of this thesis to describe all different characteristics of the existing combinations of coating-fabric. For more detailed information, the reader is referred to more specific literature as e.g. Atlas Kunststoffe + Membranen [1] and chapter 9 of the European Design Guide for Tensile Surface Structures [3].
Generally it can be stated that the advantage of PVC-coated polyester is the high tear resistance in comparison to PTFE-coated glass. On the other hand, the last one shows a better resistance to environmental degradation like temperature, solar radiation and age, but it's extremely long life span also has its price. Another disadvantage is the sensitivity for damage.

1.3.2.1 Plastic Foils

Next to woven fabrics there is also a group of foils that are suitable for tensile membrane purposes. They are made of thinly rolled or extruded homogeneous material as polyamide, polyethylene or polyvinylchloride. The transparent characteristic makes this last one loved by architects for diverse designs. It is very suitable for inflatable sculptures, as used by e.g. Buckminster Fuller and Kenzo Tange, because of its high gas diffusion resistance. However, its strength is rather low which means that it can only be used in secondary, less loaded parts when uninflated.
A stronger foil is ETFE. This material has been extruded for the first time in the seventies and is since the eighties commonly used as glass replacement for windows or as a building skin.

1.3.3 Material considered in this thesis: PVC-coated polyester

This thesis will focus on PVC-coated polyester fabric, which is the most widespread material for membrane structures, because it has the best quality-cost balance for the time being. Moreover, it is more suitable for deployable systems than glass fibers, since the latter are more brittle.
For the interpretation of the experiments and the numerical simulations that will follow, it is important to know the characteristics of this material and to understand its behavior.
In the following, the principles will be outlined. For a more detailed description, the reader is referred to the original resources [1, 12, 15 and 16].

1.3.3.1 Characteristics

Because the polyester fabric is a woven structure, the yarns are differently positioned depending on the fiber direction. The so called warp yarns are almost straight, whereas the fill (also called 'weft') fibers wave between. The consequence of this configuration is a difference in strain in each direction of the fabric when it is loaded. Furthermore, the tensioning of the fabric causes a reallocation of the fibers. The fabric will initially elongate more in fill direction because the curves are partially stretched out (Fig. 7 Woven fabric with straight warp and curved fill (a) and the interaction of warp and fill yarns under tension called crimp interchange (b) [16]). On the other hand, in warp direction the fabric will tend to become shorter, because the fibers there are forced to curve, due to the pressure exceeded by the fill fibers. This phenomenon is called 'crimp interchange' and can be analyzed from biaxial tensile tests.

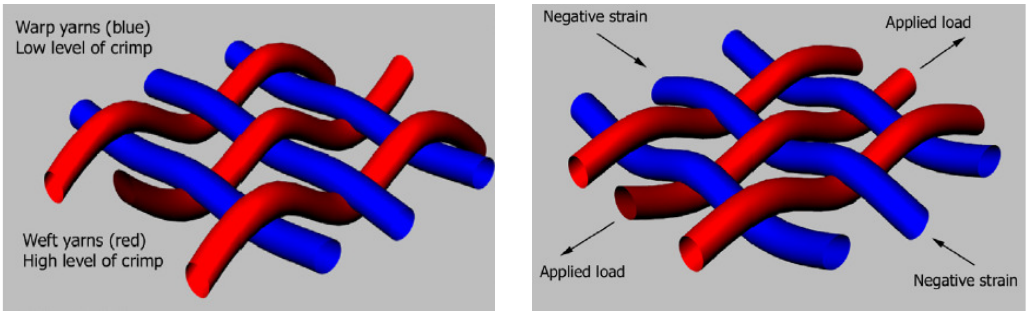

a **b**

Fig. 7 Woven fabric with straight warp and curved fill (a) and the interaction of warp and fill yarns under tension called crimp interchange (b) [16]

Furthermore, the PVC-coated polyester can be considered as a composite. The yarns provide tensile strength whilst the coating protects the weave, stabilizes it and provides shear stiffness .
Both the coating and the fibers show non-linear behavior at high tensile stress, ascribable to plasticity. Consequently, the membrane in total behaves highly non-linear, with the crimp interchange as an additional factor. The weave-structure of the yarns makes the behavior orthotropic.

1.3.3.2 Results from uniaxial tests

As can be seen in Fig. 9, the behavior of the coated fabric under uniaxial loading is significantly different in warp and fill direction. Under an increasing load, the strain in fill direction is much larger than in warp direction. For both orientations, the behavior is highly non-linear.

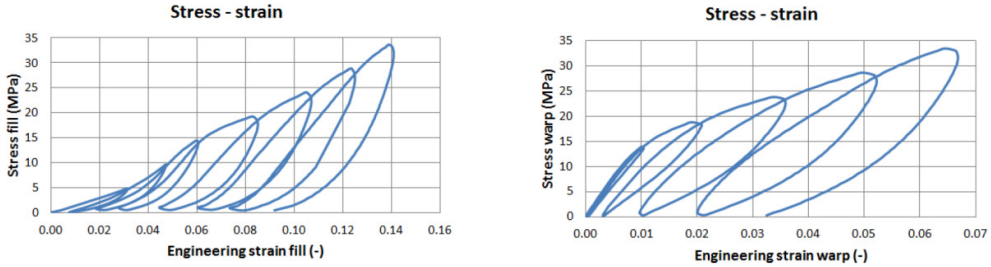

a **b**

Fig. 8 Strain in function of stress for fill (a) and warp direction (b) for uniaxial test with increasing load [15]

The main difference in behavior in the two principal directions is observed during the first phase of the loading.
Because the yarns in fill direction are originally curved, this orientation shows a very low initial stiffness. The yarns must be straightened first. This initial crimped configuration leads to large permanent strains, starting already at 5 kN (Fig. 9 b). After this stage, when the fibers are actually stretched, they respond much stiffer and linear elastic until a value of 14 MPa. When the load exceeds this limit, plasticity phenomena are observed causing even larger permanent strain.

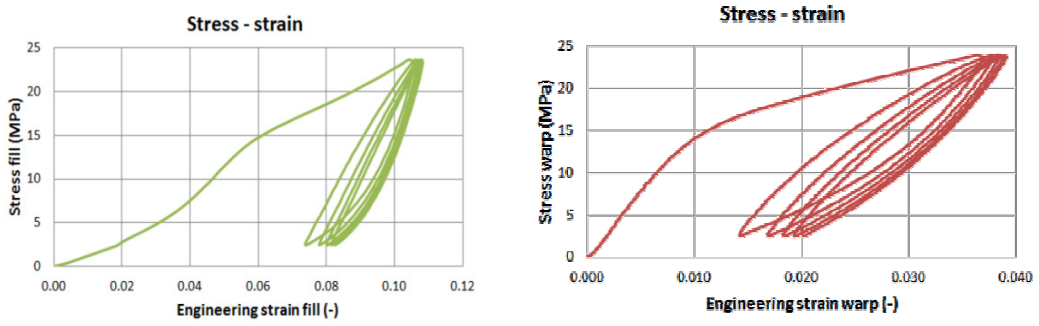

a b

Fig. 9 Strain in function of stress for fill (a) and warp direction (b) for a uniaxial cycle repetition test [15]

Meanwhile, the stress-strain curve in warp direction behaves initially linear elastic, followed by a plasticity phenomenon. The yield stress for this direction is also approximately 14MPa. When the material is loaded in its plastic regime, large permanent strains are observed after the first loading and unloading cycle. This permanent strain increases slightly in the next loading cycles, but stabilizes after 3 to-5 cycles (Fig. 9 b).
The hysteresis effect of both directions can be a result from the plasticity phenomenon, and in fill direction also the crimp could have an influence.

1.3.3.3 Results from biaxial tests

Because the interaction between warp and fill is so important, biaxial tests are essential to analyze the behavior of the material. Under biaxial loading, the ratio of the applied load will determine the equilibrium configuration of the crimp and define the permanent strain.

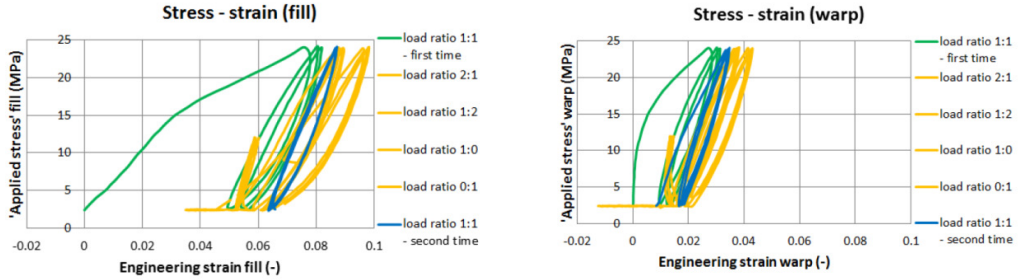

a b

Fig. 10 Results from biaxial test with different load ratios and cycles: stress-strain curve for fill (a) and warp (b) direction [15]

As can be noticed in Fig. 10, the results of the biaxial testing are similar to the ones from uniaxial loading. However, the differences between the main directions are smaller and the transition from one load ratio to another causes a small increase or decrease in permanent strain. Moreover, a different slope of the curve depending on the load ratio can be observed. This was a second observation revealed by the biaxial tensile tests, next to the phenomenon of crimp interchange. Likewise, the load history introduces plasticity phenomena which are inherently irreversible.
These results were based on a test carried out in '*Numerical assessment of material models for coated fabrics in foldable tent structures*' [15], but it was suggested that more biaxial tests should be performed in order to capture the material behavior completely.

1.4 Membranes and architecture

Membranes, as seen in the examples before, are often chosen to create something 'new' or to define an unforeseen type of space. They border a space, but not in the strict way as other building materials do. It seems as if they do not have full control of the environmental space, because of their lightness. Furthermore, they can be landscape and building at the same time, because of their naturally curved shape (Fig. 11). These specific characteristics makes them ideal for particular situations.

Fig. 11 The landscaping capability of tensile structures [17]

Moreover, membranes can make a building 'iconic', because they define both the outer image to the world and inner identity for the users of the building. But also during the time-span of a day, the appearance of the building can completely different (Fig. 12). At night, when appropriate lightning is used, the appeal of the building can change tremendously compared to daytime, due do the translucency of the material.

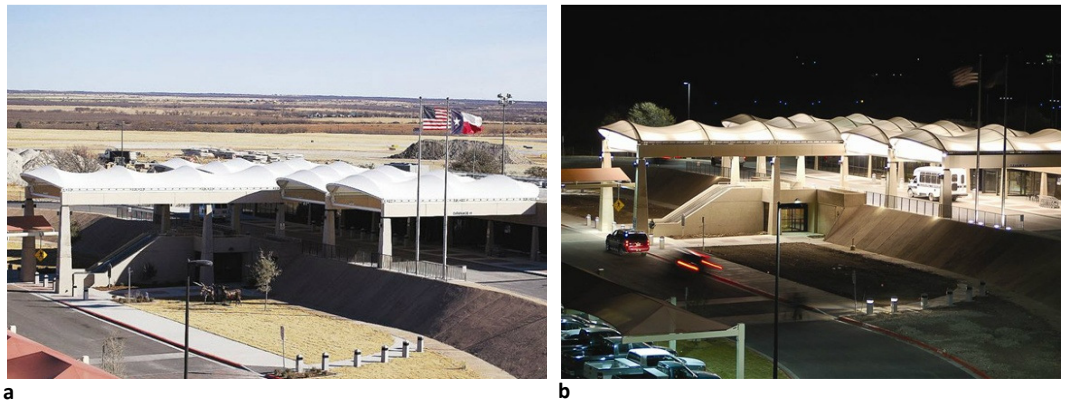

a **b**

Fig. 12 Abilene Airport by Fabritec Structures during day (a) and night (b)

However, probably the most important features of membranes, which distinguishes it from other building materials, are the flexibility and mobility. The design of a structure that can be erected over and over again on almost every location, quick and uncomplicated to deploy and easily transportable because the modest volume that it occupies when broken apart. This is the biggest advantage of tensile structures over other construction materials, especially for temporary and mobile structures that have to be moved and reused as a whole (Fig. 13).

Fig. 13 Tent of the Glastonbury festival, United Kingdom [18]

But also as part of a permanent building or in a static configuration, membrane structures can play out there flexible nature. In adaptive building parts for example, they can result in an energy efficient structure through control of natural light and internal temperature, by changing their position according to the necessity. At the same time they can reshape the interior space, metamorphosing the internal experience and user possibilities.
In what follows, this exquisite but also complicated gift will be discussed.

1.4.1 Flexibility exploited

The need and wish for adaptable skins or transformable building parts exists already for a long time. In ancient Rome for example, cotton textile was used to cover the Colloseum and provided the spectators with shade at the required time and in the right spot. Big sheets could be moved and stretched along cables, handled by experienced sailors [19].
However, it was until the mid-twentieth century that the technology reached again this point of ability to protect large spaces with opening and closing covers, e.g. for sports arenas or places for cultural events. Membranes are very popular in the design for these roofs, because of their low weight-span ratio. Moreover, they do not need intermediate supports and can be carried by frail constructions.
The feasibility to open and close or to take intermediate positions, gives the place an extension in use, as for open-air swimming pools or public places. A beautiful example can be found in the foyer of Masjid Nabawi mosque in Jerusalem (Fig. 14). The umbrellas provide the square to be used also on the hottest time of the day [20].

Fig. 14 Foyer of the Masjid Nabawi Mosque in Jerusalem (a) with closed umbrellas and (b) in fully opened configuration in order to provide shading [18]

Several designs were made in the period after World War II. It is not a surprise that architects started to look for innovative and pioneering design in those times. After the cruel experiences of the war, visionary and utopian groups broke with the bands of tradition and started to look for new forms of living, housing and building. In 1967 for example, a sheltered outdoor theater was created in the ruins of a monastery in Bad Hersfeld, which is still present [21]. The system consists of fourteen guide cables to extend the membrane, all held together by a big central mast. Although this has been and still is a successful project, it was not in every design like this. A lot of structures raised in that period, failed after only a short life time, either because the right technology was not yet available or the knowledge was still inadequate. Therefore, the ideas of too ambitious architects could not be executed properly [22].

A new hope came by the realization of the roof structure for the arena in Zaragossa after a design by Schlaich and Bergermann in 1990 (Fig. 15) [23]. An distance of 88 meter had to be spanned without intermediate supports. With the use of the 'spokes wheel'-method, the problem was solved in a very efficient way.

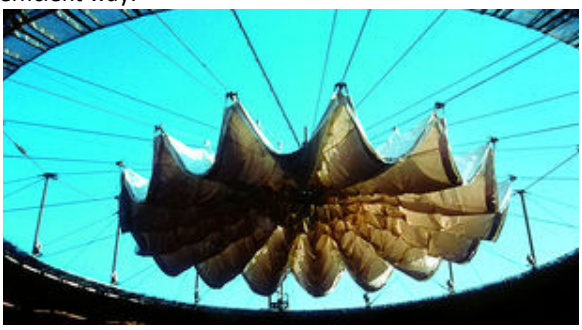

Fig. 15 Opening roof of the bullring in Zaragossa [23]

Fig. 16 Mushroom - balloons, Osaka, 1970 [24]

Adaptive structures are, as one can see, not new in the architectural field. Nowadays, goals are set every time more ambitious. As mentioned in 'Adaptive building skin structures' [25] the concepts for architecture are evolving towards responsive skins and morphing structures (e.g. Fig. 17). In an overview of the research of variable geometry structures, the distinction between two kinds of adaptable structures is made:

- compliant and bi-stable structures e.g. pneumatic concepts and (rigid) foldable origami [24, 26], and
- progressive morphing truss structures [27] and scissor like-mechanisms [28].

An example of a pneumatic structure can be found in Fig. 16. Foldable origami concepts know the most applications in space engineering [29, 30].

The second group is more ambitious. Transformations occur between more than two different shapes to constitute multiple and flexible shape alternatives. Membranes go indispensible together with this type of concepts, because other materials are do not exhibit the required flexibility. Therefore, the parallel running explorations in the field of adaptive structures can support simultaneously the research to adaptable architectural membranes.

Fig. 17 Adaptable skin of the Crystalline Towers in Abu Dhabi [31]

Despite all the diligent ideas, the applications today are still limited, partly due to the lack of analysis methods and failing knowledge about the behavior, both of the membranes and structures as separate entities, as well as of the very complex symbiosis of those two.

But the desire to realize them is present, and the demand for adaptable, interchangeable and multi-functional rooms, buildings and spaces is only increasing. The simultaneously growing need for energy-efficient, ecologic, sustainable and intelligent buildings only fuels the progress in this field.

This thesis will focus on a type of deployable system that demonstrates stable intermediate positions between fully unfolded and completely closed. The investigations presented further on, will tend to provide better knowledge in the behavior of the membrane when used in such particular mechanisms.

1.4.2 Current design problems for tensile structures

Technical textiles are composites which exhibit non-linear orthotropic behavior in function of the bi-axial stress situation. In general, design methods for structures with this kind of exceptional material divide the process in two stages: the form-finding phase and the load analysis [3].

1.4.2.1 Form finding

The goal of the form finding process is to obtain this shape of the membrane for which the stresses are equally distributed and the surface area is minimized. The final state is only depending on the predefined boundary conditions (supports, anchorages or cable edges) and the form finding properties, i.e. the desired prestress of the membrane and the cables. In this stage of design, the material properties have no influence.

In the early design period of membrane structures, this study was carried out using soap films(Fig. 18), because they demonstrate the same characteristics [32].The soap-surface takes naturally the shape of a saddle: an anticlastic curvature to carry the tension, a synclastic to derive the loads. If the project's model shows highly aberrant shapes, it is likely that there will occur troubles in its built form, e.g. accumulation of snow and water on the surface, which will lead to unexpected stress concentrations and deformations. Although the soap films are honest representations of the structure in reality and give a first impression of the efficiency of the desired construction, the process to fabricate them is very arduous. Besides that, they only account for self-weight and have isotropic properties. More practical difficulties are associated with the translation of a stable minimal surface into real tension structures, as described in '*Understanding novel structures through form-finding*' [33]. Therefore, this method became obsolete.

Nowadays, the form finding process is replaced by computer software e.g. EASY and Tensyl (see chapter 2).

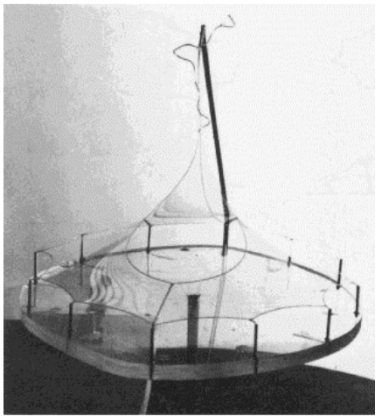

Fig. 18 Experimental approach to shape finding of lightweight structure using soap films [34]

1.4.2.2 Load analysis

The second stage of design is the load analysis. Here, the material properties are introduced. As mentioned before, the behavior of the material is highly non-linear and different for each fiber direction. Moreover, the bending and compressive stiffness is very small and can be neglected in calculations for wind and snow load [3].

Different approaches for load analysis are available. Firstly, the surface can be discretized in smaller components, seen as a cable network. The second option is to carry out a continuum based analysis. A third option is the combination of those two.

In the discrete analysis (first option), the textile is approximated by an orthotropic cable net, with constant Young's moduli in the warp and fill directions, assuming linear elastic behavior. Poisson's ratios and shear modulus are ignored [35].

The second option is a typical finite element approach, making use of orthotropic material properties including the Poisson's ratios and considering the elastic moduli (E-moduli [Pa]) both in axial and shear direction.

However, the assumption of constant E-moduli is a simplification, and introduces an error in the calculations. Of course, this leads unavoidably to approximations of the results. The small differences in the used methodology to interpret the results from experiments, can culminate in significant differences in the derived constants as e.g. the Young's moduli [36].
Therefore, up till now high 'safety factors' have to be used for the structural analysis, because the current calculation methods do not have the able to deal with the correct material behavior, the creep and tear propagation.
After a review of different codes/guides (e.g. the IASS working Group 7, the French, Italian, Japanese and German codes related to tensile structures, and the ASCE Standard), there can be concluded that in broad terms, the minimum stress factor for membrane material in permanent or semi-permanent structures is 5, and sometimes increases up to 7(!) at connection points [3].
Furthermore, when external loads are considered, the codes are designed for standardized building shapes and building behavior. This makes their application in the design of a membrane structure very difficult, since the geometry influences not only the magnitude of the loading, but also its distribution on the surface. Besides that, a good estimation of the structural behavior is complicated by the large variation in material characteristics, the deviations in strength of a virgin fabric (i.e. an unloaded fabric) to that of one applied in real constructions after degradation and the local damages that are made during fabrication and/or erection.

A round robin exercise held in 2012, exposes the urgent need for a unifying code and consistent methodologies for design. In this exercise, four case studies were analyzed through different software tools and the results concerning form, load carrying capacity, displacement and reactions were compared. The outcome, as can be seen in *'Analysis and design of membrane structures: Results of a round robin exercise*' [35], is highly varying. The lack of benchmarks for the verification of membrane structures analysis, leaves all results in dubiety, as was also pointed out in ' *Lightweight tension membranes- an overview* ' [37].

1.5 Conclusion

Tensile structures are designs of all times. In earlier days, they were constructed with natural materials, but the development of more resistant synthetic fabric, improved with sustainable coatings, gradually replaced them. Today, PVC-coated fabric is the most cost-effective available material and currently most used in membrane architecture.
Due to its flexibility and lightness, the material is beloved by architects for the application in freely formed structures. Moreover, the characteristics evoke the wish for adaptive and kinematic systems, and this tendency is fueled by developments in technology and the need for more sustainable building.
However, this kind of architecture is difficult to realize due to lack of knowledge regarding the complex material behavior and the insufficient calculation methods.
The flexible textile with its large strains and displacements requires a fundamentally different approach in design and structural analysis, compared to the well known materials as steel, concrete, wood and glass.

Chapter 2 | Approaches for the simulation of membranes

"The limitations of the human mind are such that it cannot grasp the behavior of its complex surroundings and creations in one operation. Thus the process of subdividing all systems into their individual components or 'elements', whose behavior is readily understood [...] is a natural way."

The Finite Element Method, O.C. Zienkiewicz, 1967-2000

2.1 Introduction

In this chapter, a closer look is given at the possibilities for membrane simulation in Abaqus/Standard.
First, a synopsis of available membrane simulation methods described in literature will be discussed. Next, a short delineation will be given about the theory behind the solution method in Abaqus/Standard to tackle non-linear problems. As a premise, a static solution procedure was chosen, not taking into account of velocities. The different possibilities will be tested on the simple case study of a square membrane.

2.2 Approaches for membrane simulations in previous works

In the current status for membrane simulation, two main approaches can be pointed out, depending on the results one want to identify, and the rate of detail this requires. Either the surface can be discretized as a cable network, or approached in a more detailed way as a continuum surface. Each method has its advantages and negative aspects [38].

2.2.1 The cable network

The earliest research in the simulation of architectural membranes concerned the form finding process, as was already pointed out in chapter 1 [33]. In the first place, researchers tried to translate the minimal curved surfaces into numerical models to get around the laborious and time consuming physical models as e.g. soap films (Fig. 19) or expensive real scale models. Besides that, sufficient software could allow to get more grip on the generation of cutting patterns which involves complex measurements and calculations.

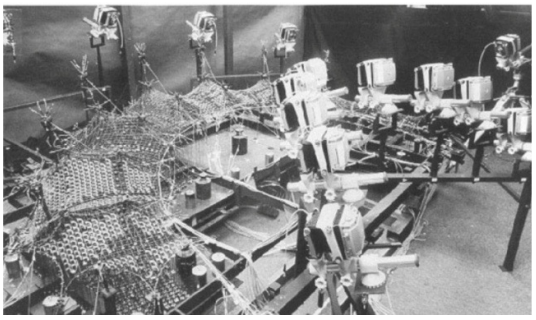

Fig. 19 Soap-film model for the Munich Olympic Stadium (1972)[39]

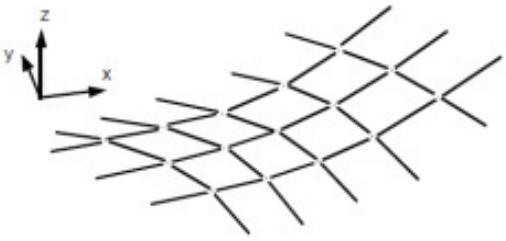

Fig. 20 Approximation of a surface as a cable network [38]

The most popular and easiest way is to rely on the cable net typology. The membrane surface is reduced to cable elements, aligned with the warp and fill direction of the fabric. Commercial form-finding software as EASY makes use of this methodology. Available calculation methods are the transient stiffness method, force density (FD) method or dynamic relaxation (DR) method. A detailed explanation of these methods would lead us to far from the subject of this thesis, but a comprehensive presentation of them can be found in '*Computational form-finding methods for fabric structures*' [38]. Also in '*Vorm-actieve constructies*' [10], the last two strategies are explained clearly.
In short, the first method assumes a linear load-displacement relationship, which demands very small steps *k*. For each intermediate position the corresponding stiffness matrix K_k is calculated, according to the displacement at that time. Every time, the residual force at the *k*th increment can be found. After several iterations, the residuals become zero and the static equilibrium is reached.
In FD, the position of one node is found by mandating equilibrium of the forces of the four branches that come together in that node. Constant values of tension coefficients are introduced, the so called force densities qm, to make the equations linear and easy to solve. If T_m is the tension in each branch, L_m the member length, the force density can be expressed as $q_m = \frac{T_m}{L_m}$.
Finally, in the method of DR masses are concentrated in the nodes, causing out-of-balance forces that make the structure oscillate about the equilibrium position. The system comes to rest by relaxing

these forces. This method is extremely efficient and accurate, further easy in understanding because of the physical interpretation.
Load analysis makes up the subsequent step in simulation. A constant elastic modulus is assigned to each direction of cables, ignoring Poisson ratios and shear. Compensated with stress factors, the computer model provides the possibility to extract the necessary data for the erection of simple constructions. For more complex configurations however, the results are precarious and the support of physical models is needed to examine the output of the software and to amend were needed.

It can be concluded that current form-finding software gives the designer a good impression about the aesthetic qualities of the project and an indication of problematic areas e.g. flat regions. A notion for wrinkled areas can be derived from negative stresses, but is not accurate. For the generation of cutting patterns (i.e. the development of a 3D-form on a 2D plane), they denote an important step forward. However, a lot of assumptions are made and over dimensioning is state-of-the-art, mainly because the material behavior is complex and static analysis capabilities are approximations. Like this, they are too indecisive to fully trust on.

2.2.2 Continuum surface

For the purpose of improvement, the strategies are evolving to more complex but at the same time more correct continuum based models. Typically this approach is used in FE-software.
Research on a good two-dimensional continuum model for membranes started already in 1929 with the tension *field* theory of Wagner[40] to simulate membrane wrinkling. Simplification and more general formulations were formed by i.e. Mansfield (1968) [41] and extension to the theory were added by i.e. Epstein and Forcinito (2001)[42].

The basis of the theory is a 2D-continuum without the ability to carry compression load and with negligible bending stiffness. Of course, this implicitly means that an infinite number of wrinkles can form, with an infinitesimally small amplitude.
When details about the wrinkling are important as e.g. the exact position, amplitude and onset, it is necessary to incorporate the bending stiffness of the material. This has been done for the first time for a heavily wrinkled membrane by Rimrott and Cvercko (1986)[43]. Consequently, shell elements have to be used instead of membrane elements, because the last ones exhibit a small compressive resistance and bending stiffness. Wong and Pellegrino [44] proposed in 2006 improvements to this approach concerning the simulation of non-parallel, non-uniform wrinkle fields.
In ' *Wrinkled Membranes- Part III: Numerical Simulations* ' [54] of the same authors, a comparison between these two approaches in made in the Abaqus software. First, a very thin membrane (thickness of 25 µm)was simulated using membrane elements, and in the second part thin shell elements were explored. It was shown that the shell elements were able to represent more wrinkles with more accuracy, despite a much larger CPU time (5 to 100 times larger, depending on the type of shell element). The choice for the type of element depends on the information and the level of accuracy one wants to achieve.
Since architectural applications do not focus on the details of wrinkles as e.g. their dept and number, but more in the area of their appearance, membrane elements seem to be convenient for the numerical simulation. These elements are able to represent the deformation of the structure, without going to deep into detail. This is the exactly the information one needs to predict the final shape of the membrane. All further analysis is given in a more general way e.g. the range of the wrinkled area and the direction of the wrinkles.
Besides, it was proved in the literature mentioned before that simulations with this type of element are able to predict accurately the stress distribution, which is from main importance in this research. The use of shell elements would be too time consuming and would introduce needless complexity, producing irrelevant information for the aim of this study.

2.3 Non-linear problems in Abaqus

Since a membrane is very flexible, caused by the lack of bending stiffness and the non-linear material properties, the structure will undergo high deformations when exposed to loadings. The relationship between the deformations and the load is also highly non-linear. Consequently it is impossible to solve the problem with a single system of linear equations and a non-linear analysis in Abaqus is necessary. The following gives the basic insight of how Abaqus calculates a solution for this type of problems.

2.3.1 Definition of the problem

In the Fig. 21 below, a typical non-linear response of a structure under loading can be seen (dashed line). The solution to determine this response cannot be calculated by the use of one linear equation. Instead, it is found by specifying the loading as a function of a pseudo-time. The time is then incremented to obtain the non-linear response for the applied load (red dot) [45].
During simulation, Abaqus/Standard finds an approximate equilibrium configuration at the end of each time increment (white dots), to come eventually to an acceptable solution after one or more iterations (=attempts). This general solution method is called Newton-Raphson method [46].

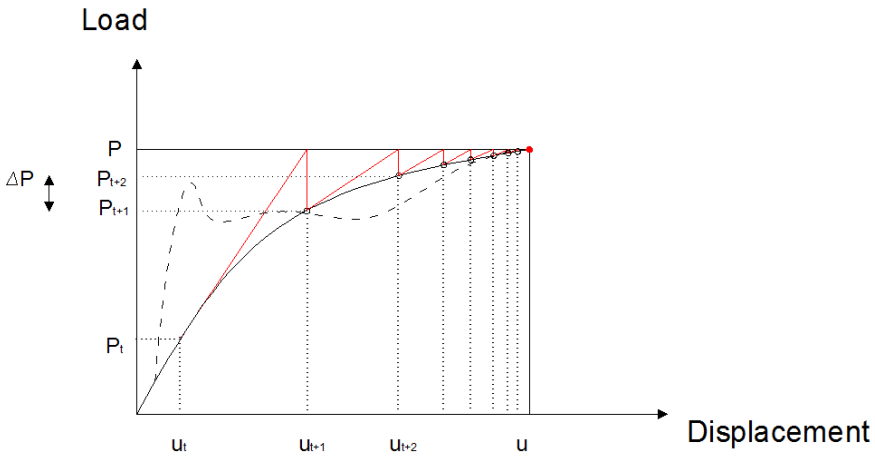

Fig. 21 Newton-Raphson method to solve non-linear load-displacement problem[45]

2.3.2 Global solution method

Like in every static analysis problem, an equilibrium status is searched, i.e. there should be a balance between external forces P working on the system and the internal forces I.

$$P - I(u) = 0 \qquad (1)$$

To find the response of the structure to a small load increment ΔP, the tangent stiffness of the structure K_0 is used to calculate a displacement correction c_a, based on its configuration at u_0 (Fig. 22**Error! Reference source not found.**). Using this correction, the configuration of the structure is updated to u_a.
This new configuration at u_a is then used to calculate I_a, which is the internal force at this updated position.

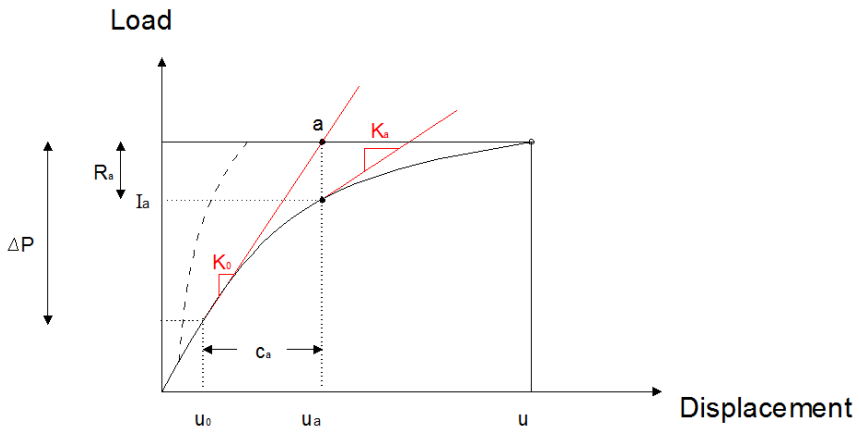

Fig. 22 Finding the response of a structure to a load increment ΔP: first iteration

When an equilibrium position is not reached, thus $P \neq I_a$, a residual force is present in the structure, calculated as follows:

$$R_a = P - I_a \qquad \textbf{(2)}$$

Obviously an equilibrium is reached when R_a equals zero at every degree of freedom in the model. In that case, the solution of the iterations (here point a) would lie on the load-displacement curve. However, R_a will never be exactly zero. Therefore Abaqus/Standard accepts the solution when R_a is less than a defined tolerance value. In this way u_a is set as the new equilibrium configuration for the structure under the applied load. This is only true if also the displacement correction c_a is considered small enough compared to the total incremental displacement $\Delta u_a = u_a - u_0$. Usually, a fraction of 1% is accepted.

The solution has not converged when R_a and/or Δu_a are too large. A next iteration is performed using the updated configuration from the previous iteration to calculate the new tangent stiffness matrix K_a and defining another displacement correction c_b that brings the system closer to the equilibrium position. This iterative process is executed by Abaqus/Standard in as many iterations as are needed. Every intermediate solution comes closer to the load-displacement curve (Fig. 23), until eventually full convergence is reached. [20]

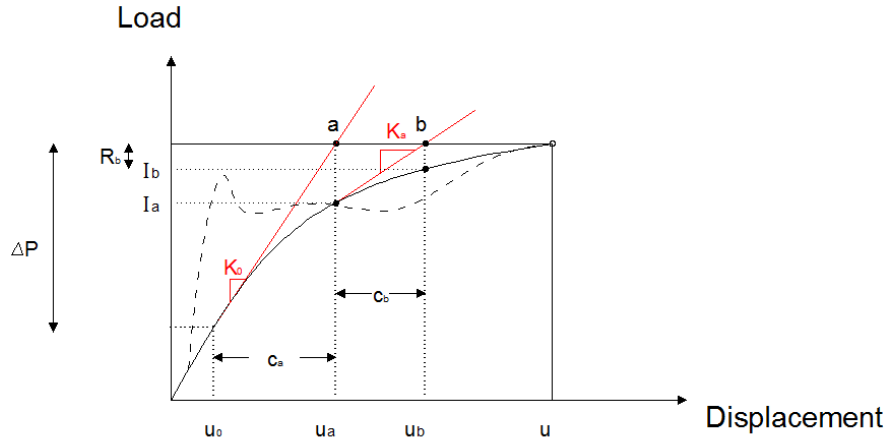

Fig. 23 Finding the response of a structure to a load increment ΔP: second iteration

2.3.3 Solution methods for unstable problems

In particular cases, the global solution method is insufficient, typically when the non-linear static problem is unstable. The origin for instabilities can be of a geometrical nature, e.g. buckling, or of a material nature, e.g. material softening, or also due to non-linear boundary conditions, e.g. contact. Also in membrane structures, instabilities occur. When a membrane structure is subjected to loading, sooner or later wrinkles will be generated. The side the membrane will choose to pop out, is unpredictable and in reality highly depending on imperfections. Furthermore, the large strains dedicated to the material characteristics, cause in instabilities while tensioned.

If the instability is localized, there will be a local transfer of strain energy from one part of the model to the neighboring parts. This kind of problems can be solved in a static analysis with the aid of artificial damping, explained in 2.3.3.1 . However, when the instability is seen as global response of the structure to an applied load, the case can be treated as a collapse problem, further described in 2.3.3.2. Each investigated method is tested on a square membrane deformed into a hyperbolic parabolic surface (hypar), documented in section 2.3.4.

2.3.3.1 Introduction of artificial damping

The method that introduces an artificial viscous force, is a developed to solve unstable non-linear problems in static analysis. In this method, the static solution of a mechanics system is referred to the steady state part of the response of the system to step loading, as pointed out by Rayleigh [47].
(in general the response = a steady state part + transient part) It converts a static system to a pseudo-dynamic one by adding fictitious inertia and damping forces.
This method knows many applications. To only name a few: it was used for stability analysis of frame structures (Brew [48]) and the analysis of plate bending [49], but was also used by Barnes [50] for form-finding of prestressed cable nets and membrane structures.
In general, the concept consists of the insertion of a viscous force when the iteration process starts to diverge, this means that the solution searched by the program is moving away from the equilibrium state. This viscous force acts as an artificial dashpot to provide the possibility of dealing with local instabilities e.g. wrinkling of the membrane, and is defined as follows:
As mentioned before, the global equilibrium is fulfilled when (1)

$$P - I(u) = 0$$

From the moment a viscous force F_v is introduced for stabilization, the equation becomes

$$P - I(u) - F_v = 0 \quad (3)$$

with

$$F_v = c\,.M.v \quad (4)$$

M in this equation is the artificial mass matrix, c the damping factor and v is the vector of nodal velocity, defined by

$$v = \frac{\Delta u}{\Delta t} \quad (5)$$

Δt is the increment of time and the nodal displacement Δu is seen from the previous iteration, thus

$$\Delta u = u_t - u_{t-1} \quad (6)$$

Hence, introducing the viscous force F_v will regularize the unstable motion of the system with the damping constant c and will eventually come to rest, this is returning to its static state. The main interest of the calculation is the final state, as it would have been found through a static analysis. This is also the reason why the this method is called *quasi-static*.
However, care must be taken in using this solution method as it has the drawback to require a longer calculation time to obtain the steady state solution, because the viscous force needs time to damp out in order not to affect the result.

Initially, the system is considered stable and at this point the damping has no effect. However, instabilities will occur during the step. When a local region goes unstable, the system releases strain energy to keep the equilibrium, which in turn is damped out by the viscous forces [51].

Different parameters determine the magnitude of the viscous force, but the most important ones are the damping factor c and the time increment Δt. Care should be taken in both defining them and attention must be paid in interpreting the results.
When a local instability takes place, large displacements occur and strain energy is released. When damping is added, a part of that energy is dissipated and permits the process to occur without very large displacements. In order to have a reliable result, attention is required in choosing the damping factor : when too high, the solution can be distorted, but if too low, the convergence behavior is problematic. The Abaqus Manual advises the dissipation energy not to exceed 5% of the total strain energy. One can choose in the settings of a simulation to define the dissipation energy fraction or immediately the damping factor itself [51].
If nonetheless a large damping factor used, the time period can be increased to keep F_v at an acceptable value, or an additional step without any damping can be carried out to achieve the static equilibrium solution.

2.3.3.2 Arc length method - Riks analysis

When the instability of the analysis is of a geometrical nature, we are dealing with global instability. When a membrane is loaded, it will tend to deform. In reality, all kind of imperfections and exterior influences regulate the direction of the deformation. In a numerical model however, all circumstances are perfect. Which side or at which place the membrane will pop out is thus unknown and difficult to decide, because all regions are equal. Abaqus offers the so called Riks method to deal with this issue of bifurcation (= two possible solutions for one load). The biggest advantage over the method with a viscous force is the absence of damping factors. However, a limitation is the fact that a Riks analysis can only be performed in one step and cannot have following steps and the calculation time is often higher[52].
When using the Riks-method, the loading P on the system does not follow a prescribed history. The load is proportionally added (in pieces λ) and forms part of the solution. Furthermore, the response of the system is supposed smooth, thus without sudden bifurcations. Assume λ to be the load magnitude parameter for loading pattern P. The actual load state at any time is given by λP, with a corresponding displacement of the structure u (Fig. 24).

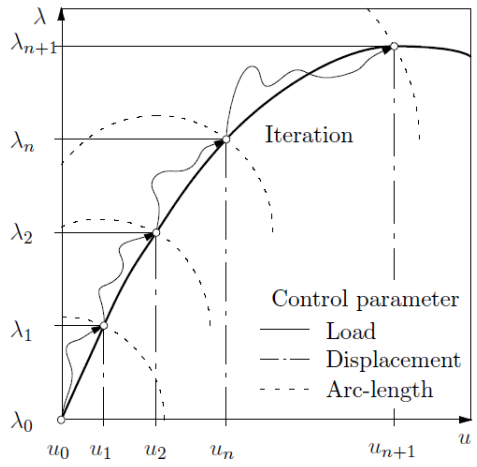

Fig. 24 Load parameter control in Riks analysis [45]

The basic algorithm to discover one single equilibrium path is still the Newton method as described in 2.3.2. The difference with the Riks algorithm is that the increment size is limited by moving a given distance along the tangent line influenced by the parameter λ. That point is then the current solution point. Then, the equilibrium is searched by drawing in the plane orthogonal to the tangent line that passes through that point, as can be seen in Fig. 25 (black dot). The path is travelled as far as needed to come to the equilibrium surface. For more detailed information, the reader is referred to the Abaqus Theory Manual [53].

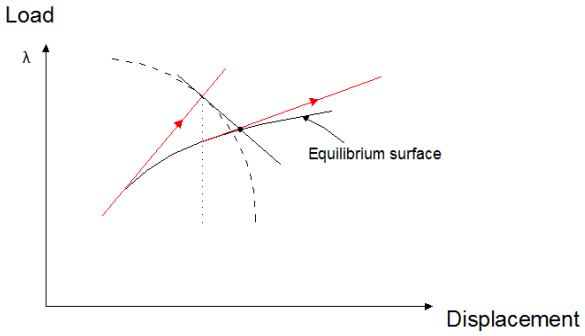

Fig. 25 Riks algoritm

This solution seems promising for the simulation of a membrane exposed to loading. Nevertheless, Wong and Pellegrino describe that the arc-length solution to appears to be insufficient in the simulation of wrinkling membranes, probably because wrinkling is a highly localized type of instability and Riks method is more appropriate for global instability [54].

2.3.3.3 Initial imperfections

To overcome the bifurcation in the analysis procedure if the membrane structure is subjected to a small compressive loading, initial geometrical imperfections can be introduced to give the structure a preference direction to pop out. In '*Wrinkled Membranes- Part III: Numerical Simulations*' [54], it was concluded that a particular magnitude for these imperfections is not critical, as well as the distribution on the surface is unimportant. The only requirement is to start an out-of-plane movement. This interference makes it much easier to get convergence.
Since a stress-free flat membrane does not exhibit stiffness perpendicular to it plane, out-of-plane loading will cause numerical singularities, and hence convergence problems [55]. In some cases it can help to add an initial tension to overcome this issue numerical singularities. However, the magnitude of the loading must be chosen small enough, so the final solution is unaffected.
A practical clarification of the 3 methods can be found in the next section.

2.3.4 Application of the solution possibilities

The three methods that were discussed in the previous section, will be explored and validated in this section using a simple square membrane model, in order to get a better vision which solution method would be convenient for the simulation of an architectural membrane.
The simulations are performed by using (1) artificial damping , (2) the arc-length or Riks method and (3) a static analysis with introduction of initial imperfections. The deformed states are compared with a analytical description of the formed surface.
As starting geometry, a plane square of 10m by 10m is given. A deformation is imposed at the corner points, moving two opposite corner 1m upwards, the other two corners 1m downwards.

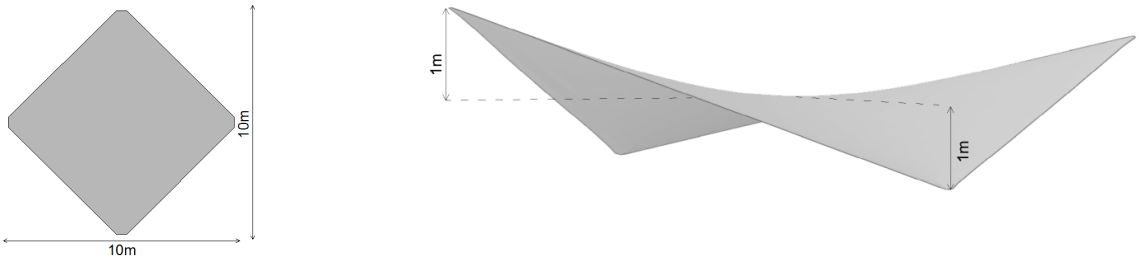

a **b**

Fig. 26 Benchmark : initial geometry (a) and deformed geometry (b)

The material was chosen isotropic linear elastic, with a Young's modulus of 1270 MPa, Poisson coefficient of 0,3 and a density of 1400 kg/m³. The thickness of the considered membrane is 1,2mm.

2.3.4.1 Introduction of artificial damping

In using the method with introduction of a viscous force, the damping factor had to be specified by trial and error.

It was already explained in 2.3.3.1 that, if the damping factor is chosen too small, one can get problems with convergence. However, if the viscous damping is chosen too high the results show distortions and are not reliable, because the system has not fully damp out the introduced viscous force.

To test this method, first a simulation was carried out with the default value of c = 2e-4, but from a post-processing analysis it could be derived that the dissipation energy in this case is way much larger (106%) compared to the total strain energy (Fig. 27). Instead, it is advised to keep the fraction of dissipation energy below 5 % and hence the damping factor as low as possible. This is necessary in order to have a reliable result (Fig. 27). As a confirmation it could be noticed in the output file that the membrane did not in achieved the obtained equilibrium position (Fig. 28).

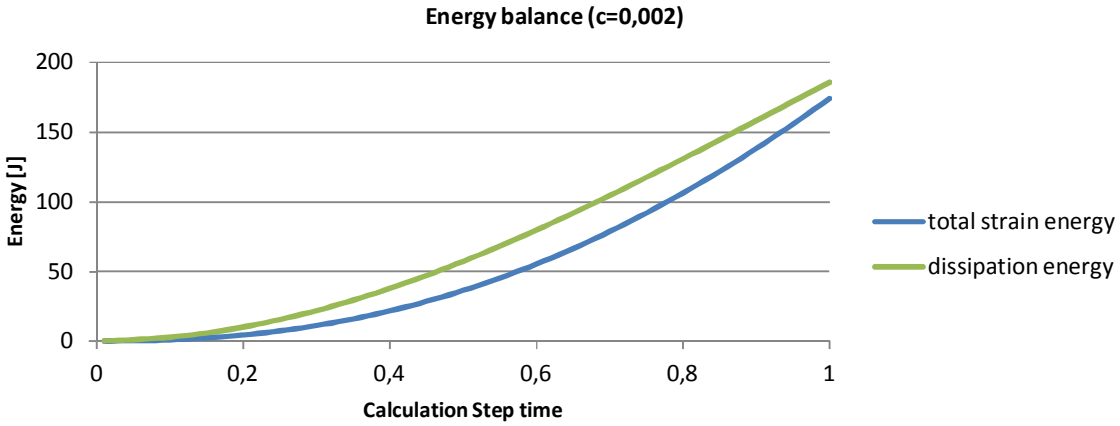

Fig. 27 Energy balance with damping factor c=0.0002

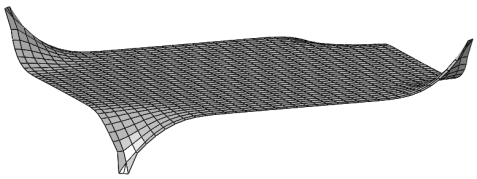

Fig. 28 Deformed state after simulation with too high damping

Since the viscous force that is introduced, is defined in equations (5) and (6), two options to lower the impact of the damping force on the result are available: either increasing the time increment Δt, or decreasing the damping factor c. Both interventions cause a lower F_v. Since they result to the same solution, it is chosen to lower the damping factor c iteratively. With a value of 2e-8 for c and the time period kept as 1, a satisfying result was obtained in regard to the fraction of dissipation energy to total strain energy (0,6%, see Fig. 29).

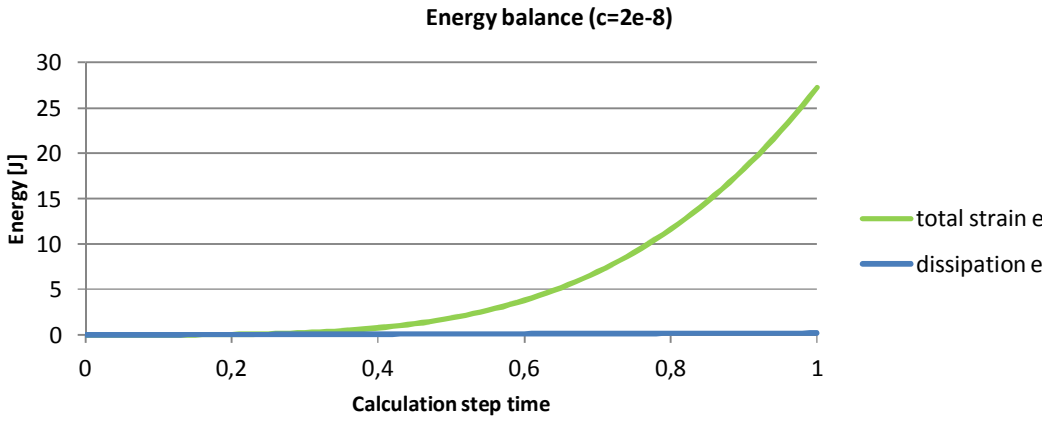

Fig. 29 Energy balance with damping factor c = 2e-8

2.3.4.2 Arc-length method

When using the arc-length method, damping factors are out of concern. What is important in this case is the increment size that must be chosen small enough, in order to keep λ small enough, as explained in 2.3.3.2. In this study, the value was set to 0,01.
The stop criterion was brought to a displacement of 1000 mm of one corner point. Nevertheless, a small prestress had to be initiated in the membrane, here applied as a displacement of 1mm in plane at every corner in order to give the membrane a very small initial stiffness.

2.3.4.3 Initial imperfection

As explained before, the biggest problem for convergence is the bifurcation that occurs in the solution procedure, due to the lack of imperfections. The program has difficulties to decide whether the structure has to move upward or downward. By introducing an initial imperfection in the form of a displacement of 10mm of the central node, a preferred direction for deformation is defined. Also in this case an initial stiffness is given to the structure by the mean of a displacement of 1mm at the corners. This is necessary because the membrane elements have no initial stiffness perpendicular to its plane. In the next step, the displacement of 1000 mm is imposed to the corner points and at the same time the initial imperfection is decreased to zero in order to have no more influence on the final shape. In this way, the introduction of damping is avoided.

2.3.4.4 Analytical formula

In Wang and Cheng [56] , an analytical description for the hyper surface as formed in this case study was found. The equation was adapted to this case to verify the results of the different solution methods with. When the origin is positioned in the center if the square, the general formula is:

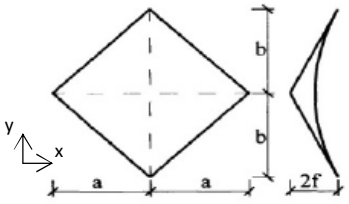

$$z = f\left(\frac{y^2}{b^2} - \frac{x^2}{a^2}\right) \quad (7)$$

In this exercise :

f= 1000 mm
a = b = 5000 mm

If now the square is rotated around the z-axis by an angle of π/4 using the right hand rule and a=b, the transformed equation of the surface is becomes [57]:

$$z = f\frac{xy}{a^2} \quad (8)$$

If we consider the origin in the corner point on the left and we fill in the values of this model, the equation becomes

$$z = 1000\left(\frac{y(x-5000)}{5000^2}\right)$$

In Fig. 30, one can see the deformations of nodes along a path from one high corner point to the center and further up again to the opposite corner (drawing in Fig. 31). It can be concluded that the three discussed strategies give the same solution, which means that each method is sufficient. For the option with a damping factor of 2e-8, there is a slight difference with the other results (max. deviation is 0,01%), due to the small residual viscous forces that remain in the model. However, the dissimilarity is very small and can be neglected. We can conclude that it is not explicitly required to use the frequency-method to define the damping factor, as long as the fraction of dissipation is low enough (under 5%).

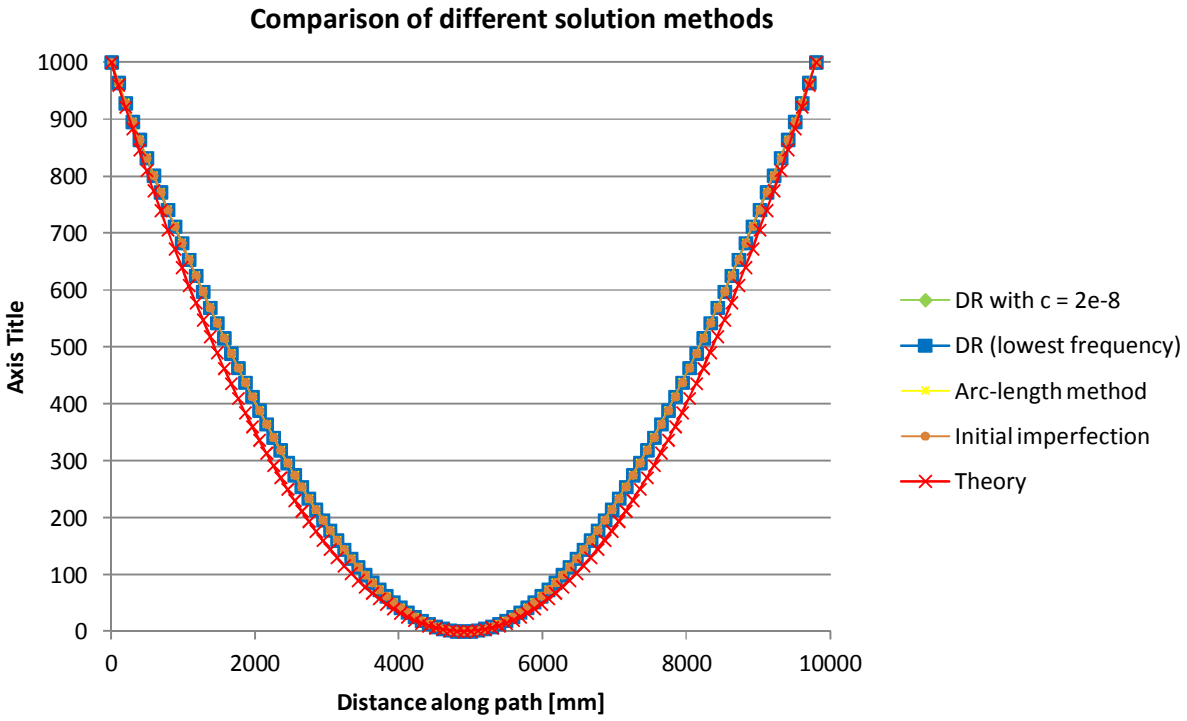

Fig. 30 Comparison of displacement along diagonal axis

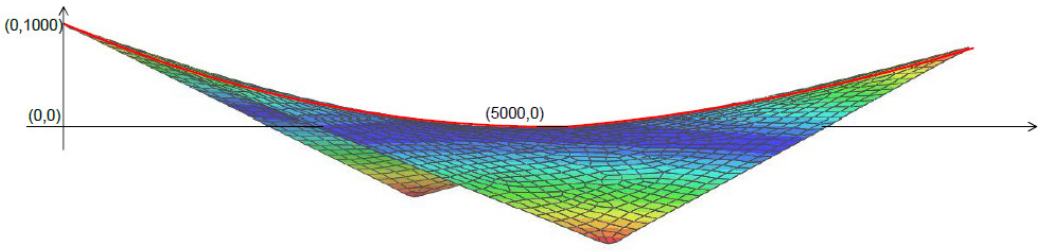

Fig. 31 (Deformed) Saddle shape with diagonal path in red

Used method	max. difference with analytical formula [mm]
Dynamic relaxation	52,9925
Initial imperfection	53,6182
Arc Length	54,10908

Table 1 Maximal deviation in Z-direction of the different solution methods with the theoretical formula

As can be seen in the graph in Fig. 30 and from the values in Table 1 above, the solution in Abaqus is very close to the analytical description. Generally spoken, the deviation is around 5% for this model.
This difference has many reasons. The most important one is the fact that Abaqus also takes into account the material properties, whereas the pure analytical description starts from an ideal non-stretchable material, and thus deforms less.
Because in the above mentioned comparison only one diagonal axis is considered, also the area of the surface is calculated and compared with the pure analytical area of a hypar, in order to get a better insight in the discrepancy of the surface as a whole. This was done with the help of Matlab.
It was found that the area of the pure analytical model is slightly larger than the surface generated by Abaqus (51×10^6 vs. 50×10^6 mm²).
This theory was verified by simulating the same problem with a very soft material (E =20 MPa). The maximal discrepancy of the resulting surface with the analytical surface counted only 46 mm, which means that the surface had deformed less and comes closer to the analytical equation than in the previous material.

In this way, the correctness of Abaqus in terms of finding the right equilibrium form is proved. It must be mentioned that it was not intended to find a minimal surface as for example is outputted by form-finding programs (e.g. EASY). Therefore, the tension in the whole surface should be equally distributed, which is not the case in this example. To reach this goal, the edges should receive a certain 'sag'. This means that the edges should not be straight, but have a curvature to the inside of the surface (mostly 5-10%)[3].

Although the different approaches are equal in accuracy, also the Computer Processing Unit - time (CPU-time) has to be concerned. An optimal simulation does not only give a good result but requires also the lowest possible time. In **Error! Reference source not found.**Table 2, one can see that the introduction of artificial damping results is the fastest method. The difference with the method with an initial imperfection is only small, but compared to the Riks method far more efficient (only 29% of the time for the arc length method is needed for a calculation with viscous force) . Therefore, the method with introduction of a viscous force will be used throughout all further simulations.

Arc-length	Artificial damping c =2e-8	Initial imperfection
65 sec	19 sec	21 sec

Table 2 Overview of calculation time for different solution methods

2.4 Conclusion

In this chapter, the importance of using a continuum based approach for the simulation of an architectural membrane is explained. Furthermore, membrane elements are proved to be the best suitable choice because they are able to generate accurately the required information regarding stress and strain, without the needless and time-consuming details as e.g. shell elements provide. With regard to the solution method, the strategy with the introduction of an artificial viscous forces to apply damping demonstrated to be the best option. Although the possible methods exhibit the same level of precision, the calculation time is significantly different. Even for this small problem, the CPU-time of the arc-length method is much larger in comparison to the technique with introduction of a viscous force. This makes the first one unattractive to use, inasmuch the complexity of the models that have to be simulated is more extensive.

Chapter 3 | In-plane loading of a triangular shaped membrane

"Sine experientia nihil sufficienter scrire potest."

Inscription in the Botanical Garden, Oxford

3.1 Introdution

On the 25th of April 2013, an experiment with a triangular PVC-coated polyester membrane was carried out at the architectural engineering lab (AE Lab) of the Free University in Brussels. The membrane was only loaded in plane. This is an intermediate and simplified step before proceeding to the more complex tests with an opening and closing movement. Although the last one is the actual topic of the KFAS project, this simplified mode, discussed in the following, is required to verify the developed non-linear material model. Moreover, the information and knowledge gained from its analysis and results can later be translated to and compared with the three dimensional setup.
In this chapter, it will be explained how the in-plane experiment was performed and how it was implemented in a numerical model. At the end, the results of the finite element model are verified by the use of experimental measurements.

3.2 Experimental setup

3.2.1 Geometry and confection of the experimental model

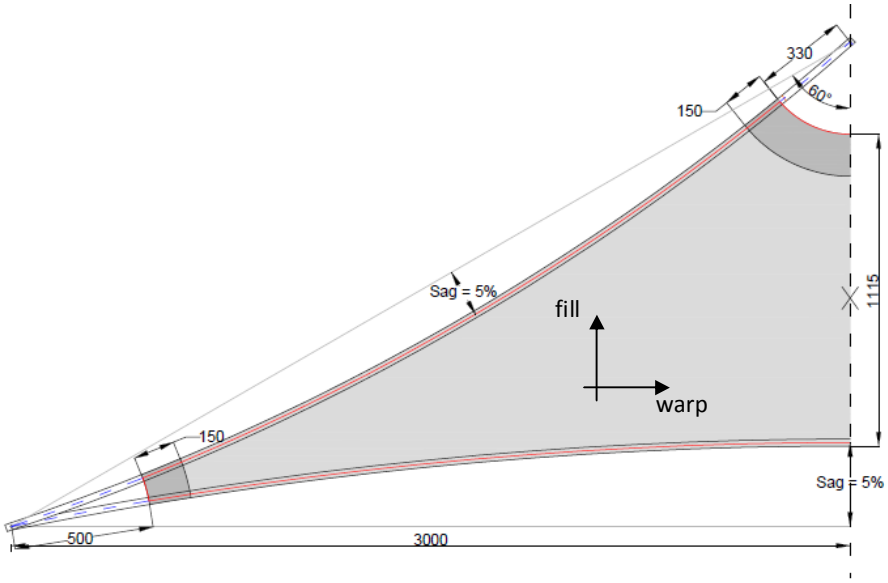

Fig. 32 Design dimensions of the model, fully symmetric about the dashed line [mm]

A triangular shaped membrane with a base of circa 6 m and a height of approximately 1,5 m was cut from a PVC-coated polyester fabric, manufactured by the company Sioen Industries and with the production code 'T2107'. The exact specifications can be found in appendix B. The warp direction was aligned with the base of the circumscribed triangle. The edges themselves were cut with a sag of 5 %, to prevent excessive high stress concentration in those areas when the membrane is under load [3]. For the same reason, the vertexes were truncated and the areas in the corners were strengthened using an extra welded layer of membrane material (dark gray area in Fig. 32). In general, these interventions are necessary because the stress concentrations at the load points can grow higher than the tension capacity of only one layer of material, which can lead to unwanted large deformations and even rupture [58]. Moreover, it diminishes the formation of wrinkles.
Polyester belts of 2,5 mm thickness and 25 mm width were stitched along the borders and were longer than the actual membrane edges. The three main reasons for their appearance are:

- reinforcing the membrane edges
- acquiring attachment points
- transferring the applied loads and equally distribute them equally on the coated fabric.

The parts outside were duplicated in thickness by stitching a second layer on top. Their goal is to improve the stiffness and minimize the stretching when loaded. In order to record only the actions of the membrane, the effect of the belts had to be reduced as far as possible. At the ends metal clamps were installed to make a connection with the surrounding supports (see Fig. 33 on the next page).

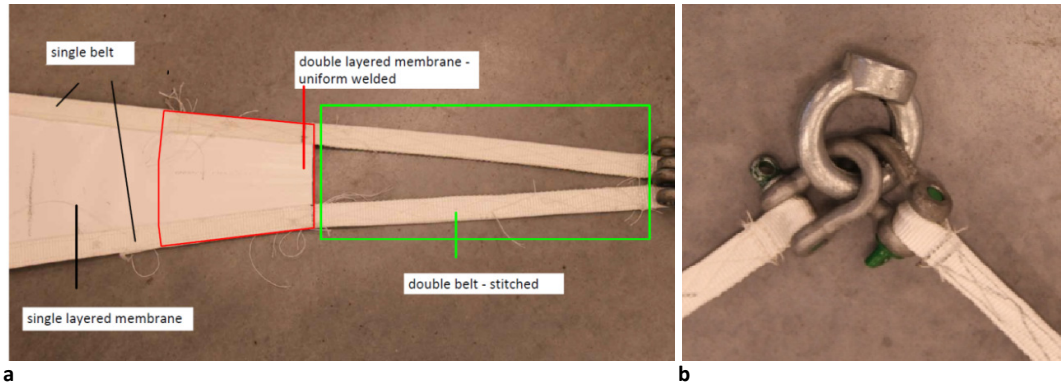

a b

Fig. 33 (a) Detail of different parts of an anchor point, here at a bottom corner, but analog for top. (b) Connection of belts to the ring of a load cell

3.2.2 Setup and loading

The triangle was positioned vertically and hung from its three corners.
In order to ease the descriptions in the following sections, names are given to the most important part of the setup. The four edges of the membrane are called edge A, B, C and D, and the corresponding sides of the circumscribed triangle are called A', C' and D'. The vertices are named to the reference point (RP) where the load is applied. Starting at the bottom left corner, RP1, RP2 and RP3 can be found in counter clockwise direction. Furthermore, also a name is given to the loads in those RPs: L_1, L_2 and L_3. The corners of edge B are called P1 and P2. An illustration is given in Fig. 34.

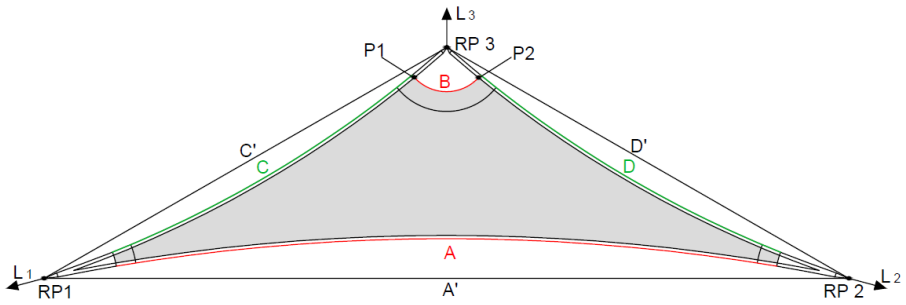

Fig. 34 Naming convention of the model

During the experiment, RP1 and RP2 were fixed, whereas the top could move up and down. The belts at RP3 came together in a ring, connected to the hook of a crane.
Every corner point was provided with a load cell to measure the tension loading continuously. Furthermore, so called 'turnbuckles' were installed in RP1 and RP2, in between the fixed structure and the load cell. These objects allow to adjust the distance between the membrane and the anchor point in order to obtain the right configuration (Fig. 35).

a b

Fig. 35 Connection details of (a) top connection: belts - end clamps - load cell - crane and (b) bottom connection: belts -load cell - turnbuckle fixed structure.

Before starting the actual loading, the membrane was slightly pretensioned to a visually flat configuration. This includes that the membrane was pulled from its corners until an almost equal load could be traced in the load cells and no wrinkles were visible. Practically, this was done by pulling up the hook of the crane until the turnbuckles were positioned alongside the belts. Subsequently these turnbuckles were slightly twisted in order to obtain a light tensioned state of the membrane. At this moment, the tension loads L_1 and L_2 reached no more than 0,18 kN and measured, whereas L_3 had a value of 0,003 kN. This pretensioned state formed the start configuration of the load test.
Consequently, all values of the load cells were set to zero in order to start the measurements from this position.

Fig. 36 Global view of the triangular shaped test setup just before loading

The experiment consisted of 2 cycles of loading and unloading. During the loading phase, the crane was moved upward until the load cells showed a value of almost 10 kN for both L_1 and L_2 .[1]
The upper load in RP3 measured at this point about 8 kN. Subsequently the membrane was brought to its initial position by lowering the crane to the same height as before the loading. Next, the first cycle was repeated once more.

The membrane showed large deformations after the first load cycle. This indicates the presence of permanent strain, and so that the occurring stresses exceed their yield limit of the material. Due to this phenomenon, the membrane slacked when it was unloaded again (Fig. 37). Moreover, the crane had to be lifted much higher during the second load phase (almost 10%) to reach again 10 kN as reaction force (RF) in RP1 and RP2.

Fig. 37 The slack in the central area after the first load cycle

[1] This value was the maximum capacity of the load cells at the bottom of the membrane.

3.2.3 DIC measurements

The displacement of the canvas and the strains that occur in the membrane are measured using the Digital Image Correlation technique(DIC). This technique requires two cameras which take a series of pictures of the dotted surface of the specimen while it is deformed due to loading. The frequency of the photos can be defined, either based on certain load step or at a preset time interval. In the studied case, the cameras were set to take pictures at a combination of these two methods. Every load increment of 0,1 kN an image was taken and as a backup, also every second. This was done to have enough intermediate data in case the load growth did not reach the speed of 0,1 kN/s .

Afterwards, the displacements - and consequently also the in-plane surface strains- could be reconstructed at each load step. The DIC software is able to measure the difference in distance between the dots on the surface by comparing all recorded images. Thanks to the use of two cameras, also the out-of-plane displacement could be traced, with the knowledge of the imaging parameters of each camera and the orientation of the cameras with respect to each other [59]. Nevertheless, the DIC measurement is not perfect and has in this experiment an inexactitude of 0,13mm. This error has many potential sources. To only name a few, there are:

- the calibration of the system
- the camera resolution
- the noise of gray values
- the different illumination conditions for the two cameras
- the image contrast
- the speckle pattern on the specimen surface.

3.3 Numerical model

3.3.1 Material model

3.3.1.1 Coated fabric

For the numerical simulation a specific user material was developed by Tien Dung Dinh [60]. The more complex multi linear elasto-plastic model, is proposed based on the data of uniaxial test with PVC coated fabric and validated afterwards with the results from biaxial tension test. Different Poisson ratios deal with the interaction between the yarns themselves as well as between the yarns and the coating.

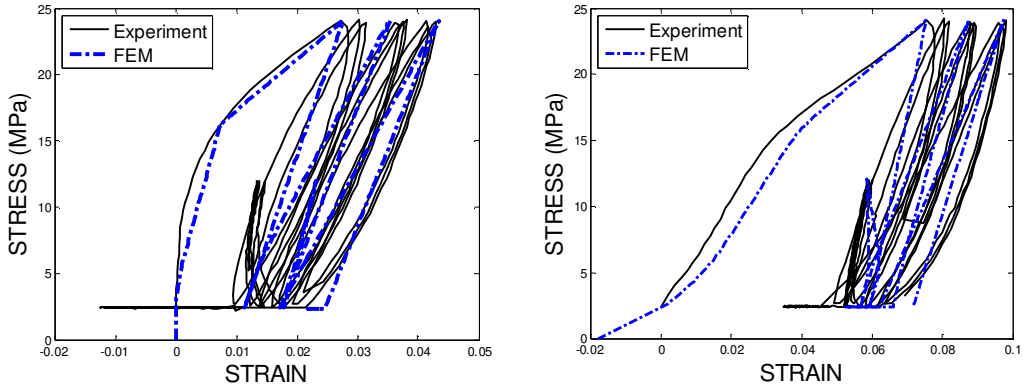

a **b**

Fig. 38 Comparison of the user material (FEM) with the experimental data from biaxial tests in stress-strain diagrams for warp (a) and fill (b) direction

In Fig. 38 it is demonstrated how the developed material model can successfully capture the non-linearities in warp and fill directions as well as the orthotropic effect. Besides, the permanent strains and load ratio dependence are simulated quite precisely in both directions.
This material model is implemented in Abaqus as a user material subroutine (UMAT).

In this study, the warp fibers are aligned with the horizontal or x-direction, while the fill direction are oriented along the Y-axis, which is in agreement with the experiment.

3.3.1.2 Belts

The material for the polyester belt is simplified with an isotropic behavior, since the exact behavior of the element itself is not the purpose of study. The assigned characteristics (Table 3) are derived from the specification sheet of the belts that were used in the experiment, and can be found in the appendix. These belts are fabricated by the company Load-Lok, England.

Property	Value
Young's modulus	2398 MPa
Density	832 kg/m³
Poisson ratio	0.31

Table 3 Material properties of the isotropic belt [61]

3.3.2 Geometry

3.3.2.1 Simplified model

The geometry and the dimensions of the numerical model are based on the original cutting pattern of the experimental setup. As it was explained in 3.2.1, some parts of the model consist out of two layers (membrane-membrane, membrane-belt, belt-belt) or are even triple layered (belt-membrane-membrane). This formation asks for special care in the implementation in Abaqus .

However, in the first simulations it was desired to test the suitability of certain solution strategies. Therefore, in the initial phase of the simulations abstraction was made of the different layers. The model consist of only one part, that is divided into relevant partitions. Each partition has its own material and thickness. In this way, constraints between the different layers are simplified, which reduces the calculation time. This makes the model a suitable medium to test how to apply the load and to check which boundary conditions give satisfying results.

The partitioning of the simplified model can be found in Fig. 39.

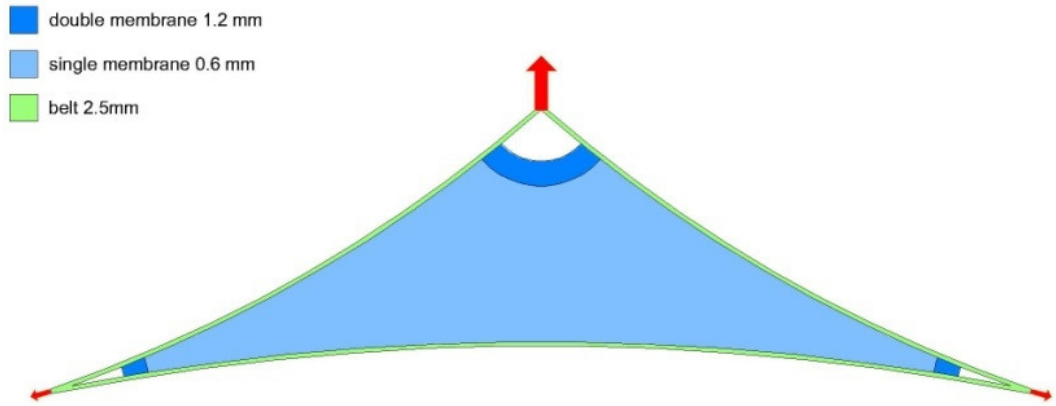

Fig. 39 Assembly of the simplified in-plane triangular shaped model

Although the calculation time of this model was very short (in terms of a few minutes), the problem with this simplification is that Abaqus automatically equalizes the mid-surfaces of each partition, which means practically that the membrane layer is not seen as a continuum surface from one partition to another (Fig. 40). Although the effect on the result is only minor, it introduces an error, especially at the transition between two segments.

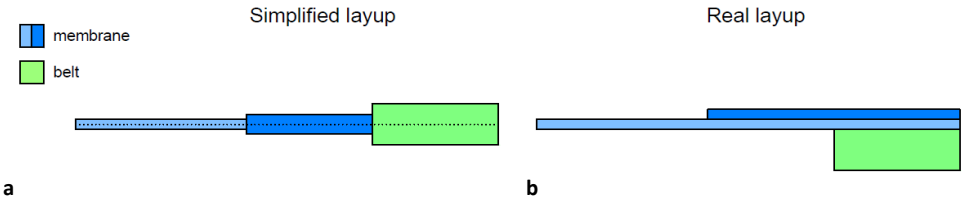

a **b**

Fig. 40 Schematic illustration of the layup in the simplified model (a) in contrast to the layup in reality (b)

To achieve more precise model, the formation of the double and triple layers had to be transformed into a more complex one. This will be explained in the next section.

3.3.2.2 Complete model

To make a more realistic configuration, there are a couple of possibilities.
First, it is tried to keep only *one part*, partitioned into areas with different thickness or material, as it was the case in the simplified model. Although now, a composite layup is picked out, which allows the adjustment of the position of the mid-surfaces and the use of multiple materials in one section. In this way, the continuity of the different plies can be managed [62]. However, the use of this method implies that the element type will be transformed into a shell element, although the section can be idealized to the one of a membrane ("Membrane only"-option). But because shell elements are used, also the so called 'transverse shear stiffness' has to be assigned. This is a penalty factor for the (reduced) integration points over the thickness and should be chosen very small in the case of thin shells. Only, the Abaqus manual is ambiguous about this value [63,64] and in literature very complicated calculations are proposed, e.g. by Hughes et al. [65]. Moreover, assigning the correct layup for each section is a laborious work and not user-friendly to adjust in case of changes. Besides that, the developed material model was designed for in-plane modeling, and thus membrane elements are preferred above shell elements. This choice is supported by advantages of membrane elements over shells regarding the endeavored solution, as was aligned in chapter 2.

Because of the aforementioned limitations, the composite lay-up approach was not found proper for this study. Alternatively, membrane elements can still be used through the creation of *different parts* for each material layer. This makes it also more easy to assign properties. The coupled regions are connected making use of the tie-constraint. This constraint ties every node of one surface to the corresponding node of the second surface, which would make them act as if they were one. To have a better convergence, it is recommended to have an identical geometry of the regions that are to be bound.
For the master-slave assignment, the largest membrane is always preferred as master surface. Only in case of the belt-belt connection, this position is assigned to the longer belt. By default, Abaqus positions every part in the same plane, namely the reference plane through the center of the thickness. Therefore, each instance has to be placed in the correct relative position.
The final layup as implemented in Abaqus can be viewed in Fig. 41.

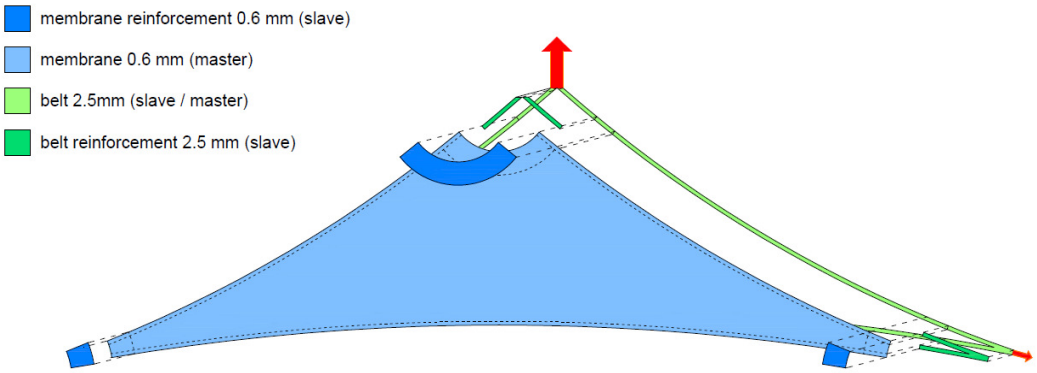

Fig. 41 Assembly of the complete numerical model equivalent to the experimental configuration

3.3.3 Boundary conditions

As it was already mentioned in the description of the experiment, the loads are imposed at the rings that connect the belt ends, constraining the displacement of the last ones, but at the same time allowing them to rotate freely. For simplicity the ring itself is not modeled, but substituted by a reference point. These are RP1, RP2 and RP3, as shown in Fig. 34. The nodes at the edges of the belts are kinematically coupled to the closest RP.[2] This means that the displacement in x, y and z-direction of all nodes will be the same as the one in the RP, as if they were connected to a ring. The rotational degrees of freedom (DOF) are not constrained. At the top, two RPs come together and are pinned in RP3. A schematic illustration can be found in Fig. 42 below.

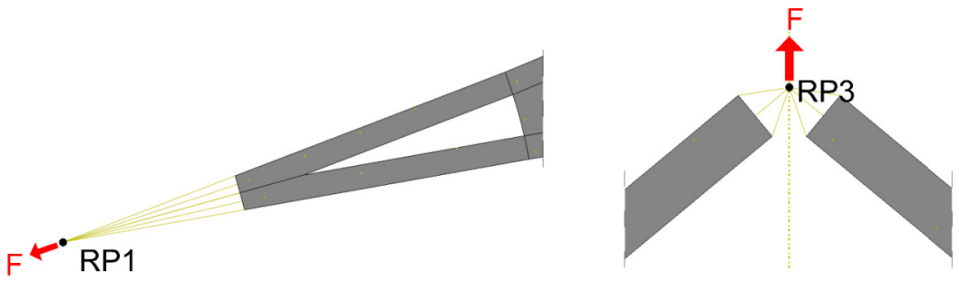

a b

Fig. 42 Load applied on a reference point (a) at a bottom corner (b) at the top). The RP is coupled with the nodes at the end edges of the belts

The actual loading of the membrane can be divided into two phases. The first step, which is the prestress phase, RP3 is held in position while both RP1 and RP2 are moved 15,55 mm away from the membrane in the line of the belts, which causes a reaction force $L_1 = L_2 = 1{,}8$ kN. This is the same value as was measured in the lower load cells after prestressing the membrane during the experiment.
In the second step the actual loading is applied on RP3, as it was recorded in the experiment. The anchor points at the bottom are this time fixed while RP3 is moved upward, until a reaction force L_3 reaches 7 kN. This value is chosen because proper experimental data are only available until this top load.

3.3.4 Efficient discretisation

Besides the element type (as discussed in 2.2.2), an appropriate mesh is of great importance for the accuracy of the result and the convergence speed. Meshing is the way the model is discretized in smaller elements to allow calculation. In general it is acknowledged that a proper element shape and efficient size are the key points for a reliable outcome.
Two kinds of element shape are relevant for in-plane membrane modeling: either triangular or quadrilateral elements. The advantage of the first one is the easy adaption to complex geometries, as mentioned in '*Wrinkling and folding analysis of elastic membranes using an enhanced rotation-free thin shell triangular element*' [66]. However, this type of element is usually overly stiff and has a constant strain over each element, which requires a miniscule mesh to obtain a sufficient precision [67]. The positive aspect of quadrilateral elements for in-plane membrane modeling is the fact that in most cases they have a better convergence rate, i.e. less computational time to reach the same result. Therefore, it is important to keep the mesh quality high. This means that the aspect ratio (i.e. proportion of width and length) does not exceed 0,1 and that the angle of each element corner is larger than 10°, optimum approximately 90° [68].
Because of all above mentioned reasons, mainly quadrilateral elements are used for the meshing of the studied model.

[2] Because the belt ends are double layered, the kinematic coupling was only attached to the border of the master surface, in this case this is always the back layer with the longest belt parts.

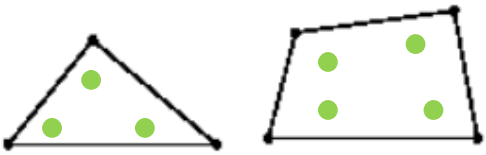

Fig. 43 Two-dimensional element shapes available in Abaqus [69], with their integration points in green

Furthermore, no reduced integration method was used, because this can have a detrimental effect on the result. In reduced integration, the different integration points of each element are taken back to only one (versus 3 or 4 whether full integration triangular or quadrilateral elements are chosen), which generally makes the result less precise (In some special cases, like shear locking, it is vice versa).

As said, the element size and shape determine the accuracy of the output and has besides that a big influence on the calculation time.
To have an idea which size is sufficient to get a reliable output in a reasonable time span, a mesh convergence test must be carried out. For this model 5 different mesh sizes were tested, starting from a very coarse one and every time refining. One point was picked out to examine the stresses. The point is situated in the area at the top of the membrane.
Furthermore, to be sure that this point is not an exception (and could lead to false conclusions), several nodes along a 'path' running from the upper left corner to a point more central in the membrane (Fig. 44) were examined additionally.

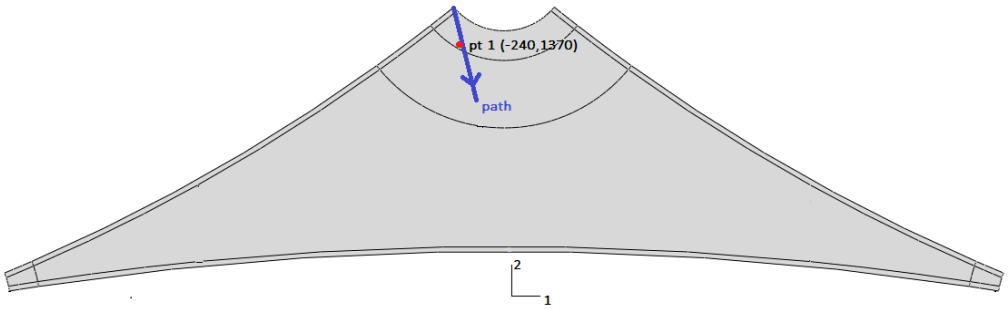

Fig. 44 Indication of examined point and followed path

The triangular membrane is loaded at the top by use of a displacement of 117 mm in RP3, causing there a reaction force of 6 kN. RPs 1 and 2 are fixed after a displacement controlled pretension of 1mm outwards in 1-direction (as shown in Fig. 41). This load scenario is in agreement with the experiment.

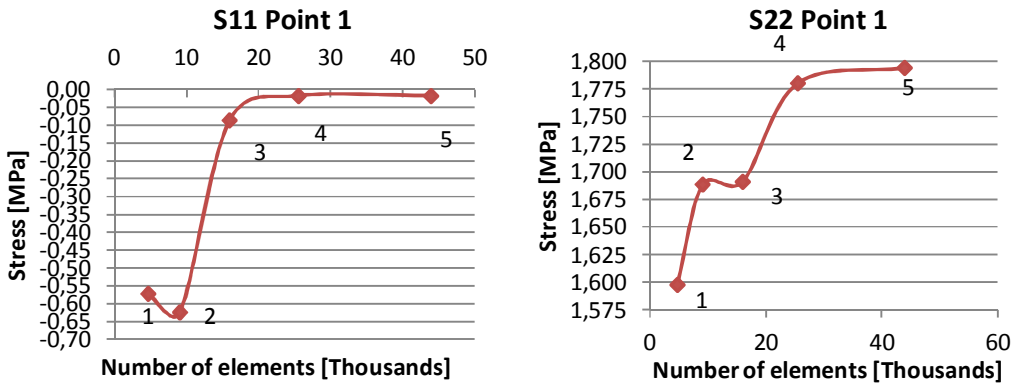

Fig. 45 Values of the stresses S11 and S22 at point 1 in the membrane for 5 different mesh sizes

From the graph of horizontal stress (S11) in point 1, it looks as if the convergence to the value of -0,017MPa starts between mesh 3 and 4, which corresponds with a slightly compressed state. This is reasonable since the applied load causes large vertical tension in that point.
Also for the vertical stress in the same point (S22), the solution starts to stabilize at mesh 4, to a value of 1,8 MPa.
In this problem, the result with a finer mesh of 45000 elements may be a little closer to the fully convergence state, but the minor improvement does not compensate the much higher calculation time, as can be found in Fig. 46. The calculation time of mesh 5 is more than 12 times the calculation time with only half the amount of elements.
Up till now, it can be concluded that a satisfying convergence rate is obtained with mesh 4 (26000 elements).

	Number of element	CPU time [s]
1	5000	60
2	10000	300
3	17000	1800
4	26000	6720
5	45000	86400

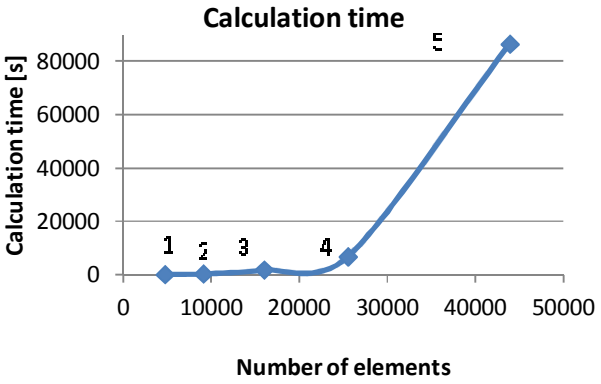

Fig. 46 Computational time of the 5 different meshes in function of their number of elements

To be sure that this is not an exceptional point, the stresses in several points along the path were also plotted for the different mesh models (Fig. 47 and Fig. 48). The position of the path was chosen in the top region, which is the most critical area of the studied case, and runs from one loading top to a point at a more central location (illustration in Fig. 44).

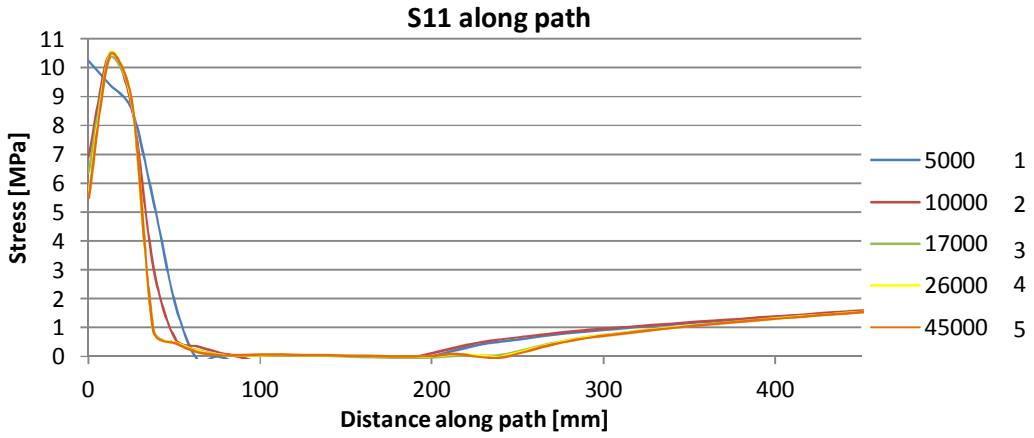

Fig. 47 Stress S11 along a path running from the upper left membrane corner to the central area for 5 different mesh sizes

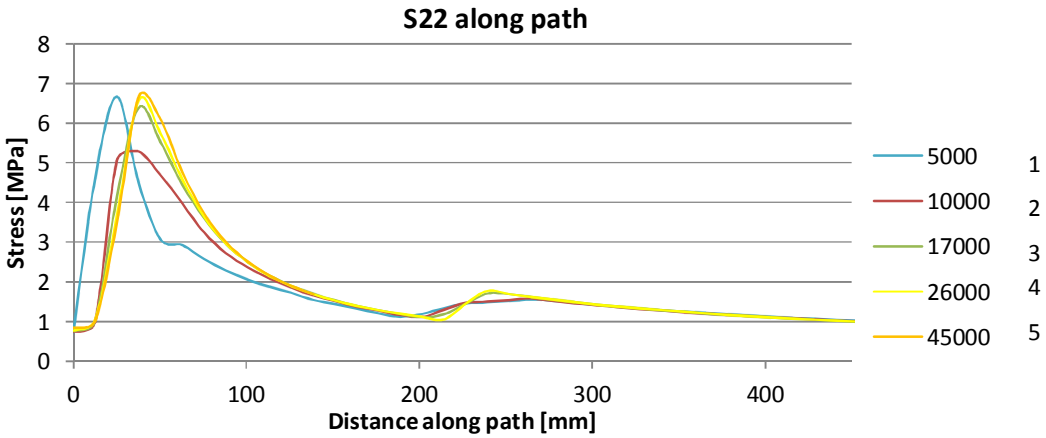

Fig. 48 S22 along a path running from the upper left membrane corner to the central area for 5 different mesh sizes

Fig. 47 and Fig. 48 indicate that the first two meshes with about five and ten thousand elements are too rough to give a good representation of the state of the membrane. Mesh 3 comes close to the end solution, but 26000 elements generate an accurateness that is almost equal to the precision with nearly double the amount of elements. This confirms the option for mesh 4 with 26000 elements, which has the optimum size concerning calculation time and precision.

Fig. 49, the chosen mesh is presented. Because the central part is the area of interest, therefore the mesh is chosen finer in this area. More to the side, the mesh becomes coarser. In the apexes a structured mesh is used with only quadrilateral elements approximated as squares, while in the center a free meshing is applied, with as well quadrilateral as triangular elements.

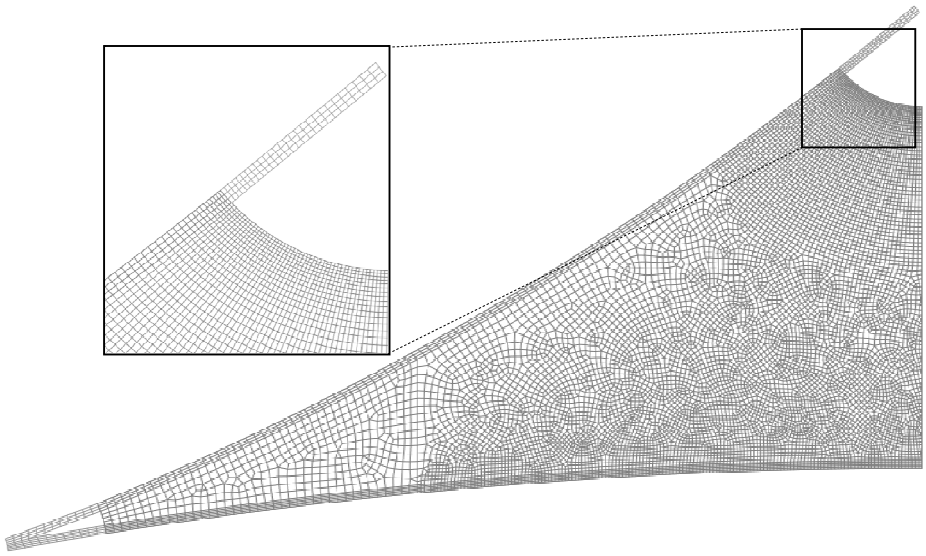

Fig. 49 Mesh used in the FEM model

3.3.5 Damping factor

As said before, the chosen solution method for the numerical calculation introduces an artificial damping to ease convergence. The value of the damping factor c was found by a trial and error method, checking for every value the balance between dissipated energy and total strain energy. As was explained in chapter 2, the ratio of these two should stay below 5%.
Eventually, damping factors of 2e-6 and 1e-7 for respectively the prestress step and actual load step have proved to be appropriate. The values enact an proportion of dissipation/strain energy of 0,5%, which is far below the limit to have a reliable result. Consequently the damping factors in this case will not affect the solution due to remaining residual forces.

3.4 Comparison of the results

The most important goal of the simulation of the tensioned architectural membrane, is the prediction of the stresses and strains of the coated fabric under an applied load. Therefore, the output from Abaqus was verified and validated through comparison with the DIC results.
The comparison will be carried out on two levels:

(1) *Qualitatively* :to get a first impression of the matching areas and the performance of the numerical model, the contour plots of strains, produced by both Abaqus and the DIC software, are compared. Visually it can be seen if the behavior in general resembles to the experimentally recorded actions.[3] Furthermore, a closer look is given to the relation with the stress patterns. Because they cannot be derived experimentally, the numerical simulations give an important insight in the magnitude and distribution of the stress in all directions, and enables to investigate their relationship with the strain.

(2) *Quantitatively*: to get a more precise idea of the quality of the numerical result, the values of strain in different points along 'paths' are tracked and compared with experimental data. Three lines are chosen in such a way that an overall image of the strains in the membrane can be captured. The origin is located in the center of base A' of the circumscribed triangle (for a review of the naming conventions, the reader is referred to Fig. 34, p.29). The x-direction (1-direction) is horizontally aligned and the y- axis (2-direction) is positioned vertically. In all further descriptions, this coordinate system is respected.[4]

- Path 1 runs vertical from a point in the top near the corner of edges B and C, until 550 mm above the base of the circumscribed triangle A', or 250 mm above the edge A of the membrane.
- Path 2 starts at the center of the top area and continues diagonally to a point in the left corner.
- Path 3 is horizontally positioned, starting and ending 1000 mm from the central vertical axis and is situated at 900 mm in the positive y-direction.

An illustration of the paths with inclusion of the coordinates of their start and end point can be found below in Fig. 50.

The abovementioned methodology is used to compare first the horizontal strain, ε_{11} (3.4.1), followed by the vertical strain, ε_{22} (3.4.2), and finally also the strain in shear direction, ε_{12} (3.4.3).
In order to gain also insight in the progress of the strain between the initial and final state of the membrane during both the experiment and the simulation, three load stages are examined.
Therefore, 3 well-chosen values of the reaction force L_3 in RP3 at the top of the membrane are picked out, according to the available experimental data : an initial position at L_3 = 2 kN, a more intermediate position at L_3 = 4 kN and the final state for L_3 = 7 kN are broadly examined.

[3] For the contour plots, the results from Abaqus are given in logarithmic strains ($\varepsilon_{\log}$), while the experimental data are expressed in Lagrangian strain ($\varepsilon_{\mathrm{lag}}$). Since we are dealing with very small strain values, the difference is negligible as proved in following example.
The formula to transform Lagrangian strain into logarithmic is[12]: $\varepsilon_{log} = \ln\left(\sqrt{2 * \varepsilon_{lag} + 1}\right)$
If we have for example an experimental strain of ε_{lag} = 0,02 , this value is equivalent to ε_{log} =0,01996. Since we are dealing with very small strain values, the difference is negligible. For reasons of precision, the values for the graphs are all transferred to logarithmic values, but this was not possible for the contour plots.

[4] It was not possible to filter out the points with *exact* coordinates as in the experiment. The reason for this is that the geometry of the membrane in the experiment in pretensioned state (which forms the reference geometry for the DIC measurements) is slightly different from the theoretical geometry that is implemented in Abaqus. Of course, the regarded points are chosen as close as possible, but a small discrepancy is insurmountable.

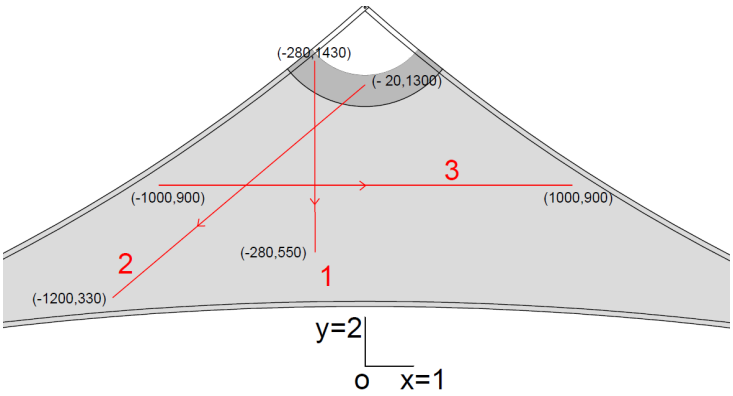

Fig. 50 Schematic overview of paths along whom the strains are compared (coordinates are in [mm])

In the graphs that will follow, the geometry of the model is every time displayed in the background. The x-axis of each graph is aligned with the investigated path. In this way it is easier to translate the curves to their physical meaning.

3.4.1 Horizontal strain ε11

3.4.1.1 Contour plot simulation

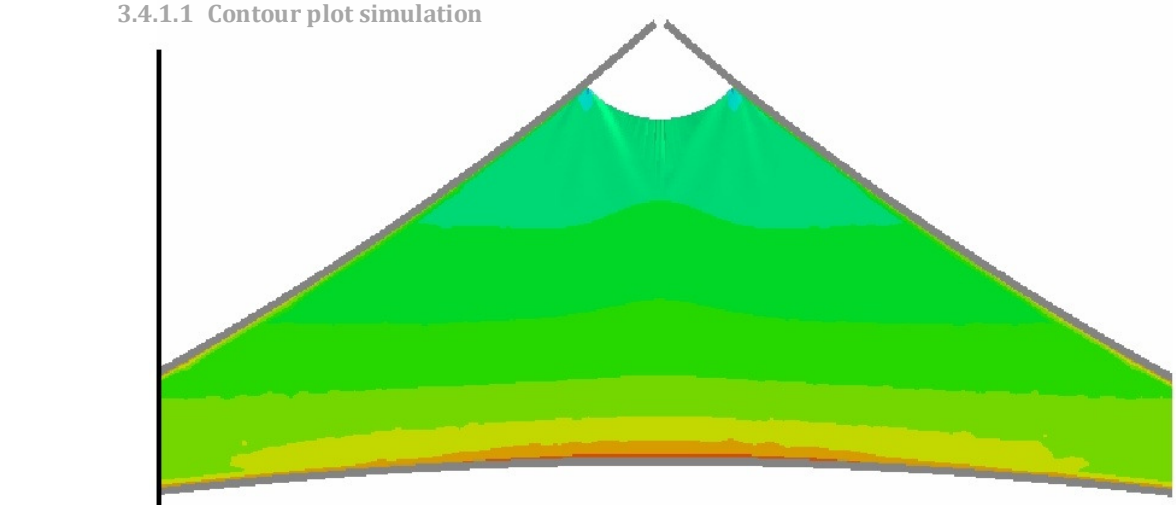

Fig. 51 Contour plot simulation for horizontal strain ε_{11} [-] at L_3 =2 kN

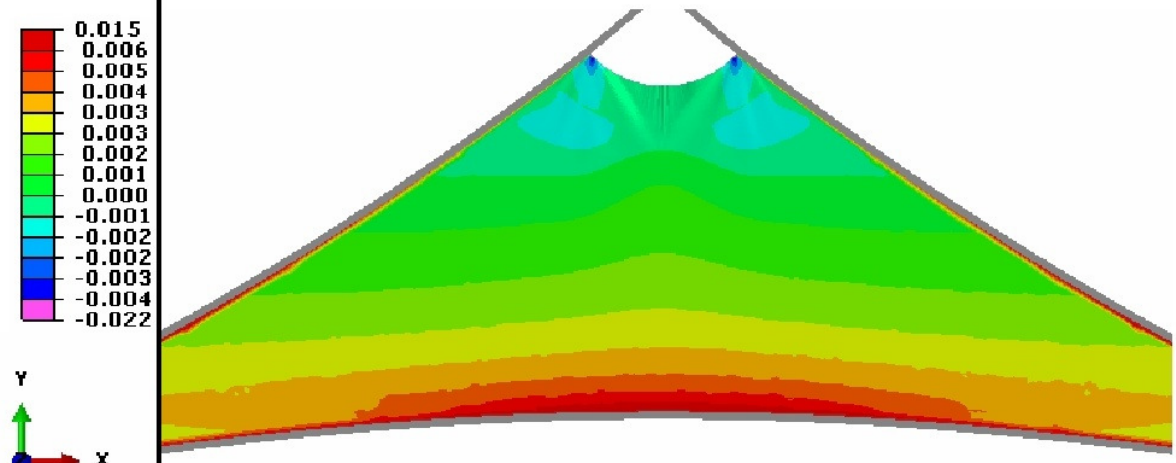

Fig. 52 Contour plot simulation for horizontal strain ε_{11} [-] at L_3 =4 kN

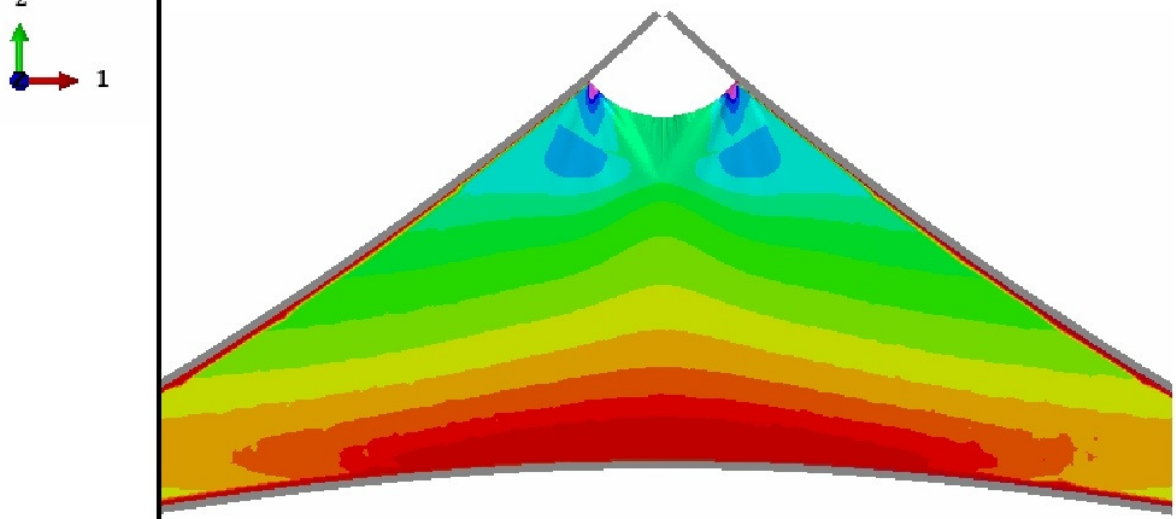

Fig. 53 Contour plot simulation for horizontal strain ε_{11} [-] at L_3 =7 kN

3.4.1.2 Contour plots experiment

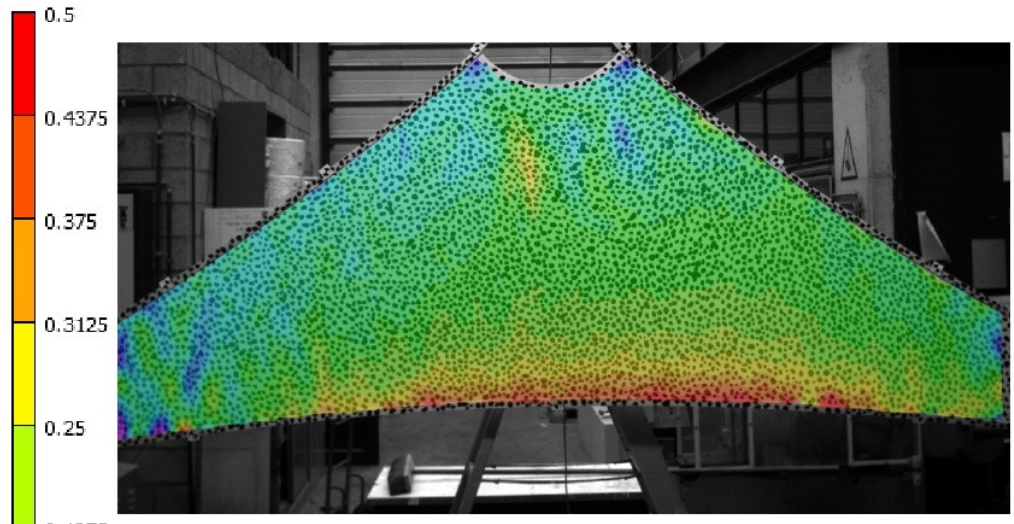

Fig. 54 Contour plot experiment for horizontal strain ε_{11} [-] at L_3 =2 kN

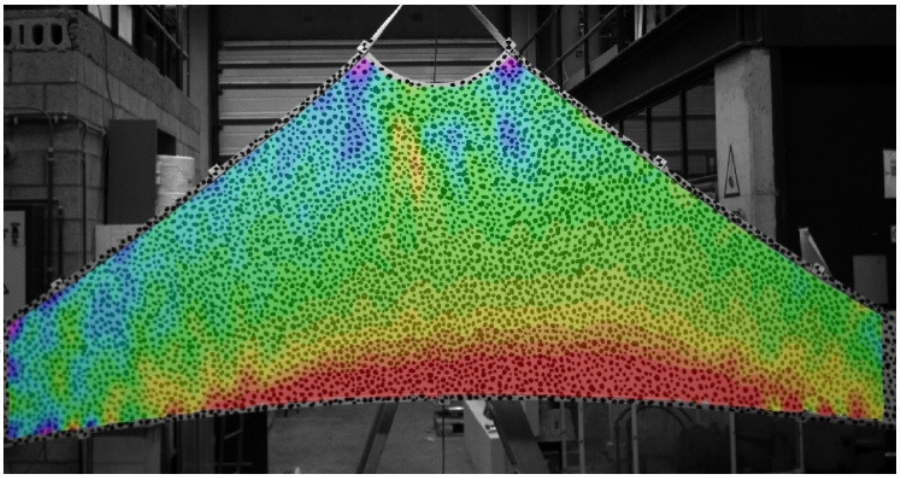

Fig. 55 Contour plot experiment for horizontal strain ε_{11} [-] at L_3 =4 kN

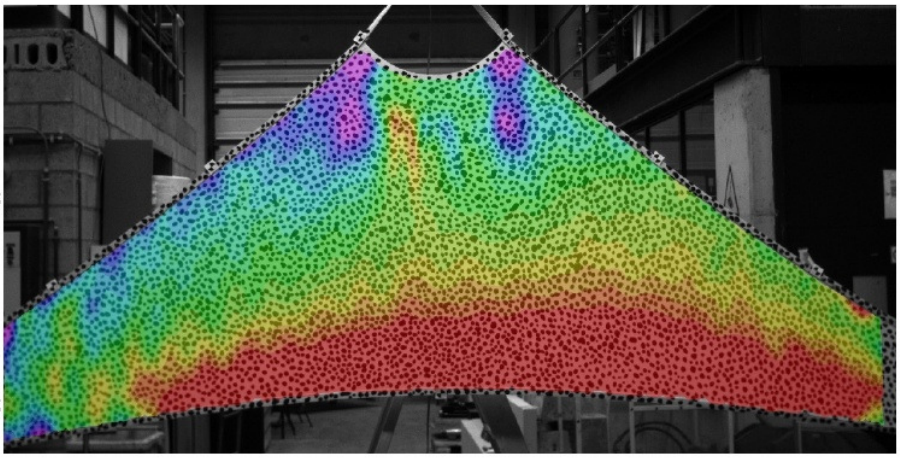

Fig. 56 Contour plot experiment for horizontal strain ε_{11} [-] at L_3 =7 kN

3.4.1.3 Qualitative comparison ε_{11}

As can be seen in the contour plots in 3.4.1.1 and 3.4.1.2, the region at the bottom edge A is clearly simulated in resemblance to the experiment and this for all stages of loading. This part of the membrane is in tension, due to tensioning of the anchored bottom points RP1 and RP2. A slight asymmetry is noticeable in the DIC pictures of the experiment, probably due to a imperfections during the experiment (Fig. 54-Fig. 56). In reality it was not possible to apply an exactly equal preloading on the anchor points, nor to impose an exactly centric load by pulling up the crane. In contrast to this, the simulations do not suffer from these imperfections in reality. As long as the geometry of the model is perfectly symmetric about the y-axis, so is the output of the strain and stress. From the stress pattern in Fig. 57, we can see that the maximum horizontal stress σ_{11} at the bottom is almost 15MPa. This is the yield stress for the fibers in warp direction. It means that permanent strains will remain in the coated fabric when it is again unloaded. This was also observed during the experiment (Fig. 37).
At the top, compression in x-direction is visible. Two reasons can be found for this. Firstly, the belts at the top of the membrane move towards each other under the upward motion of the hook. This results in a loss of pretension in the top region and even pushes the membrane slightly together. Therefore, negative horizontal stresses can be observed in the Abaqus model (purple region in Fig. 57). A minimal value of -0,4 MPa is laid down.

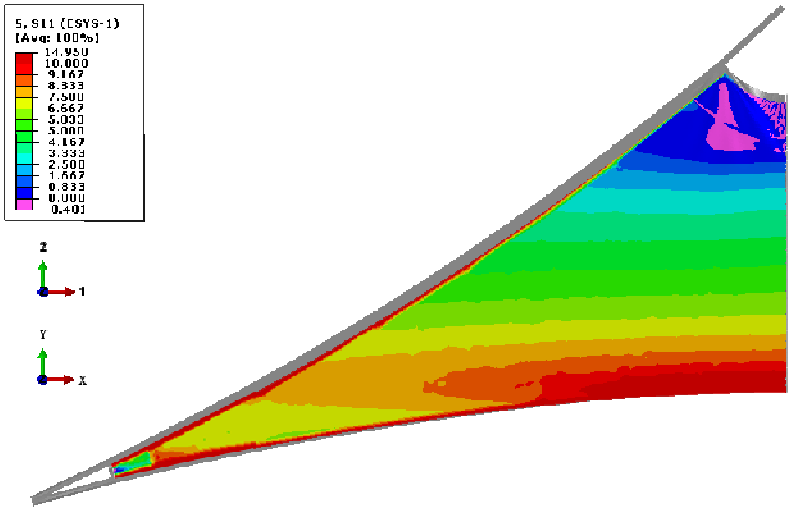

Fig. 57 Horizontal stress σ_{11} for a top load of L_3 = 7 kN [MPa]

A second cause could be found in the crimp interchange (1.3.3.1). The imposed load is oriented along the fill yarns (y-direction) and straightens them preparatory to stretching. In turn, this action makes the warp yarns curve and thus compresses them.
The phenomenon of the compressed top edge (edge B) is more expressed in the experiment whereas the simulation shows slightly lower values of negative strain. This can also be derived from the graphs of path 1 and 2.

At this point, it can be stated that qualitatively the Abaqus result is a good representation with respect to the evolution in horizontal strain in the membrane under top load.

3.4.1.4 Path values ε_{11}

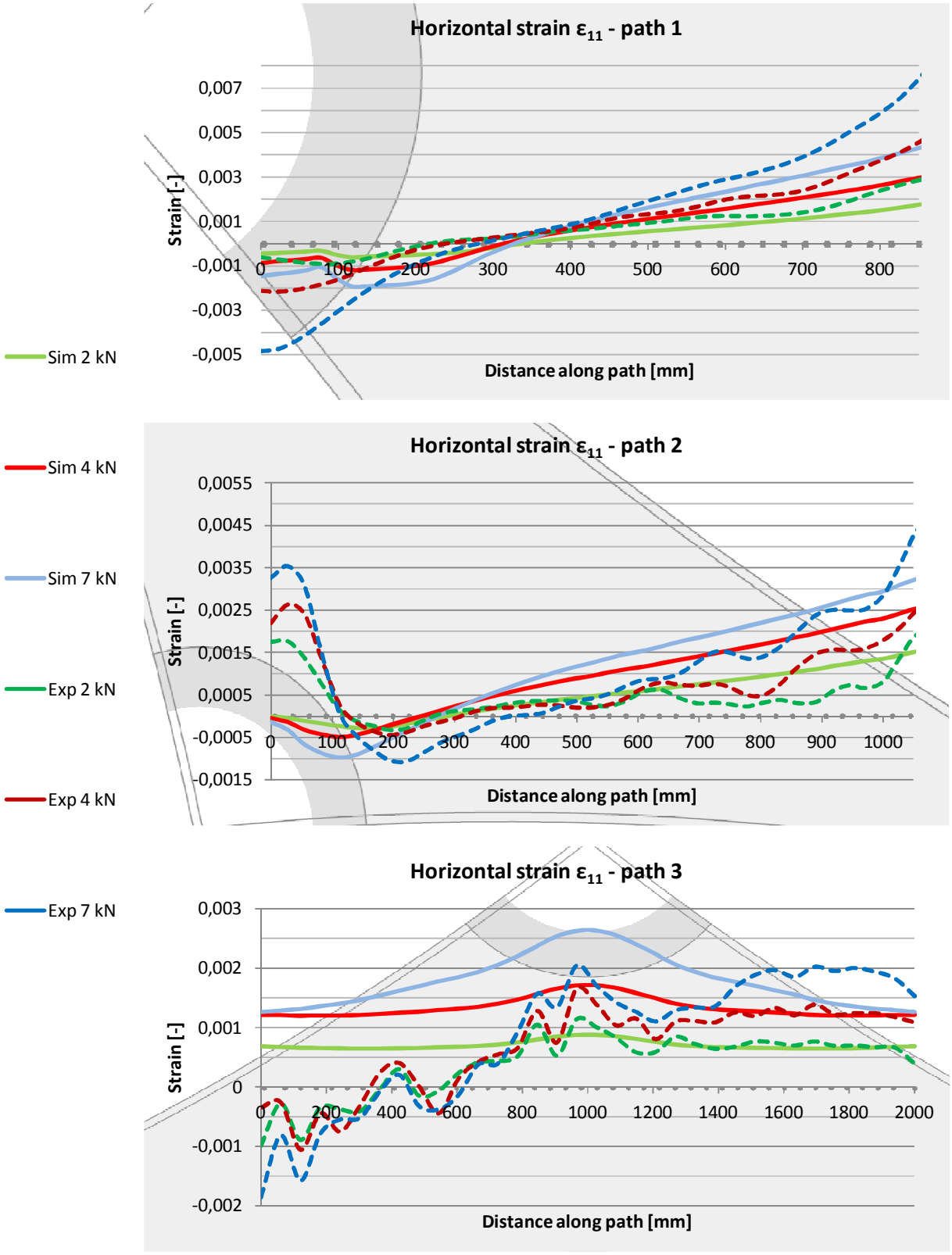

Fig. 58, Fig. 59, Fig. 60 Horizontal strain along resp. path 1,2,3 - experiment vs. simulation for L_3 = 2, 4 and 7 kN

3.4.1.5 Quantitative comparison ε_{11}

First of all, the propagation of the curves along the distance is in every path of the same nature. This means that the overall behavior of the membrane is simulated well (Fig. 58-60). It can be seen that also quantitatively the simulation is very similar to the experiment.
For path 1, the curves are alike, except for the start and end values at L_3 = 7 kN, the miscorrelation is slightly larger (blue lines). In these regions, the simulation produces only the half of the value measured in experiment (-0,0021 vs. -0,0048 compressive strain in the beginning and 0,0045 vs. 0,0078 tensile strain at the end of the path).
Moreover, the imparity in the top area manifests itself also in the second path.

The average of the horizontal strain is, depending on the load stage, only 0,0001 and 0,0002 (see Table 4) higher than the experimental value, whilst the value in the top region shows differences of more than 0,002. This indicates that there could be a mistake in the comparison. As mentioned before, it must be taken into account that the investigated points are not exactly the same as in the experiment. Since the area at the top shows high local diversity in stress and strain, points in the neighborhood of the start points on path 1 and 2 vary considerably.
Next to that, the area at the top shows light wrinkles in the simulation. Although this is pure geometrical deformation of the elements, it gives an indication where in reality the membrane will wrinkles too. On the other hand, during the experiment no wrinkles in that area were recorded in the first load cycle. This discrepancy is a second plausible declaration.
In the areas further to the center, the sensitivity for exact location is less distinct while the membrane behaves more stable there.
In path 3 the asymmetry that was observed from the contour plots is clearly expressed. On the other hand, the output from the simulation is perfectly symmetric.
In Table 4 an overview is given of minimum and maximum values for each considered load case and each path. One can see that the values of the experiment and the simulation are very close to each other. In path 3 the most obvious aberrance is noticed, due to the asymmetry mentioned before. To avoid this problem, the averages of only half the path are also calculated (i.e. only the positive x-direction, so the matching area). The values in that case are significantly better.

		ε_{11} - path 1			ε_{11} - path 2			ε_{11} - path 3		
		2 kN	4 kN	7 kN	2 kN	4 kN	7 kN	2 kN	4 kN	7 kN
Min	sim.	-0,0006	-0,0012	-0,0019	-0,0003	-0,0005	-0,0010	0,0006	0,0012	0,0013
	exp.	-0,0009	-0,0022	-0,0049	-0,0003	-0,0004	-0,0011	-0,0010	-0,0011	-0,0019
Max	sim.	0,0019	0,0032	0,0045	0,0016	0,0027	0,0034	0,0009	0,0017	0,0026
	exp.	0,0032	0,0057	0,0078	0,0020	0,0027	0,0047	0,0011	0,0017	0,0020
Avg	sim.	0,0004	0,0007	0,0010	0,0005	0,0010	0,0012	0,0007	0,0013	0,0018
	exp.	0,0008	0,0011	0,0015	0,0005	0,0008	0,0011	0,0004	0,0007	0,0009
Avg HALF path 3	sim.							0,0007	0,0013	0,0018
	exp.							0,0007	0,0012	0,0017

Table 4 Overview of minimum, maximum and average value of horizontal strain along paths 1,2 and 3 at different load stages for L_3

In general it can be said that for each increment of load, also the mismatch with the experimental data grows. This finding is visualized in the box plots in Fig. 61.
The reason for this can be found in the material model. The properties were assigned based on biaxial tests with equal loading for warp and fill direction (load ratio 1:1). In the experiment of the with triangular shaped membrane, this load ratio is not present. In the beginning the membrane is equally tensioned, but the upward movement of the hook at the L_3 increases till 7 kN, while L_1 and L_2 in the bottom corners are about 9 kN. Therefore, with each load increment of the top, the load ratio in the

membrane dissociates itself always further from the ratio 1:1. The lack of biaxial tensile tests with other different load ratios did not allow to implement the behavior under these circumstances in the material model. This is something that can be improved in the future.

In general it can be stated that the error has an average of about 50%. Although this value is not small, it must be taken into account that the horizontal strains are on a scale of 1/1000. Values of 1,5 times the experimentally measured ones, are not so different when we look from an architectural point of view. For example, the maximum strain at 7 kN for path 3 is 0,0026 according to the simulations. This means for a structure of 10 meter an elongation of 2,6 cm. If we base the calculations on the experimental data, the maximum strain is 0,002 and results in an elongation of 2 cm. In architectural terms, this is only a minor difference, with an negligible influence on the structure.
Moreover, in most cases the simulated strain is larger. This slight overestimation of the strains in the calculations is safe to rely on when it comes to building, because it will result in a slightly stiffer structure than necessary.
The median deviation is the largest along path 2. This path crosses the membrane diagonally and traverses in this way areas of more varied loading. This could result in more deviation than the other paths.
Furthermore can be noted that all paths show excessive outliners (This is not fully visible in the chart, but values more than 300% were established.) This can be attributed to all inequalities between the experimental setup and the 'perfect' numerical model as there are e.g. the small asymmetric load, the minor difference in geometry, the error of the DIC and unstable output from the experiment, and the not fully correct material model in the simulations. The values must be approached in this perspective.

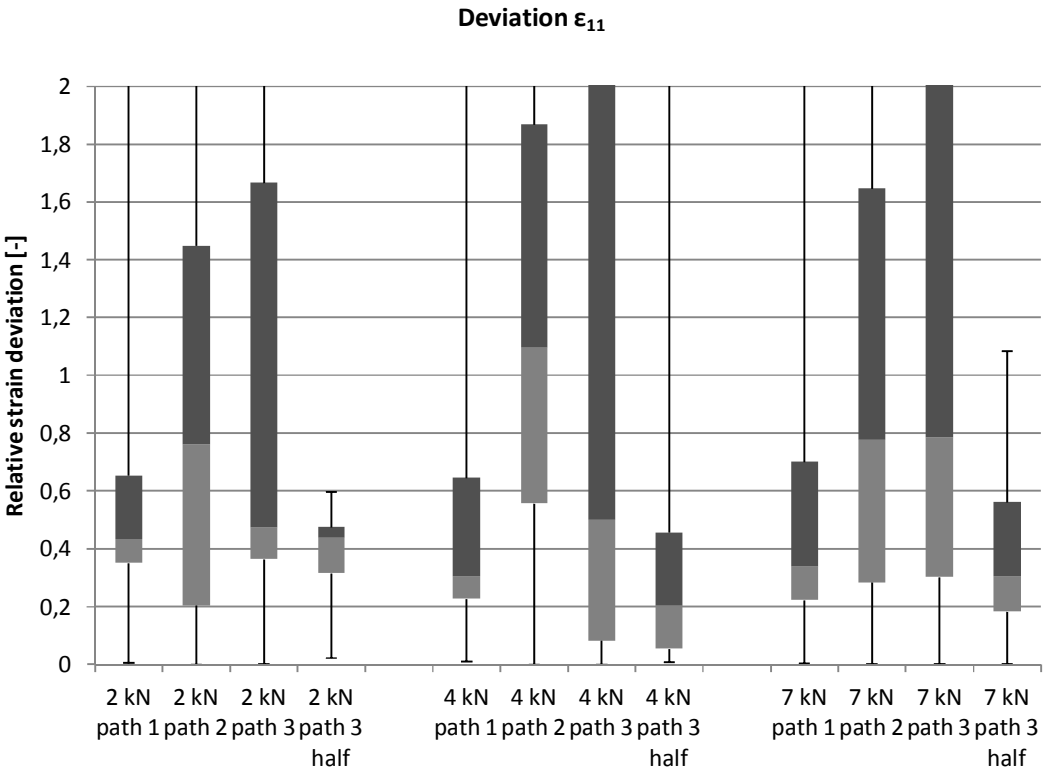

Fig. 61 Relative deviation between experimental and simulated horizontal strain for different load stages (L_3 = 2 kN, 4 kN and 7 kN) for path 1, 2 and 3

It can be stated that the simulation is in good correlation with the experiment concerning the horizontal strain. For the investigated paths, the tendency of the strains is alike, but generally can be said that the values of the simulation are 50% larger than the experimentally recorded strain ε_{11}.

3.4.2 Vertical strain ε_{22}

3.4.2.1 Contour plot simulation

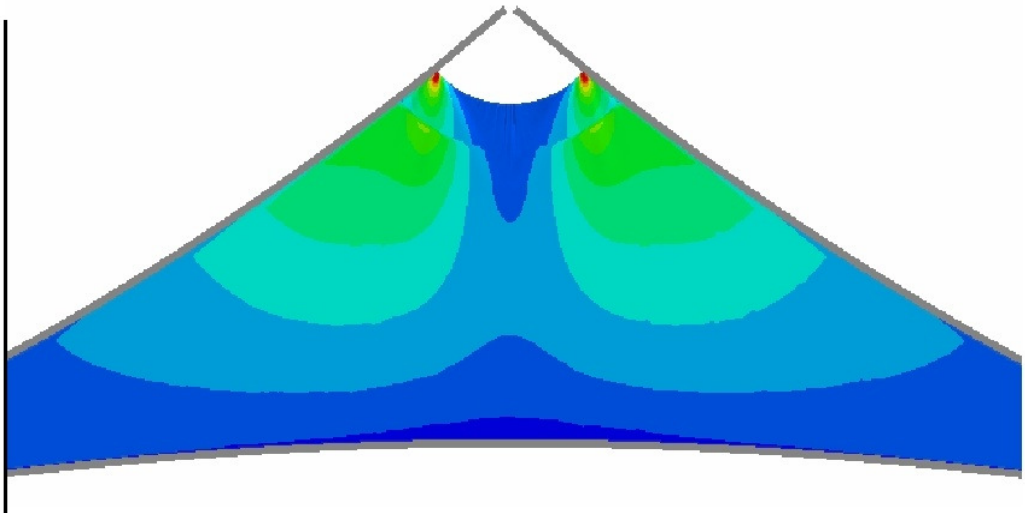

Fig. 62 Contour plot simulation for vertical strain ε_{22} [-] at L_3 =2 kN

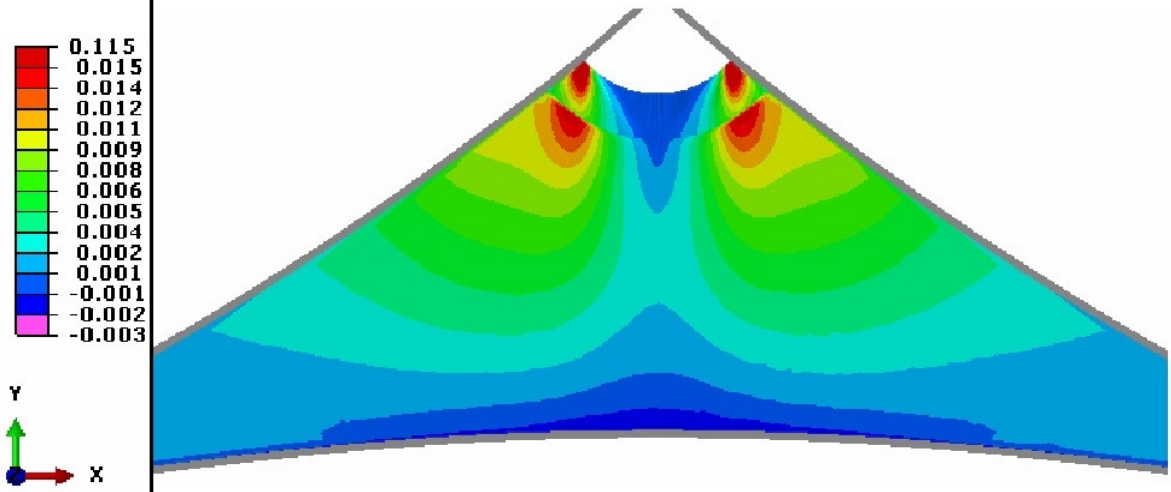

Fig. 63 Contour plot simulation for vertical strain ε_{22} [-] at L_3 =4 kN

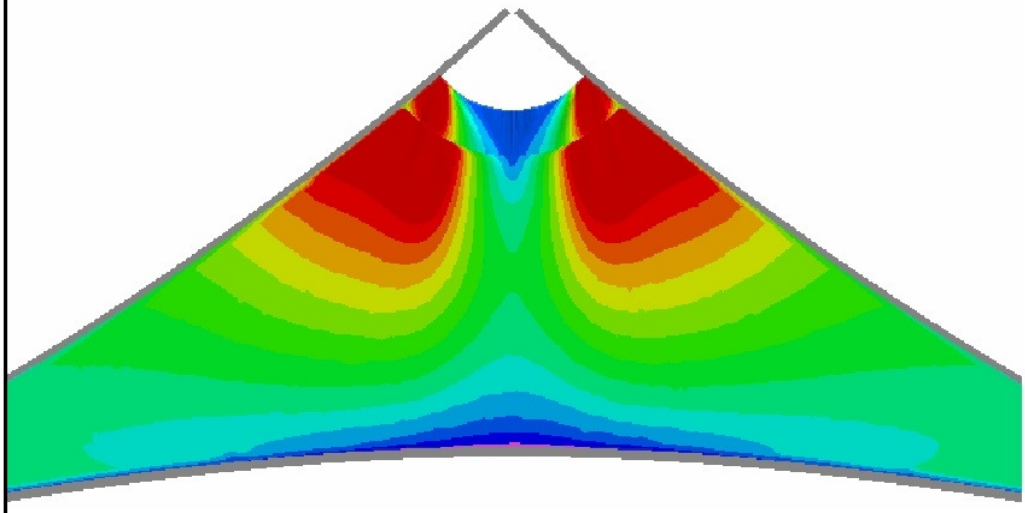

Fig. 64 Contour plot simulation for vertical strain ε_{22} [-] at L_3 =7 kN

3.4.2.2 Contour plots experiment

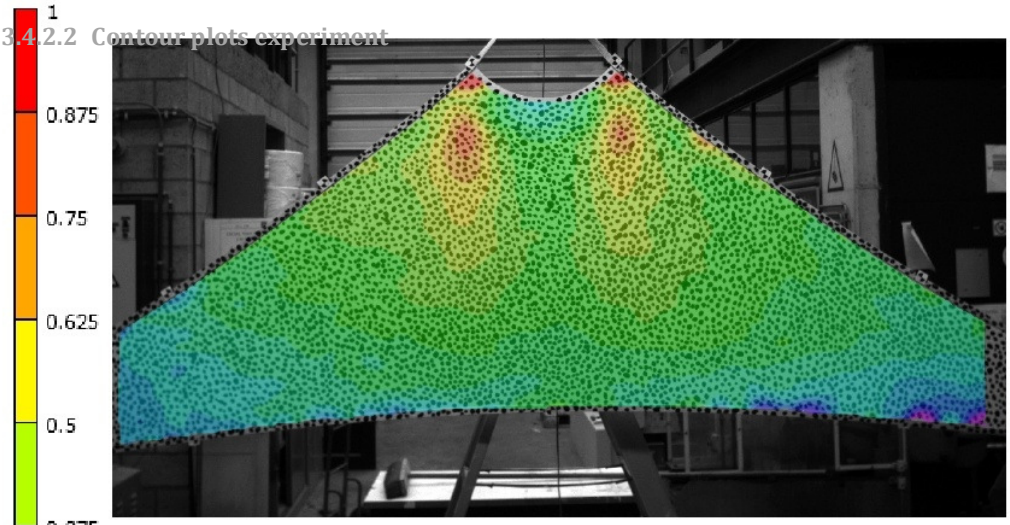

Fig. 65 Contour plot experiment for vertical strain ε_{22} [%] at L_3 =7 kN

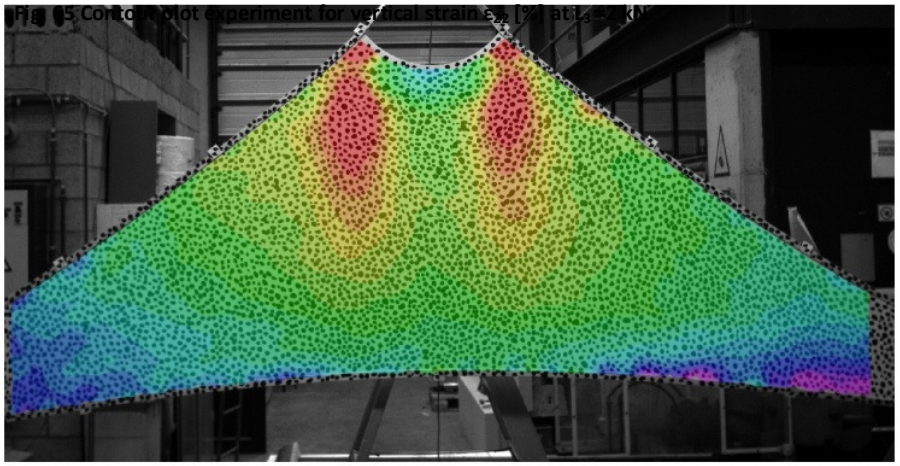

Fig. 66 Contour plot experiment for vertical strain ε_{22} [%] at L_3 =4 kN

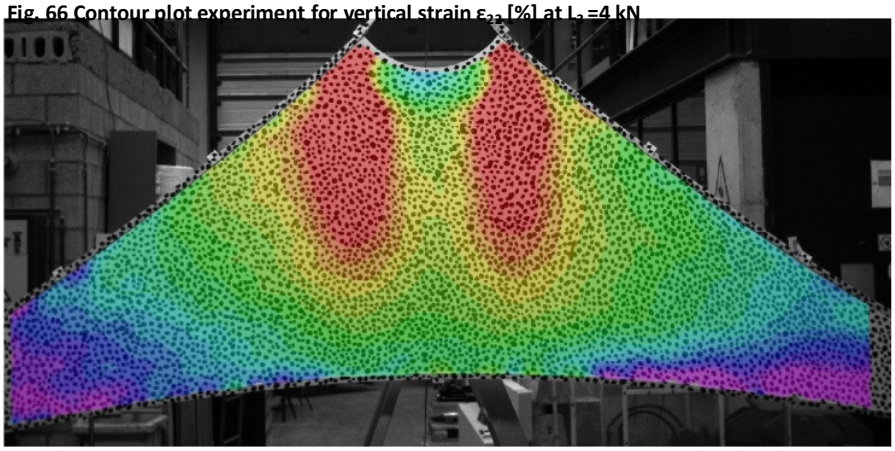

Fig. 67 Contour plot experiment for vertical strain ε_{22} [%] at L_3 =7 kN

3.4.2.3 Qualitative comparison ε_{22}

Where negative strain was measured for the horizontal strain, (positive) tensile strain can be noticed in y-direction and vice versa. The applied load propagates through the connecting belts and is transferred to the membrane in particular in P1 and P2. Therefore, the yarns in that area are locally extremely charged. Vertical tension stresses (σ_{22}) between 10 and 25 MPa in the corner area are measured (Fig. 68) for a load L_3 =7 kN. This means that the plastic regime of the fill yarns is exceeded and permanent strain will remain in the membrane. This phenomenon could also be seen in the experiment (Fig. 37). Furthermore, the influence of the reinforcement layer at the top is clearly demonstrated. A large part of the tension stresses is intercepted before proceeding to the single layered membrane, which reduces them tremendously before they propagate to the single membrane layer (from 22 MPa to ca. 1 MPa). Therefore, the largest vertical stress traced in the single membrane layer is only 4,15 MPa. This indicates that no permanent vertical strain in that partition will occur at a top load $L_3 \leq 7$ kN.

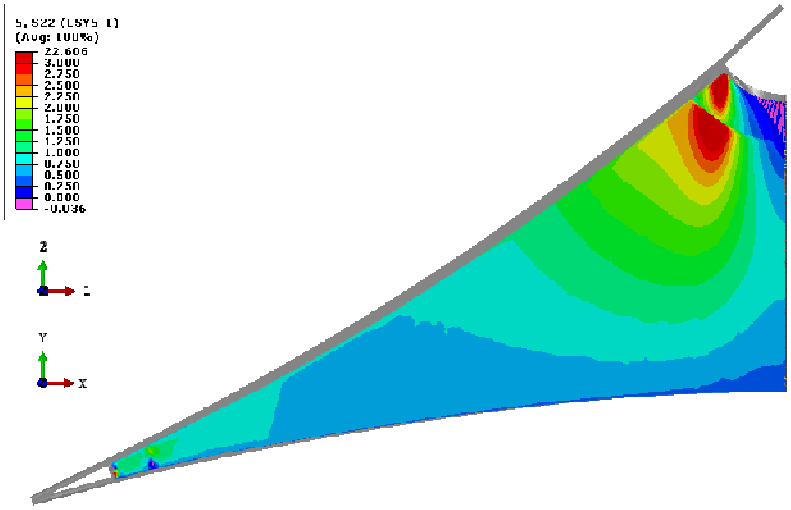

Fig. 68 Vertical stress σ_{22} for a top load of L_3 = 7 kN [MPa]

The effect of the reinforcement layer is not only noticeable in the contour plot of σ_{22}, but is also visualized in the contour plots of the strain, both experimentally an from the simulation (Fig. 62 - Fig. 67). For the lower load rates (L_3 = 2 kN and L_3 = 4 kN) the strain is restrained to the local area around the P1 and P2, but becomes more continuous for the larger loading (L_3 = 7 kN). This is because the stresses in that case is too large to be sufficiently reduced by the reinforcement layer.
The area at the center of the membrane is rather neutral and is simulated in correspondence for all loading rates. At the top edge, the membrane is lightly in compression, which is again a result of the inward rotation of the belts under the increasing load. Also this phenomenon is likewise reproduced by Abaqus.

The only major difference is the region at the bottom corners of the membrane. The experiment showed high negative strains (till 0,01), but there is not such appearance in the simulations.
An explanation for the negative strains in this area could be the compression of the membrane corners due to the pretension and the loading. During the experiment it could be seen that the apexes are heavily deformed (Fig. 69), which points out a loss of tensile stress. In the simulation this phenomenon is only minor displayed. The reason for this could be found in the element size and shape, because the deformation in a model with membrane elements is purely geometric and depends only on these two parameters. The elements themselves have no bending stiffness. Another cause could be the small difference in boundary conditions between the numerical model and the experiment.
However, it is difficult to do judge what eventually causes the noticed discrepancy. The corner areas were not recorded with by the DIC cameras, hence there is nothing to verify with. This is something that should be investigated further, but the limited time span of this thesis did not allow to do the experiment again to investigate also this area.

a

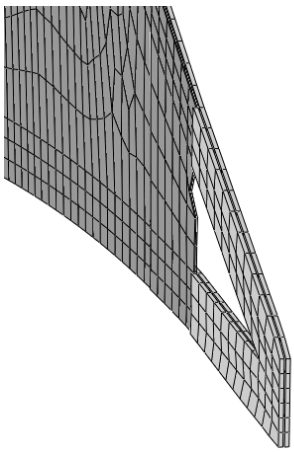

b

Fig. 69 Deformation at the bottom right corner (RP2) at a top load of L_3 = 7 kN. Experimental photo (a) and simulation output (b)

3.4.2.4 Path Values ε_{22}

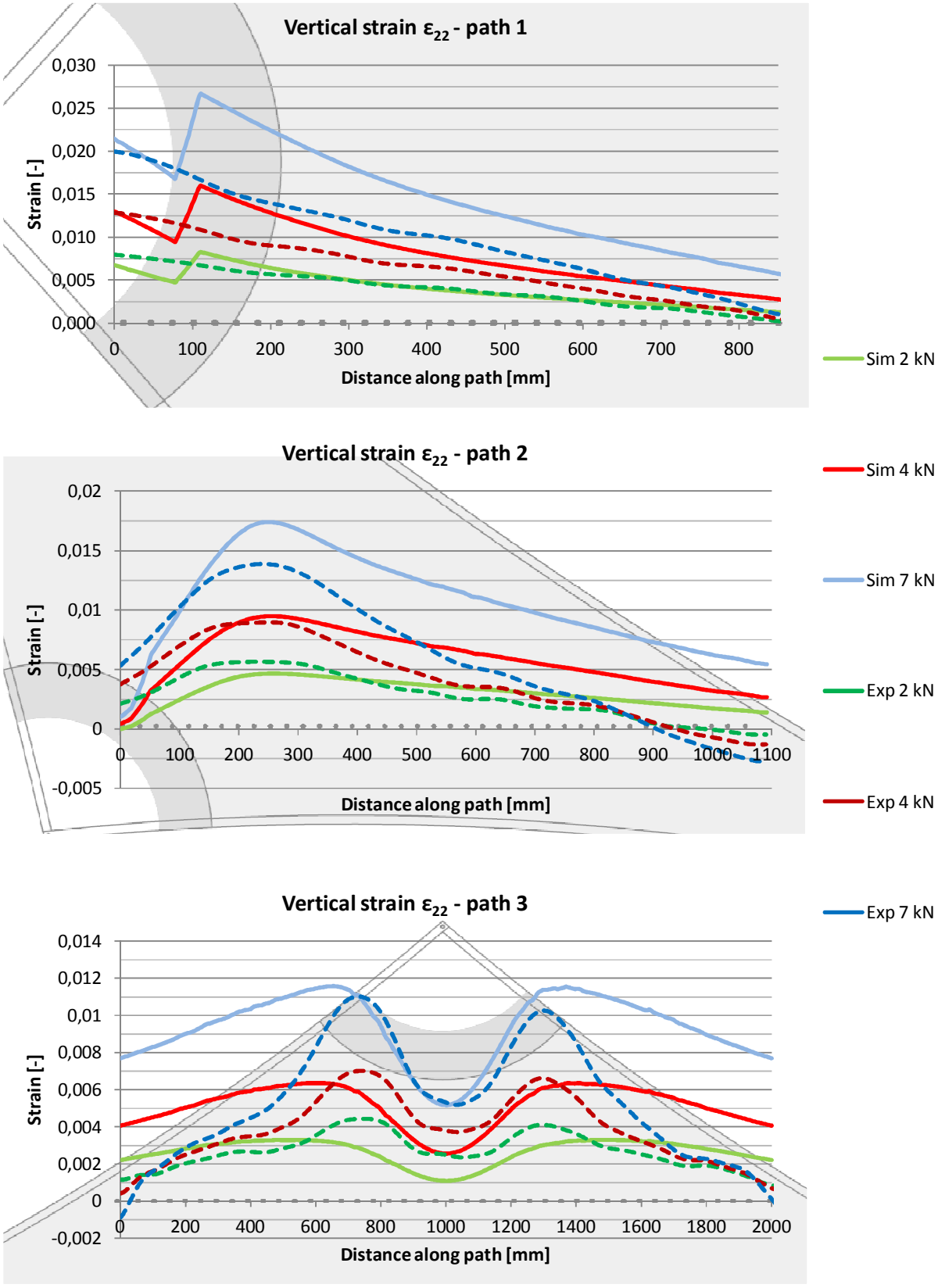

Fig. 70, Fig. 71, Fig. 72 Vertical strain along resp. path 1,2,3 - experiment vs. simulation for L_3 = 2, 4 and 7 kN

3.4.2.5 Quantitative comparison ε_{22}

The applied loading on RP3 is aligned with the fill yarns. Before it was already delineated that fill yarns are initially in a crimped position, which makes them able to elongate much more than the warp yarns. That is the reason why the strains are of a higher ratio (1/100) than the ones measured in horizontal direction (1/1000).
If we have a look at the graphs in 3.4.2.4, one can see that the curves show the same propagation over the distance along the path, as it was also noted for the horizontal strains.
Also for ε_{22}, the miscorrelation with the experiment is mainly expressed at the top area, which is visualized by the start points of path 1 and 2 (Fig. 70 - Fig.71). An closer look to the material model could clarify this difference. The implemented material model has a very small compressive stiffness. Since the area underneath edge B is under compression due to the slightly inward movement of P1 and P2 when RP3 is moved upward, the simulation showed wrinkles in this area. However, these wrinkles were not clearly observed in the experiment, probably because the compressive stiffness in reality is higher, especially in the top area where a reinforcement layer is attached. This could declare the large deviations in the beginning of path 1 and 2, as established in Fig 58-59 for horizontal strain, Fig.70-71 for vertical strain.
Furthermore, in path 1 it is demonstrated how the vertical strain declines. Around P1 the strain is very large, but eventually vanishes at the center of the membrane. This gives a good idea how far the strains propagate through the membrane, and to which distance a certain loads affects the fibers in the membrane. Also for this path the highest ε_{22}-values are marked, because it is positioned in the most critical area in the membrane. Strains up to 0,0267 are calculated, which is 0,0067 higher than in the experimental results (Table 5).

The asymmetry that was displayed in the graph for path 3 for ε_{11}, is now not anymore expressed (Fig.72). The unequal pretensioning at the bottom corners and/or slightly eccentric load in RP3 does not affect the vertical strain in such an extent as it did for the horizontal strain. The two areas perpendicular underneath P1 and P2 that exhibit increasing tensile strain for increasing L_3 (Fig. 62 - Fig. 67), are translated to local maxima of the curves of Fig. 72. However, this path shows an inferior resemblance with the experimental data, especially at the start and end points. This discrepancy can be attributed to their location. The start and end points are located near to the reinforcing belts that are attached to the edges. Their influence could declare deviation between the simulation and the experiment.

In Table 5, one can view the maximal, minimal and absolute values measured along the different paths, this time for the vertical strain, for each considered load rate. The values of the experiment and the simulation are very close to each other, if we keep in mind that the scale of the values is 1/100. What can be pointed out is the fact that the values of the simulation are in most cases higher than those of the experiment. This fact was also denoted for horizontal strain.

		ε_{22} - path 1			ε_{22} - path 2			ε_{22} - path 3		
		2 kN	4 kN	7 kN	2 kN	4 kN	7 kN	2 kN	4 kN	7 kN
Min	sim.	0,0011	0,0025	0,0053	0,0000	0,0004	0,0011	0,0011	0,0026	0,0052
	exp.	-0,0004	-0,0002	0,0003	-0,0005	-0,0013	-0,0028	0,0008	0,0004	-0,0009
Max	sim.	0,0083	0,0160	0,0267	0,0047	0,0095	0,0173	0,0033	0,0064	0,0116
	exp.	0,0080	0,0128	0,0200	0,0056	0,0090	0,0139	0,0044	0,0070	0,0110
Avg	sim.	0,0040	0,0081	0,0145	0,0030	0,0059	0,0107	0,0027	0,0051	0,0094
	exp.	0,0038	0,0060	0,0094	0,0084	0,0041	0,0060	0,0027	0,0039	0,0054

Table 5 Overview of minimum, maximum and average value of vertical strain along paths 1,2 and 3 at different load stages for L_3

To have a better insight in the discrepancy with the real setup, also for the vertical strain box plots are made for each path and each load stage, representing the relative difference. Similar as for the horizontal strain, the deviation for path 1 is much smaller than for the other paths.

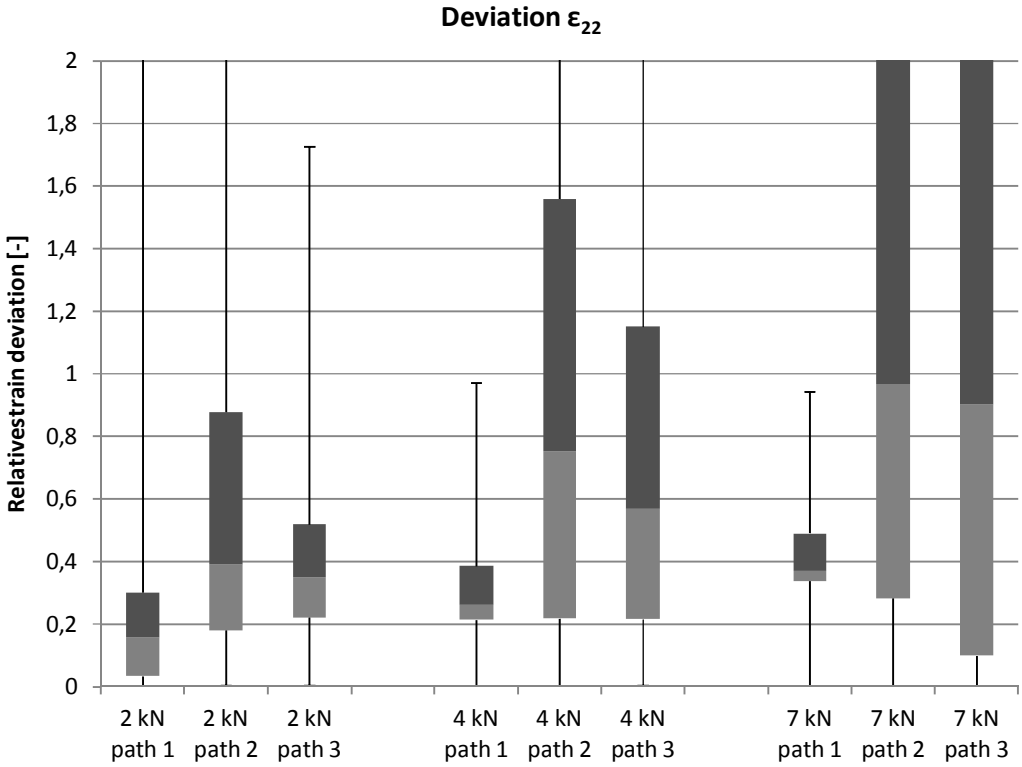

Fig. 73 Relative deviation between experimental and simulated vertical strain for different load stages (L_3 = 2 kN, 4 kN and 7 kN) for path 1, 2 and 3

For the strain in fill direction, an average deviation of ca. 50% is declared. Path 1 is the closest to the experiment, with an average difference of only 26%.
In general, this means that also for the vertical strain, the simulation gives a satisfying representation of the reality.

3.4.3 Shear strain ε_{12}

3.4.3.1 Contour plot simulation

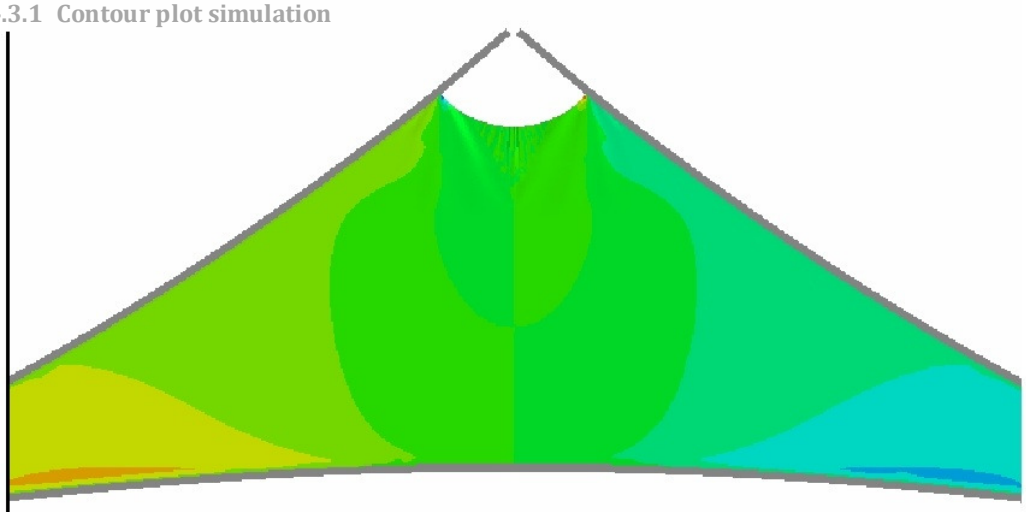

Fig. 74 Contour plot simulation for shear strain ε_{12} [-] at L_3 =2 kN

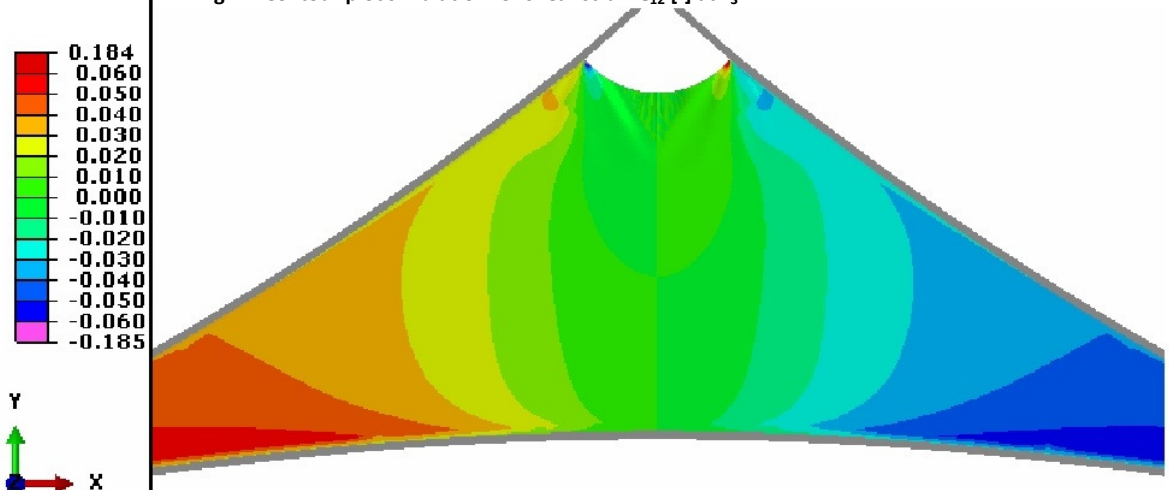

Fig. 75 Contour plot simulation for shear strain ε_{12} [-] at L_3 =4 kN

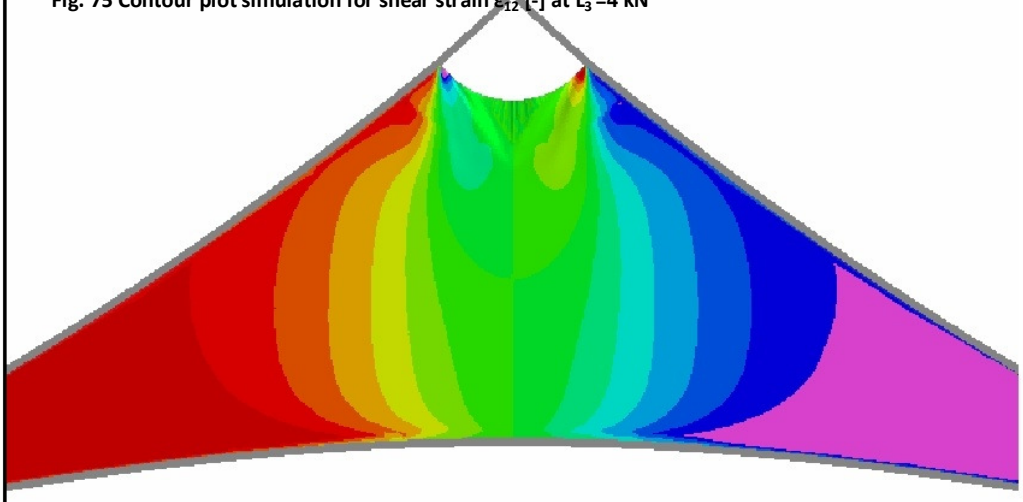

Fig. 76 Contour plot simulation for shear strain ε_{12} [-] at L_3 =7 kN

3.4.3.2 Contour plots experiment

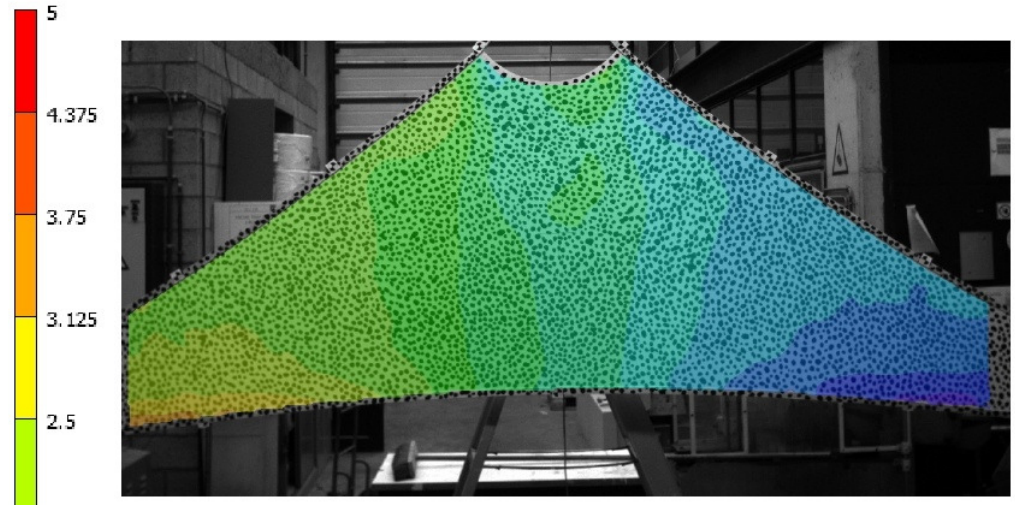

Fig. 77 Contour plot experiment for shear strain ε_{12} [%] at L_3 =2 kN

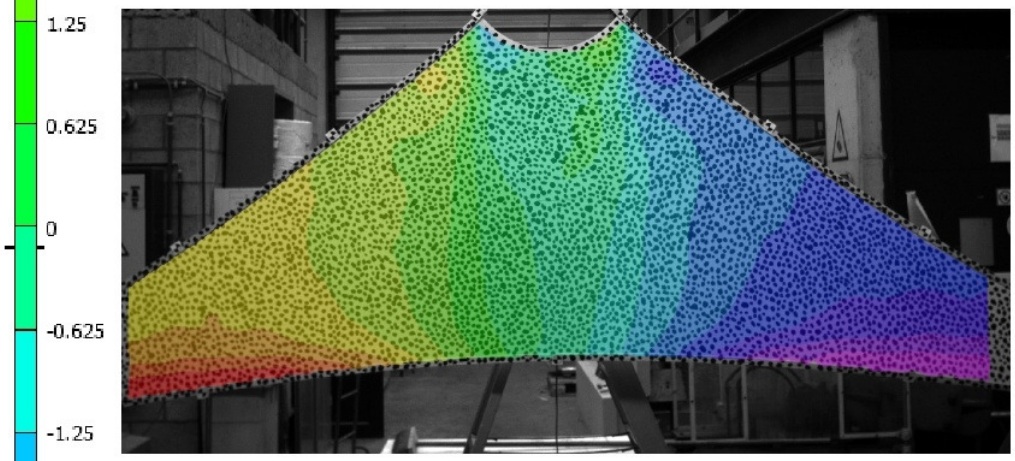

Fig. 78 Contour plot experiment for shear strain ε_{12} [%] at L_3 =4 kN

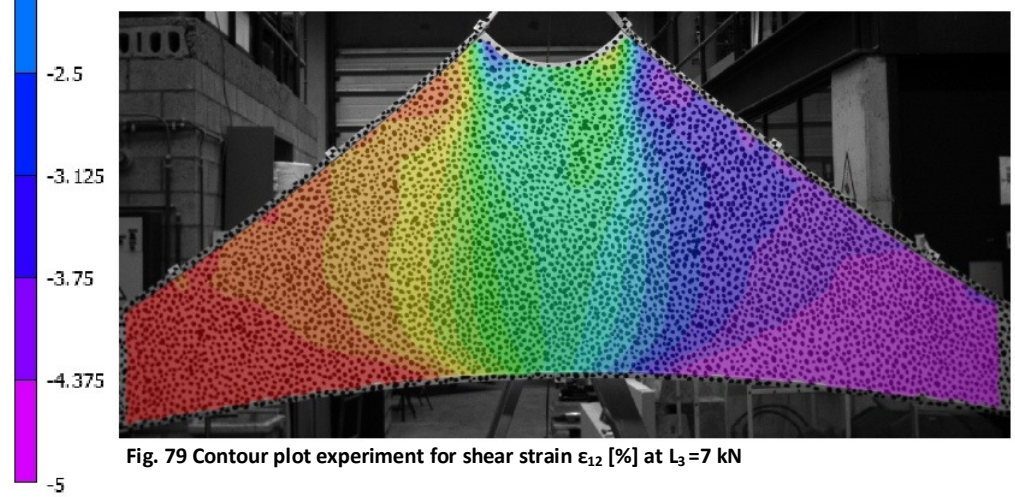

Fig. 79 Contour plot experiment for shear strain ε_{12} [%] at L_3 =7 kN

3.4.3.3 Qualitative comparison ε_{12}

The contour plots for shear strain are - compared to the other strain directions - in best correlation to the experimental result. It is clear that the simulation gives an exact representation of the real spectrum, and this for all load stages. The shear is inversed symmetric about the y-axis.
Because the load is applied symmetrically, the shear strain is neutral in the center of the membrane and augments as the distance to the center increases. One side of the membrane is subjected to positive shear strain, while the other side demonstrates negative values.
Notice also the phenomenon in the top corners P1and P2 of the membrane. When the load increases, the shear in the corners areas has an opposite sign (negative on membrane side with positive shear and vice versa). With augmenting load, this action is more expressed. It can be physically declared by the movement of the belts during the load phase. When the hook is moved upward, the unstitched belt ends rotate a little and impose an opposite force in the corner points P1 and P2.

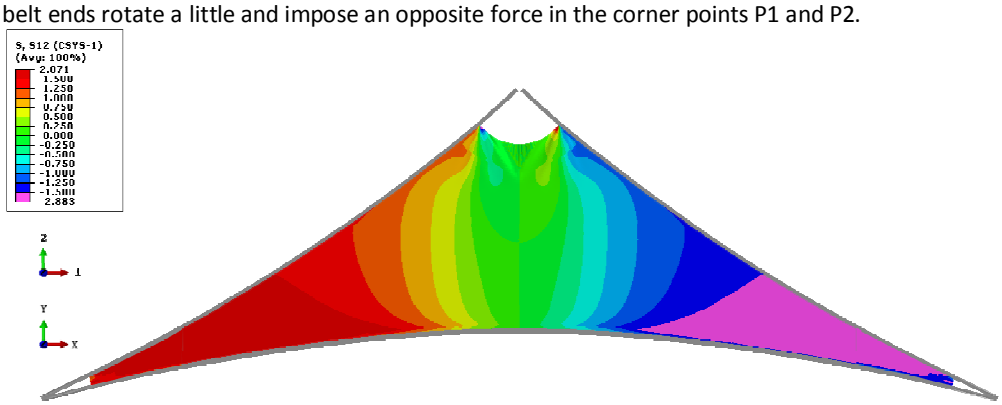

Fig. 80 Shear stress σ_{12} for a top load of L_3 = 7 kN [MPa]

The pattern of the shear strains is a result from the shear stresses in membrane at the corresponding load stage. In Fig. 80 an illustration of the shear stresses at a top load of 7 kN is given. One can see that the spectrum of σ_{12} is of the same kind of the strain ε_{12}.
As it was already pointed out in previous research by e.g. Brigdens and Birchal [71], the maximum stresses in a woven fabric under load will usually occur in weave directions, due to the low shear stiffness (about 20 MPa) compared to their tensile stiffness (typical values between 200 and 2000 MPa). This is also noticed in the results form Abaqus. Where horizontal and vertical strain showed maxima of 14 and 22 MPa (Fig. 57 and Fig. 68), the maximal value in shear direction is limited to 2,8 MPa (Fig. 80).

3.4.3.4 Path values ε_{12}

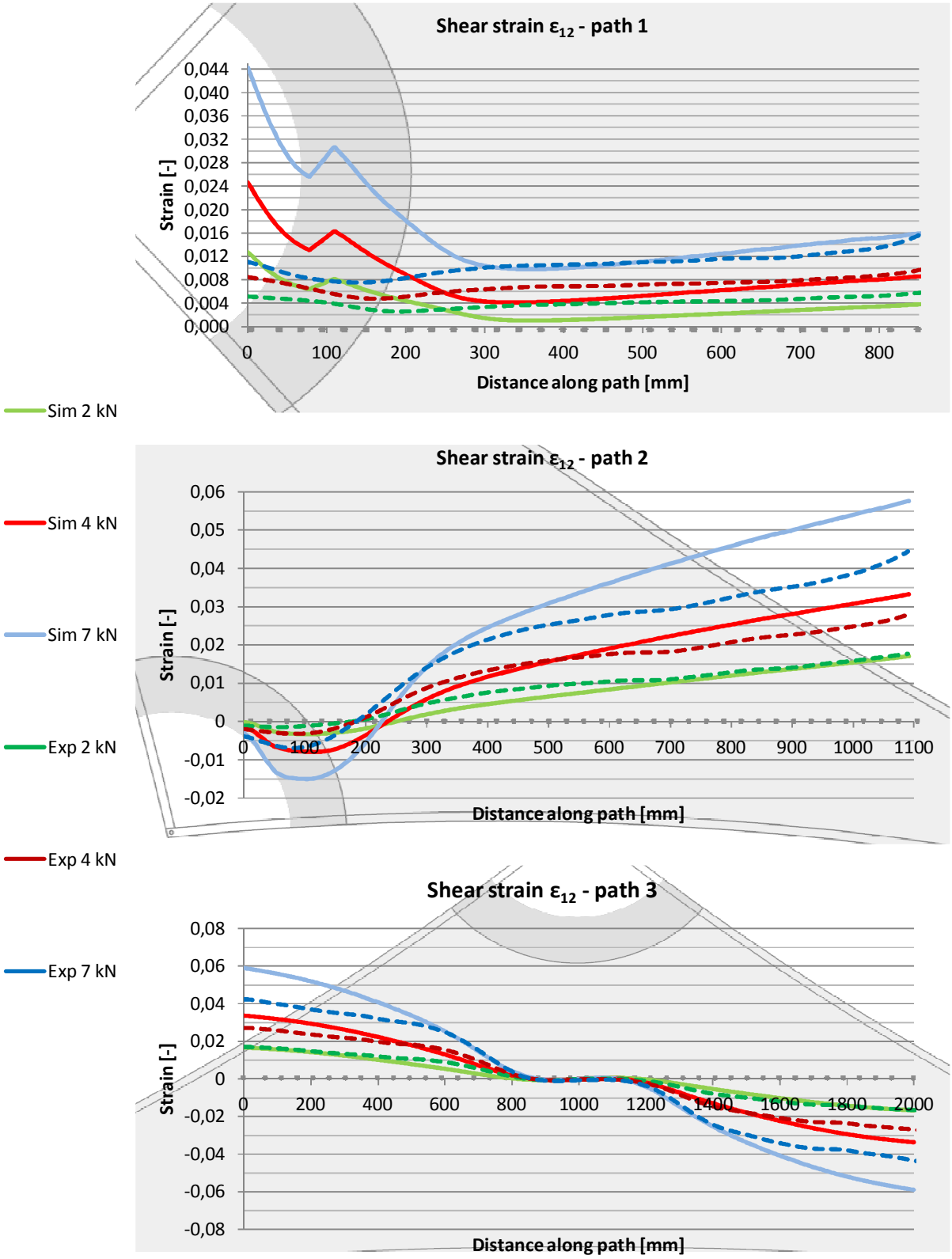

Fig. 81, Fig. 82, Fig. 83 Horizontal strain along resp. path 1,2,3 - experiment vs. simulation for L_3 =2, 4 and 7 kN

3.4.3.5 Quantitative comparison ε_{12}

Also for the shear direction, the values are of a scale of 1/100, similar to the magnitude that was recorded for ε_{22}. However, in this case the values have a wider spectrum and vary between the limits of -0,06 and 0,06 for a maximum top load of L_3 =7 kN.
This phenomenon is satisfyingly displayed in the graph of path 2 for one side of the membrane (Fig 82). At the beginning of the path the shear strain is close to zero, because no stress is measured in that location. The value grows with each step travelled further away from the center, along the line of the path. Depending on the applied load, the value at the end of the path differs roughly between 1,7% and 5,7% for the simulations, and between 1,7% and 4,4% for the experimental setup.

In the curves for path 1 (Fig.81), one can recognize the neutral region at the center of the membrane. The curves are almost stable and very close to zero. Also the phenomenon in the corner top P1 (as discussed in 3.4.3.3) can be recognized. For L_3 = 2 kN, the strain in that corner is still relative low, but increases very fast when RP3 is pulled upward, due to the belts that try to move P1 and P2 inwards.

In Fig. 83, one can see clearly the reversed symmetry about the y-axis of the model. At the edges of the membrane, ε_{12} has either a high positive or negative value, followed by a diminution towards the middle of the triangle and finally neutralizes itself in the central area. This phenomenon is satisfyinly represented by both the numerical and experimental graph.

For a top load of L_3 = 2 kN, the graphs are almost exactly represented by Abaqus. The averages values along each path are almost equal for the experiment and the simulation, as can be extracted from Table 6. Also for ε_{12}, the difference between the numerical curve and the experimental curves increases as the top is more tensioned (i.e. if L_3 augments). For example, this is expressed in the more dissociating values for the average as the load increases, e.g. for path 2: this path shows a difference in average of 0,0016 with the experiment at a top load of 2 kN, and this deviation enlarges up till 0,0051 for a top load of 7 kN. This is due to the change in load ratio, as was explained in 3.4.1.5.

		ε_{12} - path 1			ε_{12} - path 2			ε_{12} - path 3		
		2 kN	4 kN	7 kN	2 kN	4 kN	7 kN	2 kN	4 kN	7 kN
Min	sim.	0,0010	0,0041	0,0098	-0,0033	-0,0079	-0,0149	-0,0166	-0,0337	-0,0589
	exp.	0,0026	0,0048	0,0075	-0,0014	-0,0031	-0,0069	-0,0168	-0,0273	-0,0440
Max	sim.	0,0127	0,0246	0,0442	0,0170	0,0332	0,0570	0,0166	0,0337	0,0590
	exp.	0,0063	0,0113	0,0195	0,0177	0,0279	0,0444	0,0170	0,0272	0,0423
Avg	sim.	0,0035	0,0081	0,0162	0,0068	0,0146	0,0266	0,0000	0,0000	0,0000
	exp.	0,0042	0,0072	0,0110	0,0084	0,0138	0,0215	0,0001	-0,0001	-0,0005

Table 6 Overview of minimum, maximum and average value of shear strain along paths 1,2 and 3 at different load stages for L_3

Relative seen to each other, the dissimilitude of the shear strains between the numerical result and the experiment is in the order of 26%, but the median difference varies between 17 and 60%. This can be seen in Fig. 84 on the next page.

As was expected from the matching contour plots, the discrepancy for the shear strain is much lower than for the strains in other directions.

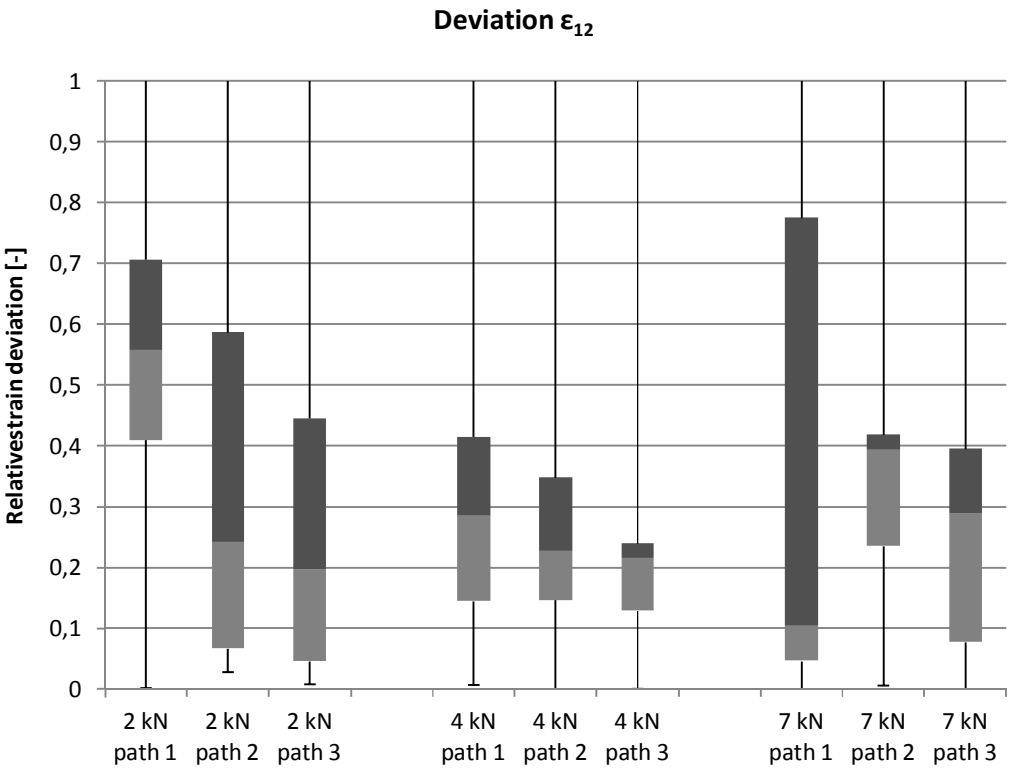

Fig. 84 Relative deviation between experimental and simulated shear strain for different load stages (L_3 = 2 kN, 4 kN and 7 kN) for path 1, 2 and 3

3.4.4 Conclusion of the compared paths

Qualitatively seen, it can be concluded that the numerical simulation gives a satisfying representation of the real actions in the membrane. The correlation between the contour plots from Abaqus and those from the DIC measurements is recognized for both horizontal and vertical strain, but shows the best equivalence for the shear direction.
Also from a qualitatively point of view, the numerical model performs the best in representing ε_{12}, with an average deviation of 26% for all load stages and all investigated paths. For horizontal and vertical strain, the values are slightly higher, varying about 50%. Only path 1 shows better correlation. Depending on the investigated strain, the median difference for this path varies between 26 and 35%.

Although the deviations seem high, they must be approached in the perspective 'perfect' simulation versus experiment. The most important influence are listed:

- The geometry of the experimental setup is not perfect, since we are dealing with real material. The fabrication and preparation of the setup introduced in this experiment an average imperfection of 4,47% according to the design geometry.
- The compared paths do not have *exactly* the same position, due to the minor difference in geometry and the imperfect alignment of the experimental setup.
- The experimental data is not as stable as the output from the numerical program: varying values and local aberrations cause excessive outliners.
- The DIC measurements introduce an error of 0,13mm.
- The material model used for the simulations has a only a very small compressive stiffness, resulting in the formation of wrinkles at the slightest pressure force.
- The numerical model is based on biaxial tests with a load ratio 1:1, which is different from the load case in this experiment.

This last one results in larger deviations as RP3 is moved further upward, since the load ratio differs each time more and more from 1:1.

If now the average deviation is calculated, considering all paths and all strain directions, average values of 37%, 43% and 53% can be measured for respectively a load of 2 kN, 4 kN and 7 kN in RP3 . This considerable augmentation could be diminished by improvement of the user material. Therefore, more biaxial tests for different load ratios should be performed.

In general is observed that Abaqus calculates slightly higher the values concerning the strain. Consequently, the numerical calculations overestimate to a limited extent the occurring strains, which will result in the choice for a slightly stiffer and hence safer design.

3.5 Conclusion

At the AE Lab of the VUB in Brussels, an experiment with a triangular shaped membrane has been performed. A PVC-coated sample of 6 m by 1,5 m was loaded in-plane only, using a displacement applied on the top of the triangle. This experiment and research is an intermediate step in the KFAS project, before proceeding to a more complex kinematically adaptive construction.
The displacement of the membrane has been recorded by the use of two DIC cameras, and hence the strain patterns for each load increment could be collected.
Thereafter, a numerical model in agreement with the experimental setup was designed in the FEM-program Abaqus. With a developed user material that is able capture the non-linearities in warp and fill direction, the simulation was performed, using membrane elements.

To evaluate the results from the simulation, the contour plots produced by Abaqus were compared with those from the DIC software. It could be established that the overall behavior of the membrane in the simulations is equivalent with reality. The areas of strain are very alike, and this for all analyzed load stages (2 kN, 4 kN and 7 kN).
Furthermore the progression of the strain along three well chosen paths were generated for each direction (ε_{11}, ε_{22} and ε_{12}), in order to investigate in detail the generated results and the correlation with the experiment.
It could be concluded that the tendencies of horizontal, vertical and shear strains along each path are in good agreement. Qualitatively, the results show average deviations between 26 and 50 %, depending on the path and load rate. On the first sight, these are high values, but account must be taken for the many influence that affect them and the scale we are working on. To only name the most important ones, the slight difference in chosen paths and geometry, incompleteness of the material model and local aberrations in the data from the experiment, affect to the result.

These findings indicate the room for improvement, both in the experimental and numerical field. For example, during the performed experiment no information is gained about the bottom corners of the membrane . Experimental data of that area that could reveal present ambiguities, especially about the negative vertical strain in the bottom region of triangular membrane.
For the numerical part, extensions to the user material are recommended, in order to capture also the behavior for load ratios that differ from 1:1. Furthermore, research to the low compressive stiffness must be carried out.

Chapter 4 | Comparison with simplified material models

"We should make things as simple as possible, but not simpler."

Albert Einstein, 1979-1955

4.1 Introduction

The user material subroutine, implemented in the numerical model in chapter 3, proved its performance and good correlation with the experimental data has been achieved. To have an idea about the improvement of the user material over more simplified material models, an additional study is carried out, which compares the UMAT with (1) isotropic and (2) orthotropic material. Especially the last case is interesting to investigate, since orthotropic material is state-of-the-art in design of tensile membrane structures . For both cases, the same geometry and boundary conditions are used as for the numerical model described in 3.3.2.2, only adjusting the material parameters.

4.2 Isotropic material

The earliest design models for membrane architecture were based on an isotropic material behavior, by analogy with e.g. soap-structures. This was already outlined in chapter 1. Of course, it is a very bad resemblance of a membrane in reality, but to see the evolution and development in time and the effect of equal behavior in all directions in contrast to the more complex models, an analysis with a constant Young's modulus is carried out. Its value was based on uniaxial test. For the thickness and the density, values equal to the simulation with the user material were used. The properties as implemented in Abaqus are listed in Table 7.

Property	Value	Property	Value
Young's modulus	1270 MPa	Thickness	0,6 mm
Poisson ratio	0,313	Density	1416 kg/m³

Table 7 Material properties of an isotropic material model based on the results of uniaxial tests

4.3 Linear elastic orthotropic material

On the other hand, current design methods still make significant assumptions concerning the material properties. In most calculations methods nowadays, the Young's moduli are chosen constant for each fiber direction, resulting in a linear elastic orthotropic material model. Although this is an approach that is closer to reality than the isotropic one, the assumptions mostly result in an over dimensioned structure and hence material waste [72]. To gain more insight in the improvement of the user material on this issue, a simulation with an orthotropic material model is carried out.
The imposed Young's Moduli are derived from biaxial test [15]. The thickness and density of the coated fabric, as well as the shear modulus , are the same as in the case of the user material. The values for all properties can be found in Table 8.

Property	Value	Property	Value
Young's Modulus warp	1130 MPa	Shear Modulus	20 MPa
Young's Modulus weft	825 MPa	Poisson ratio	0,3
Thickness	0,6 mm	Density	1416 kg/m³

Table 8 Material properties of an orthotropic material model based on the results of uniaxial tests

4.4 Comparison

The results of the simulations that were carried out with an isotropic and linear elastic orthotropic material can be found on the next pages. The contour plots for horizontal, vertical an shear strain are shown at the final state of the membrane, thus at a load level L_3 = 7 kN. In order not to overload with needles digression, the intermediate results for 2 kN and 4 kN are dropped. Besides, the chosen load level provokes strains of considerable size, as it could be analyzed from both the experiment and the simulation with the UMAT. Therefore, this load is found sufficient to give an impression about the performance of each the material model. [5]

After the qualitative comparison, points along a path are traced and the values regarding stress and strains are compared for all investigated material models. Only one path was picked out as medium for comparison, namely path 2 from the investigation in chapter 3 (For the exact location, the reader is referred to Fig. 50 p. 40). This path runs from a central point in the top of the membrane to a point near the left bottom corner, and crosses the most important and varying regions of the membrane. Therefore, it is able to provide a representative image of the occurring action in the mode when it is subjected to load.

[5] The contour plots from the experimental data and from the simulation with UMAT can respectively be found on the first and last page of this book. If folded out they enable the reader to compare easily with results from other simulations that will be shown in the following. The horizontal, vertical and shear strains are presented for a load level L_3 = 7 kN.

4.4.1.1 Contour plots isotropic material

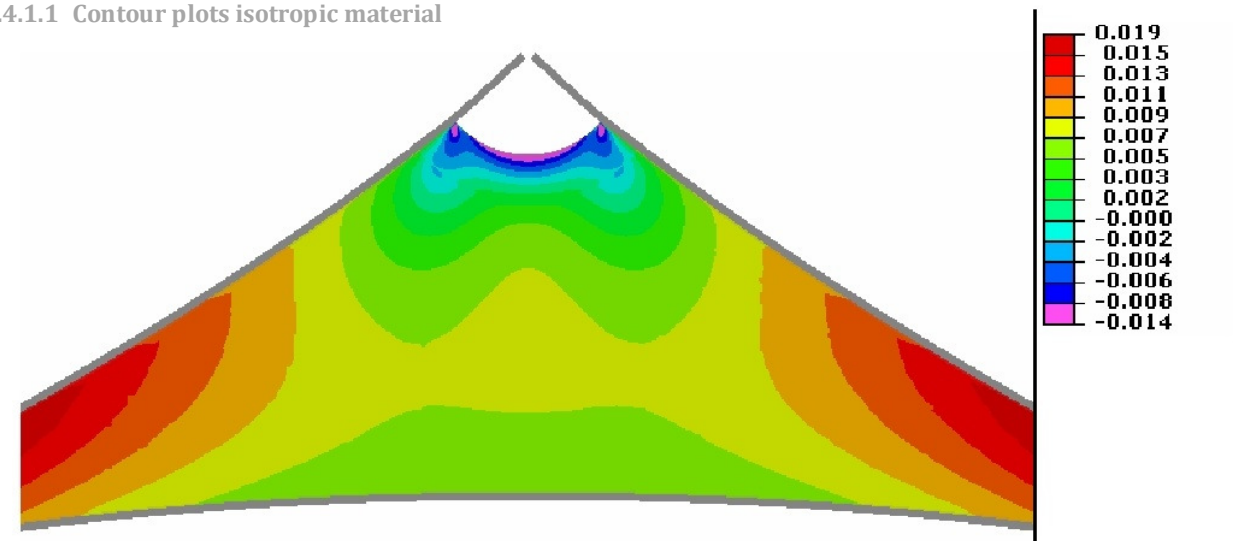

Fig. 85 Contour plot isotropic material for horizontal strain ε_{11} [-] at L_3 =7 kN

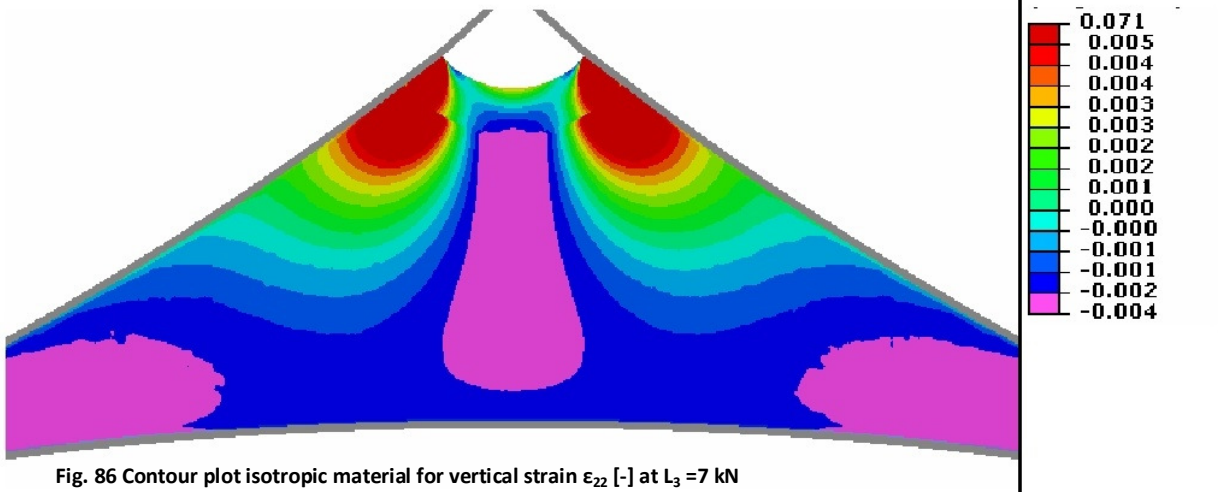

Fig. 86 Contour plot isotropic material for vertical strain ε_{22} [-] at L_3 =7 kN

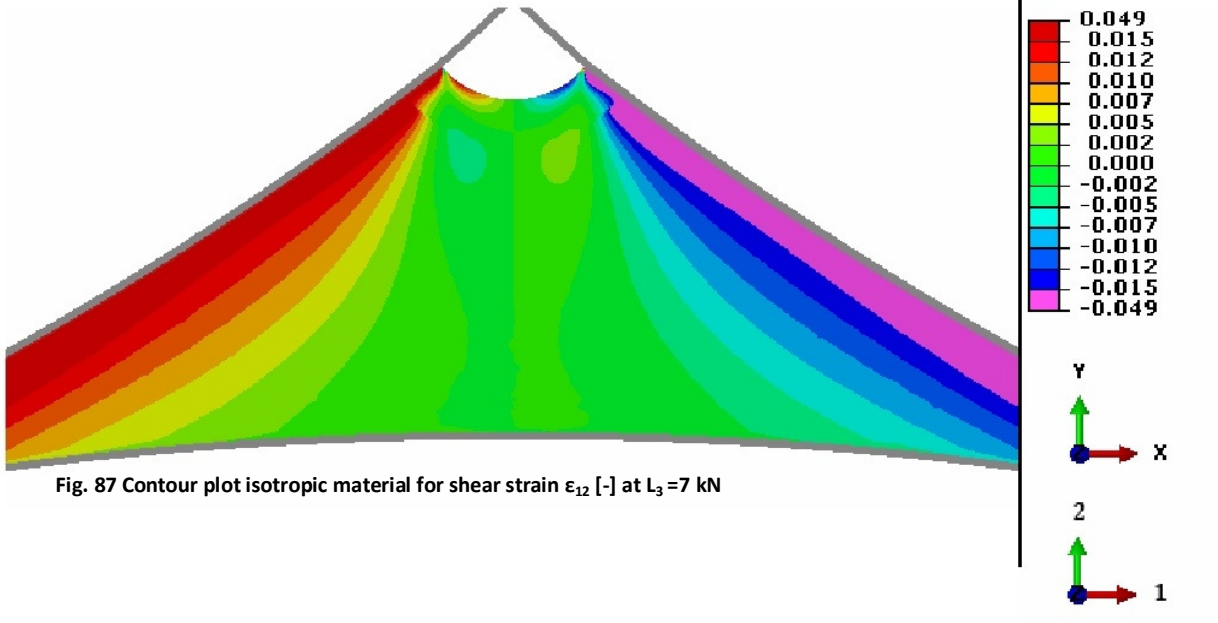

Fig. 87 Contour plot isotropic material for shear strain ε_{12} [-] at L_3 =7 kN

4.4.1.2 Contour plots linear elastic orthotropic material

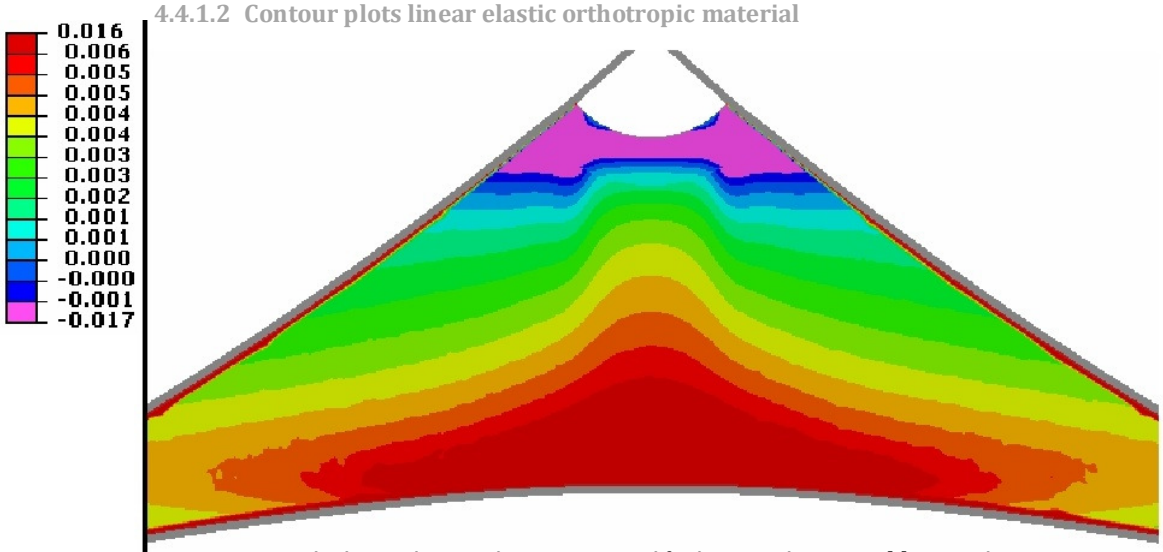

Fig. 88 Contour plot linear elastic orthotropic material for horizontal strain ε_{11} [-] at L_3 =7 kN

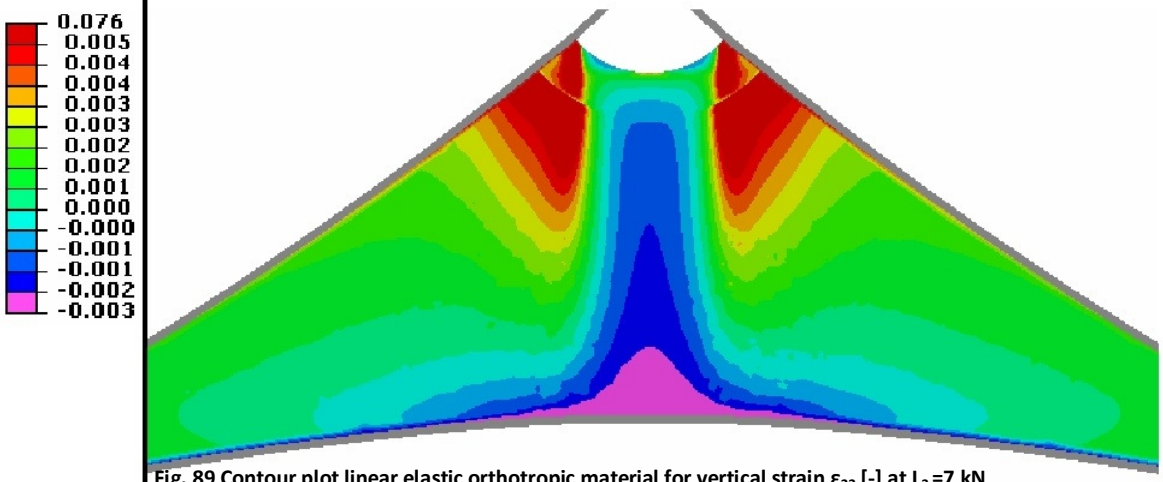

Fig. 89 Contour plot linear elastic orthotropic material for vertical strain ε_{22} [-] at L_3 =7 kN

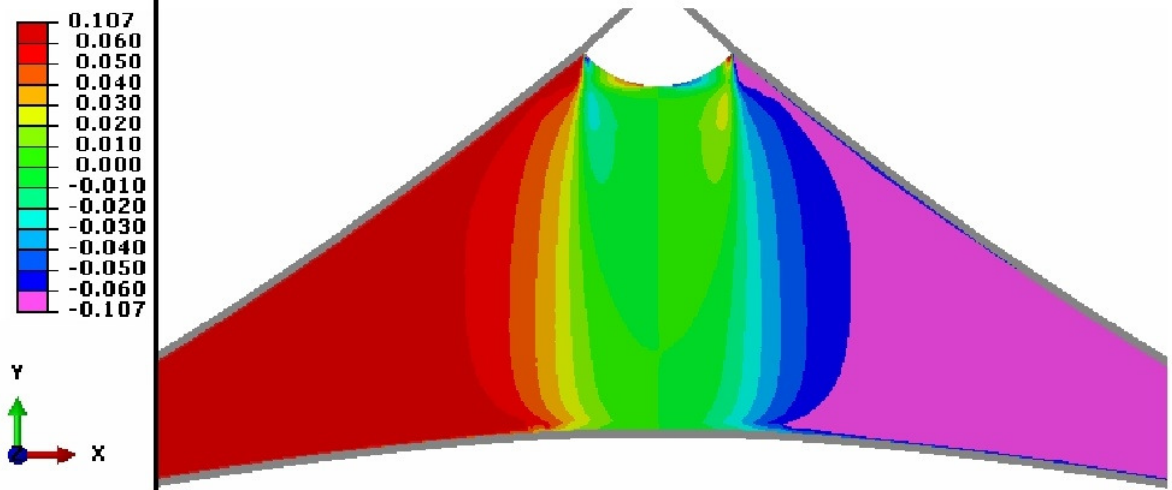

Fig. 90 Contour plot linear elastic orthotropic material for shear strain ε_{12} [-] at L_3 =7 kN

4.4.1.3 Qualitative comparison

From the contour plots, it can be seen that the difference of the simplified materials with the experimental data is significantly larger than those of the UMAT.
Globally, the orthotropic material indicates the correct areas for tension and compression, but they are rather rough estimations and provide not the detailed information as the user material does. For example, the area at top edge B is simulated as a complete area in compression, without de detail of the neutral region in the middle.
Furthermore, both simplified material models show bad correlation for the central area of the membrane, especially when one concerns about the vertical stains (Fig. 86 and Fig. 89). They demonstrate negative strains instead of a neutral/tensioned region.
However, the isotropic material exhibits the best resemblance with the experiment for the strains in load direction (ε12), compared to the horizontal and shear strain. These last ones show conflicting results with the reality. For example in the horizontal strain plot (Fig. 85), the bottom border should be in higher tension than the sides, but complete opposite results are presented.
On the other hand, the orthotropic material is able to represent the shear strains in a correct way (Fig. 90**Error! Reference source not found.**), while the isotropic is not able at all (Fig. 87).
This difference can be clarified by Hooke's law, which expresses the relation between the shear modulus G, the elasticity modulus E and the Poisson's ratio for a homogeneous, linear elastic isotropic material [73]:

$$G = \frac{E}{2(1+v)} \quad \textbf{(9)}$$

Accounting for the material properties that can be found in Table 7, the shear modulus for the isotropic material becomes 483,625 MPa. This is much higher than the shear modulus of the orthotropic material (20 MPa), and declares the high neutral area in the central part of the membrane, as it can be found in Fig. 87.

Another striking remark is the low value of strain, especially in fill direction (y-direction), for both materials, when places side by side with the experimental data. This means that the material strength is largely overestimated, which explains the use of high safety factors in the design with constant Young's moduli. The material is assumed to behave stiffer than will occur in reality.
To gain more information about the quantitative differences, the values of strains and stresses are compared in the following section.

4.4.1.4 Quantitative comparison

For the investigation of the stresses and strains, path 2 (Fig. 50) was picked out as a medium for comparison. This path describes the most important regions of the membrane and therefore gives a satisfactory overview behavior in the model. On the next page, the graphs for ε_{11}, ε_{22} and ε_{12} can be found (respectively Fig. 91, Fig. 92, Fig. 93 Horizontal, vertical and shear strain in comparison to the experimental data for 3 different materials 91, Fig. 92 and Fig. 93). It is immediately recognizable that the UMAT is able to represent the tendency of the strain much better than the other 2 materials, and the produces values are very close to those of the experiment. The curves for isotropic an linear elastic orthotropic material exhibit only to a limited extent the trend of the experimental strains, with less detail of the changes along the distance. Moreover, the scale is of another order. It is strikingly demonstrated that the results achieved with the UMAT are much closer to the ones of the experiment.
Moreover, the simplified material models propose in some areas completely opposite values, in particular in the beginning of the path for horizontal and vertical strain. In the places where the experiment shows positive strain, the isotropic and linear elastic orthotropic models show negative, and hence indicate a loss of stress while this is not the case.

These findings point out the vast improvement that is achieved when an elasto-plastic multi-linear material model is used instead of a simple iso- or orthotropic materials with constant E- modul(us)(i).

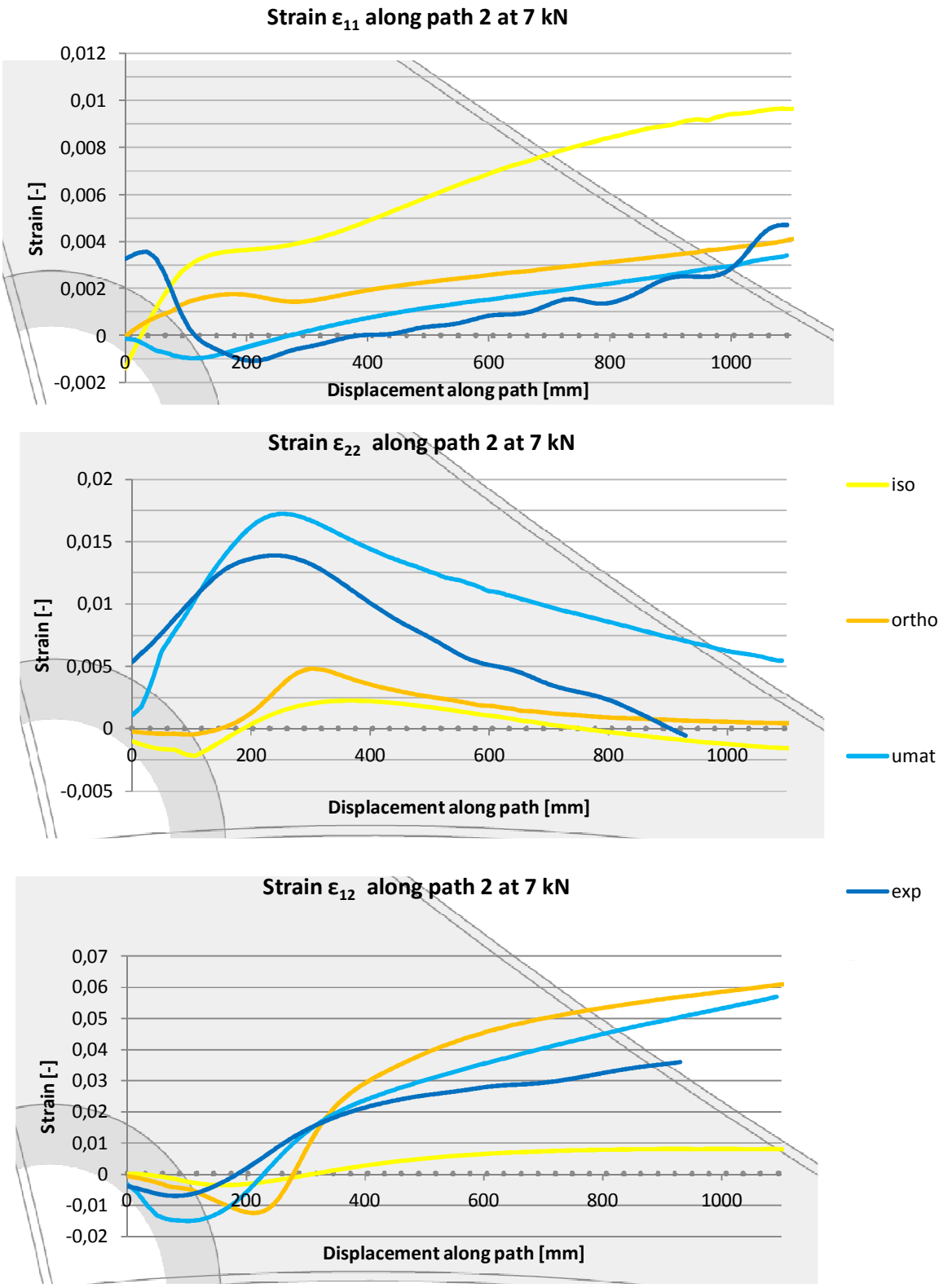

Fig. 91, Fig. 92, Fig. 93 Horizontal, vertical and shear strain in comparison to the experimental data for 3 different materials, along path 2 at a top load of L_3 = 7 kN

To visualize the discrepancy with the experiment, also diagrams of the deviations for the different materials are plotted (Fig. 94).

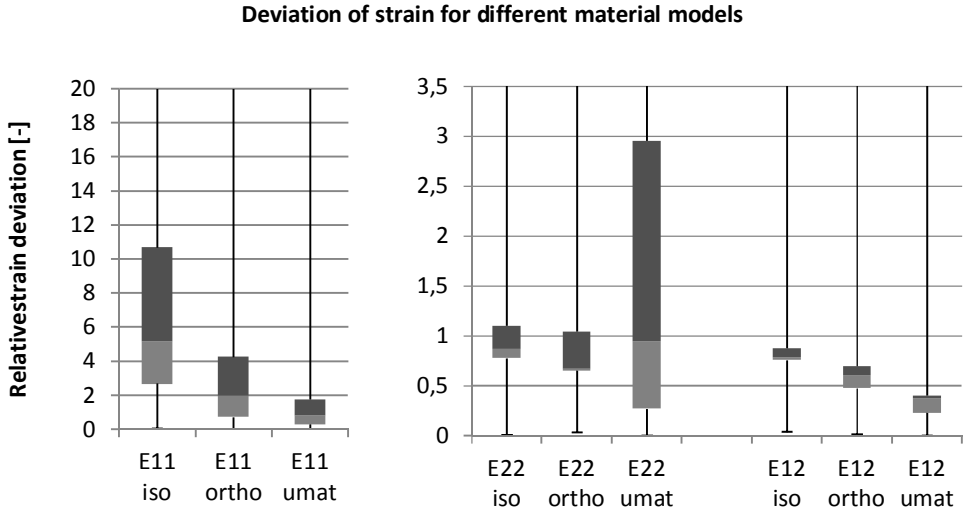

Fig. 94 Relative deviation of horizontal, vertical and shear strain from the experimental data for 3 different materials

It can be noticed that the difference of the user material compared to the experimental data is significantly smaller for horizontal and shear strain. For vertical strain ε_{22} however, the deviation is much larger. Presumably, this is caused by the settings of the user material model. In fill direction the initial stiffness is very low (160 MPa) and proceeds soon into a plastic regime, which triggers large strains (starting at 5 kN, see Fig. 38 p.31). It is plausible that the E-modulus based on biaxial tests with load ratio 1:1 is set to small. Therefore, it is recommended to do additional experiments for different load ratios, in order to capture also the behavior in these circumstances.

Furthermore, it is noticed that the isotropic model presents stresses that are approximately 1 to 3 times higher than the ones demonstrated by the user material (Fig. 95-97). On the other hand, the stresses produced by the linear elastic orthotropic material are much closer to the stresses in the model with a user material, but are rather a rough estimations (a relative deviation of 30% with the user material is measured). This gives an indication of the overestimation of the stresses when a simplified model is used, which leads to a thicker and stronger fabric choice and hence waste of material to build a structure. The use of the more complex but more precise user material could lead to a vast improvement in this field.

Besides the difference in output, also the calculation time is significantly different for the investigated materials. Between the linear elastic orthotropic and isotropic material models, the difference is only small, but the UMAT needs circa four times the calculation time. It can be denoted that the more complex the material, the longer the CPU time. However, the required time for the user material is still within reasonable limits. Table 9 gives a summary.

Material model	CPU time [min]
Isotropic material	17
Orthotropic material	21
User material	75

Table 9 Overview of the calculation time as function of the material model

The main reason for the increased calculation time is the appearance of wrinkles, which are not simulated with by the simplified material models. The user material exhibits a very low compressive stiffness compared to the other two materials. and together with the lack of bending stiffness of the membrane elements, pure artificial wrinkles are formed during the simulation. This causes a much higher calculation time, but gives at the same time an indication of the areas where wrinkles will appear in reality.

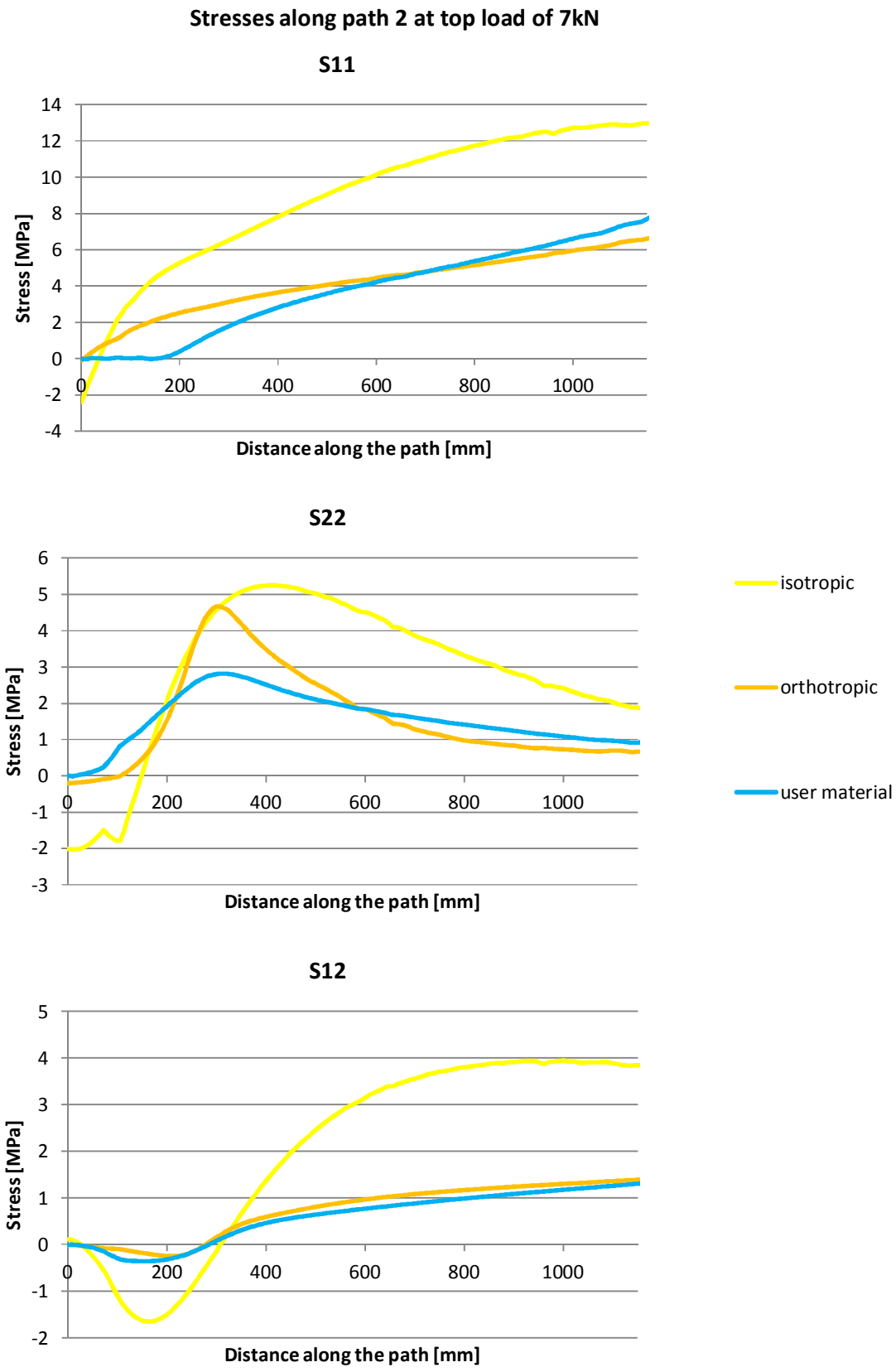

Fig. 95, Fig. 96 and Fig. 97 Horizontal, vertical and shear stress in comparison to the experimental data for 3 different materials, along path 2 at a top load of 7 kN

4.5 Conclusion

The UMAT has proved clearly its advantages over on isotropic material, and produces more precise results compared to linear elastic orthotropic material. This last one is able to present a rough estimation of the occurring stresses and strains in the membrane, but lacks the accuracy and detailed information the user material can provide. The average overall deviation with experimental data for the strains in all directions are respectively for the isotropic, linear orthotropic and the user material 227% , 109% and 70%. This indicates an improvement of 39% of the user material over orthotropic material and almost 70% over the isotropic material with regard to the calculated strains.

Chapter 5 | Influence of the fiber direction

"The excessive increase of anything causes a reaction in the opposite direction."

Plato , 427-347 B.C

5.1 Introduction

In the previous models, the warp fibers were aligned with the x-axis of the coordinate system, i.e. the horizontal direction of the membrane. It is known from the material properties of coated fabric that the fill fibers show more extensive strain in the initial loading phase in comparison to the warp yarns [74]. In addition, they demonstrate also earlier permanent strain (starting at 5MPa versus 14 MPa for warp fibers)[75]. Because the loading in this research is mainly applied in y-direction and hence predominantly charges the fill fibers, large vertical strains are measured. These strains could be reduced by changing warp en fill direction of the fabric, and aligning the initially stiffer warp direction with the load orientation. [6]

This assumption tested in two ways. First, by changing only the fiber direction in the reinforcement layers at the vertices. This is the place where the largest stresses were measured. Second, by redirecting the warp fibers of the all coated fabric in the model, thus including as well the large membrane surface as the strengthening parts and aligning them with the vertical axis.

Unfortunately, no experimental data is available for these adjustments. Even though the numerical model demonstrated trustworthy results in account for the original fiber direction (analyzed in Chapter 3), it is advised to double check with real tests in the future.

5.2 Inversed fiber direction in reinforcement layers

As can be seen from the contour plots of the stresses in Fig. 57, Fig. 68 and Fig. 80, the largest stresses appear in the top part of the membrane. For horizontal direction, the maximum negative strain was measured in the top area, for a value of -0,04 MPa. On the other hand, in vertical direction tensile stresses up to 22 MPa occurred, which is far beyond the yield stress (fill) fibers.

In the experimental setup, the fibers of the reinforcement had the same orientation of the large fabric part, namely warp in x-direction and fill aligned with the y-axis. Because of the reinforcing function, it is interesting to test the influence of change in fiber direction of the double layers in the apexes of the model. We expect an increase of stress, but a decrease in strain, if the stiffer warp yarns are aligned with the load direction.

For the simulation, the model as described in 3.3.2.2 was used, but now with changed fiber orientation of the reinforcement layers at the apexes. A schematic illustration is given in Fig. 98. Again the membrane is loaded in RP3 at the top for a load of L_3 = 7 kN. The results are presented and discussed in the following sections.

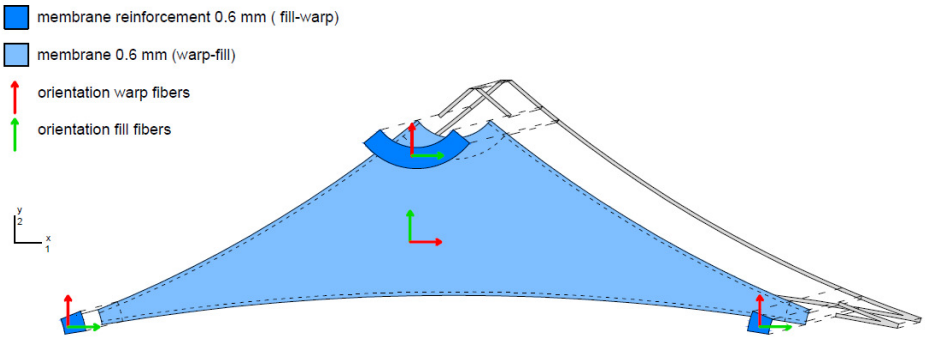

Fig. 98 Schematic presentation of the fiber direction for the model with inversed orientation in the reinforcement layers

[6] In what follows, the indication for a yarn orientation with warp along the x-axis and fill in vertical position will be 'warp-fill oriented', while 'fill-warp oriented' will be used for the opposite case.

5.3 Inversed fiber direction in all membrane parts

During the fabrication of the experimental model, the patterns for the different membrane parts were cut from a roll of coated fabric. The warp fibers are positioned along the length of the cloth, due to the weaving process(Fig. 99).

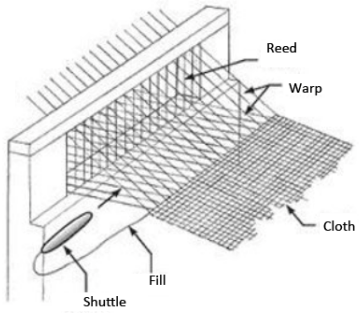

Fig. 99 Weaving process of textile with indication of warp en fill yarns

Due to the limited width of the roll, it was not possible to change the fiber direction of the largest membrane part. To avoid welded seems that would introduces impurities in the model, it was decided to orientate the warp fibers along the longest side of the circumscribed triangle (side A'). Although, it would be more logic to align the warp fibers in the direction of the applied load. Since they exhibit a stiffer initial behavior, they can confine excessive strains in a better way than the initially crimped fill fibers when the membrane is loaded.
To test the effect of changed warp and weft orientation of the entire model, an additional simulation was carried out with all warp fibers positioned in vertical direction, as schematically illustrated in Fig. 100. Also for this model, a load of 7 kN is applied on RP3. The results are presented in the following sections.

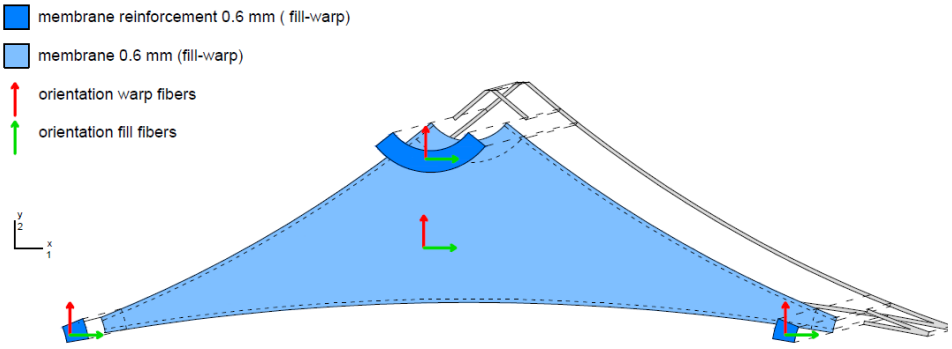

Fig. 100 Schematic presentation of the fiber direction for the model with inversed orientation in all parts

5.4 Comparison

In 5.4.1 and 5.4.2, the contour plots of both investigated cases concerning the fiber direction are presented. Again, only a top load of L_3 =7 kN is considered. The strains in horizontal, vertical and shear direction are shown. [7]
Fig. 101 Horizontal strain ε_{11} for model with inversed fiber direction in the reinforcement layer at top load of L3 =7 kN
Fig. 102 Horizontal strain ε11 for model with completely inversed fiber direction at a top load of 7 kN

[7] To compare with the original situation, the reader can again fold out the contour plot of the user material and the experimental results, provided at respectively the beginning and the end of this book.

5.4.1 Contour plots inversed fiber direction in the reinforcement layers

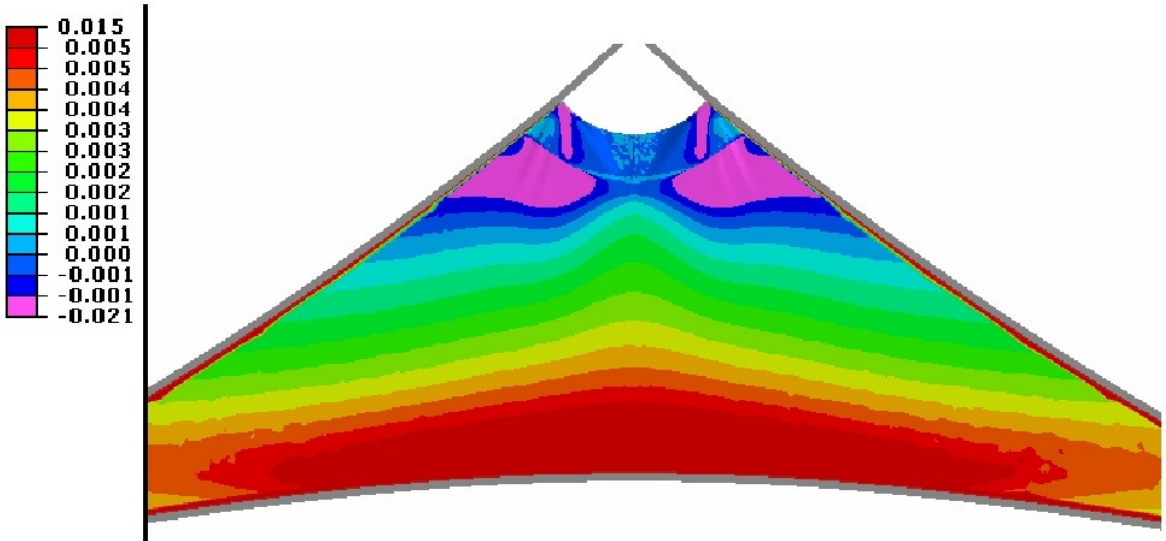

Fig. 103 Horizontal strain ε_{11} [-] for model with inversed fiber direction in the reinforcement layer at top load of L_3 =7 kN

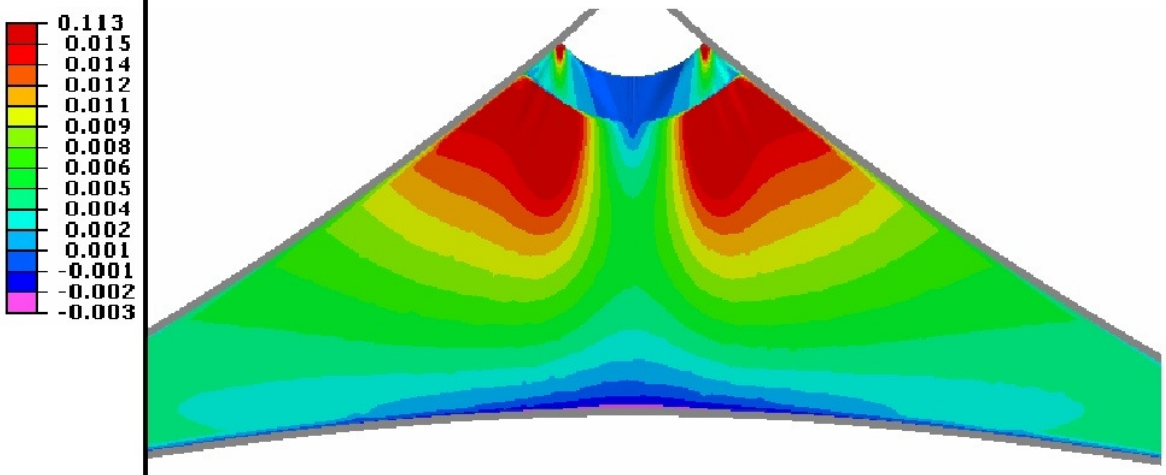

Fig. 104 Vertical strain ε_{22} [-] for model with inversed fiber direction in the reinforcement layer at top load of L_3 =7 kN

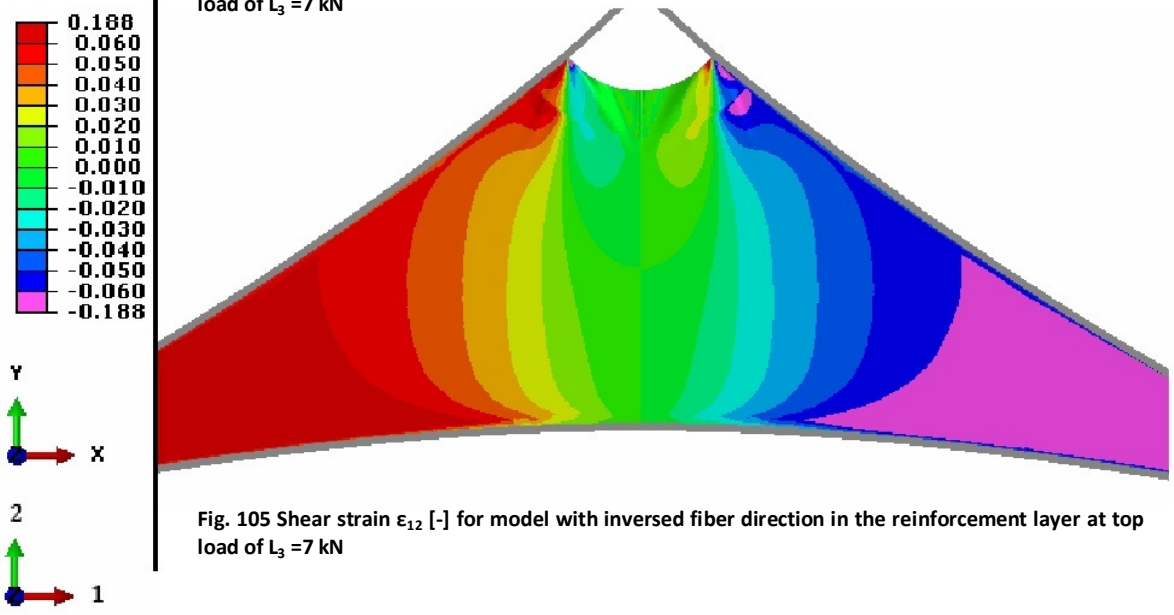

Fig. 105 Shear strain ε_{12} [-] for model with inversed fiber direction in the reinforcement layer at top load of L_3 =7 kN

5.4.2 Contour plots inversed fiber direction in all membrane parts

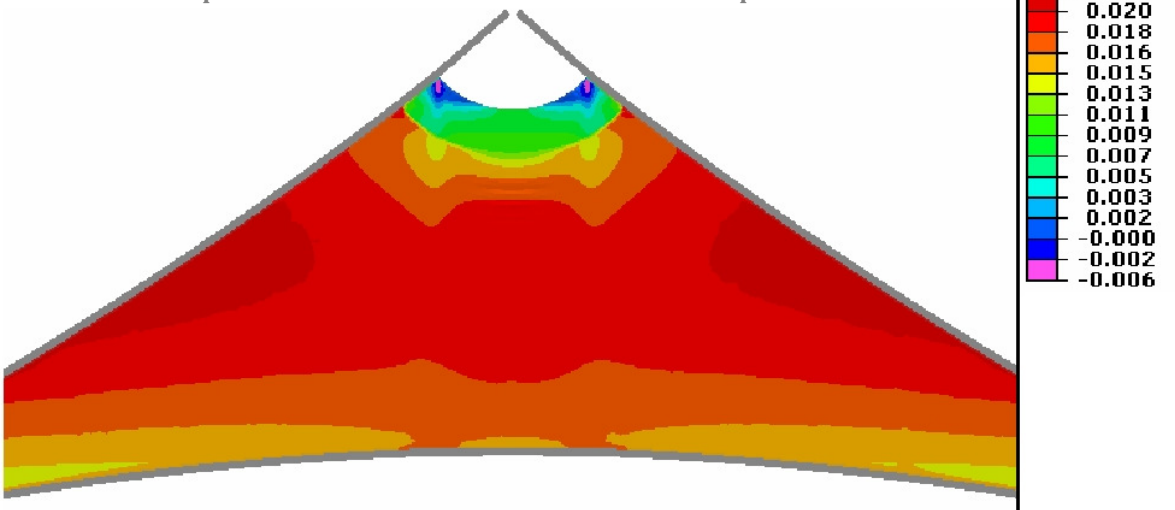

Fig. 106 Horizontal strain ε_{11} [-] for model with inversed fiber direction in all membrane parts at top load of L_3 =7 kN

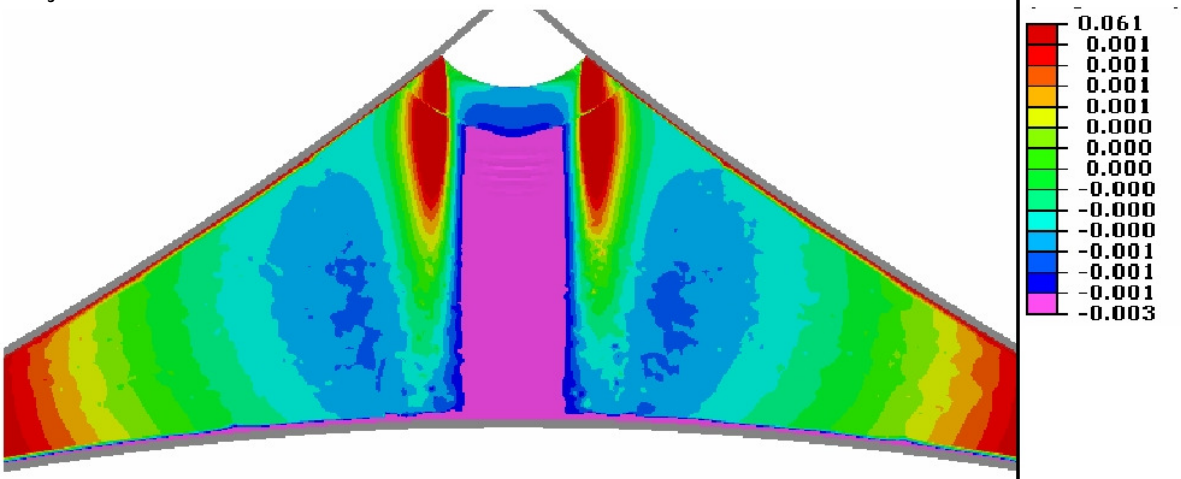

Fig. 107 Vertical strain ε_{22} [-] for model with inversed fiber direction in all membrane parts at top load of L_3 =7 kN

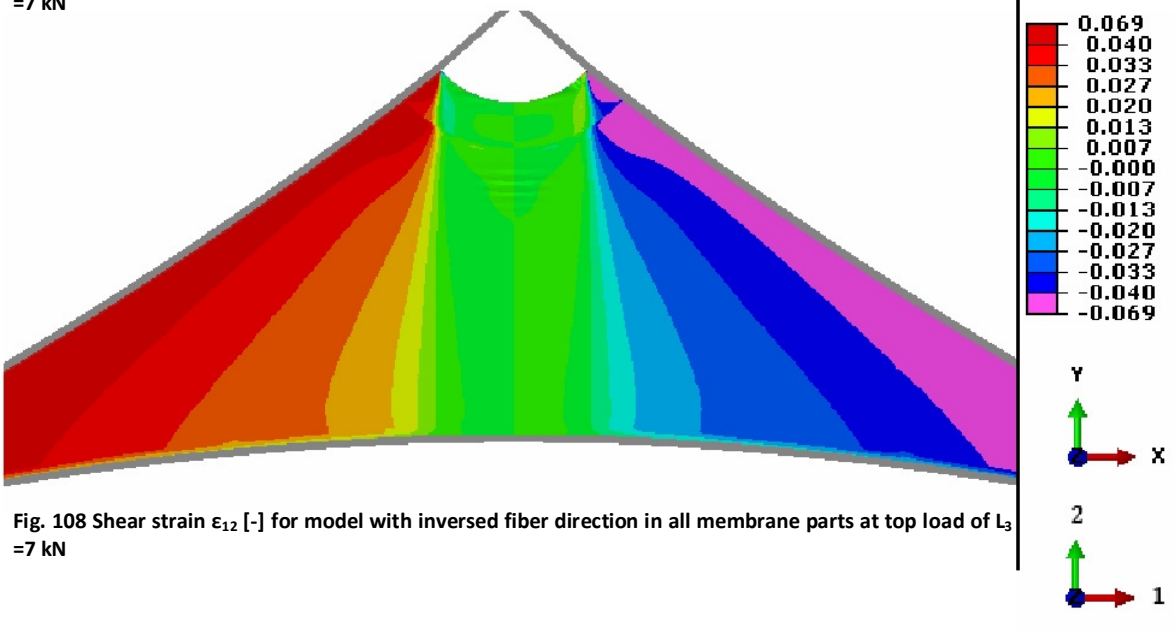

Fig. 108 Shear strain ε_{12} [-] for model with inversed fiber direction in all membrane parts at top load of L_3 =7 kN

5.4.3 Qualitative comparison

The change of fiber direction in the reinforcement layer is clearly noticeable in the contour plots of horizontal and vertical strain (Fig. 103 and Fig. 104). The compressed area for ε_{11} in at the top of the membrane has increased significantly and is not anymore only concentrated in the 2 corner points P1 and P2, but more equally distributed over the whole top area. This indicates that the membrane will wrinkle heavier than in the case of equal fiber directions.
The tensile stresses in the top part have increased enormously. The maximum vertical stress σ_{22} has now a value of 47 MPa(!) (Fig. 109). However, the cooperation of the stiffer warp fibers in the reinforcement layer with the softer fill fibers of the larger membrane part prevents this last one from deforming easily. This was not the case in the original global warp-fill orientation. The displacement of the upper joint RP3 in is constrained to 182 mm in order to cause a reaction force of 7 kN, versus 189 mm in the original part. Hence, the overall stretching of the model has decreased with 7 mm. Therefore, the strain ε_{22} is much smaller in this upper area.
On the other hand, the stress that progresses to the single layered membrane partition do not proceed 6 MPa. This indicates that the stress and strain in that area is does not significantly differ from the model with global warp-fill orientation. This finding shows again the importance of the reinforcement layer, as was already pointed out in 3.4.2.3.

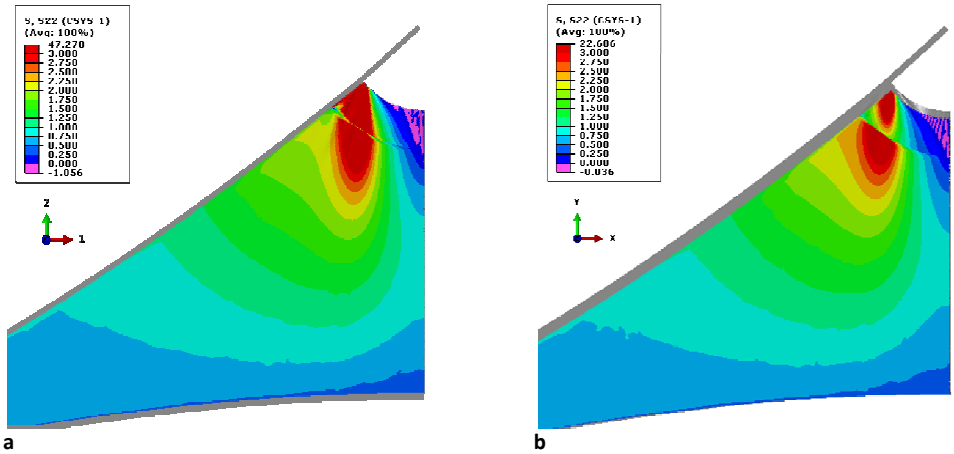

a **b**

Fig. 109 Distribution of vertical stress S22 in the top corner of the membrane with fill-warp orientation in the reinforcement layer (a) in comparison to the original stress distribution with warp-fill orientation (b)

When a closer look is given at the contour plots of the model with complete inversed fiber direction, we can see many differences from the original orientation. For the horizontal strain, the tensile area that was present at the lower part of the membrane, now covers almost the complete membrane. Only the top shows a small remaining neutral area, with slightly compressed regions at the corners.
Furthermore can be remarked that the tendency of the patterns for the fill-warp direction shows more analogy with an isotropic material. This phenomenon is also described in ' *Form and function: The significance of material properties in the design of tensile fabric structures*' [76], and can be declared as follows.
The user material is implemented with adaptive Young's moduli. However, in the initial phase of loading, they can be approximated by E_{warp}=1270 MPa and E_{fill} = 160 MPa [75].
In the originally oriented model (warp-fill orientation), mainly the fill yarns are charged. Their initial waviness, called crimp, is stretched out before the yarns are actually loaded. The change in configuration of the fill yarns exerts a force on the warp yarns. This interaction is called crimp interchange and was already described in chapter 2 (Fig. 7).
Meanwhile, when the fiber orientation is inversed, mainly the warp yarns take account for the applied load, as is the case in the studied model here. Because they are already straight in the beginning, the effect of crimp interchange is now less expressed. Since the load is applied along the vertical direction, the stiffness of the warp fibers predominates, and so the behavior of the membrane as a whole is closer to that of an isotropic.

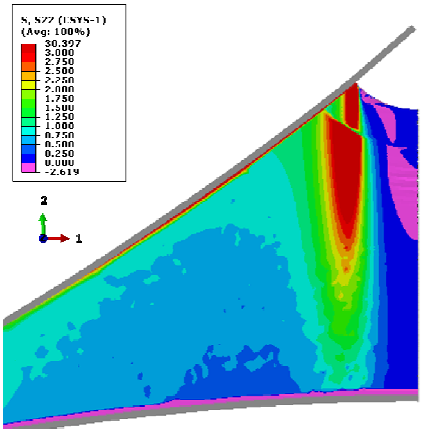

Fig. 110 Distribution of vertical stress S22 in the top corner of the membrane with fill-warp orientation in all membrane parts

In Fig. 110, one can clearly notice that the stress S22 has propagated much further through the membrane and is more locally situated than in the other studied cases. This confirms the idea of the decreased effect of crimp interchange in case of global fill-warp direction. Because of this stress concentration underneath the corners, the yarns that are situated on this location are extremely high stretched (up to 6%), but this large strain stays local and does not spread to the rest of the membrane. However, the diminishing effect of the fill fibers on the warp yarns is now also of less influence. Therefore, the displacement of RP3 is now 201 mm (12 mm higher than warp-fill orientated fabric) for a load of 7 kN.

Table 10 gives an overview of the displacements of RP3 that were required in order to reach a reaction force of 7kN. This gives an indication of the stretchability of the model as a whole.
It can be noticed that the change in orientation of the reinforcement layer causes less elongation (4%), while for the fill-warp orientation of the complete model a much higher displacement (6%) was established.

Material	Displacement of RP Top for a load of 7 kN
UMAT- warp-fill oriented	189 mm
UMAT- double layer fill-warp oriented	182 mm
UMAT - completely fill-warp oriented	201 mm
Orthotropic material	192 mm
Isotropic material	126 mm
Experiment	344 mm

Table 10 Overview of required displacement of RP Top in order to reach a reaction force of 7 kN in function of the material properties

5.4.3.1 Quantitative comparison

To have a better insight in the effect of change in fiber direction, the strains ε_{11}, ε_{22} and ε_{12} are plotted along the same 3 paths as were investigated chapter 3. The following graphs show the relation between the original warp-fill oriented model, the model with inversed orientation in the reinforcement layers and the completely fill-warp oriented model, and this for a top load of L_3 = 7 kN. Subsequently, the same was done to know the influence on the stress. The same graphs, but this time with the effect on σ_{11} , σ_{22} and σ_{12} are also displayed.

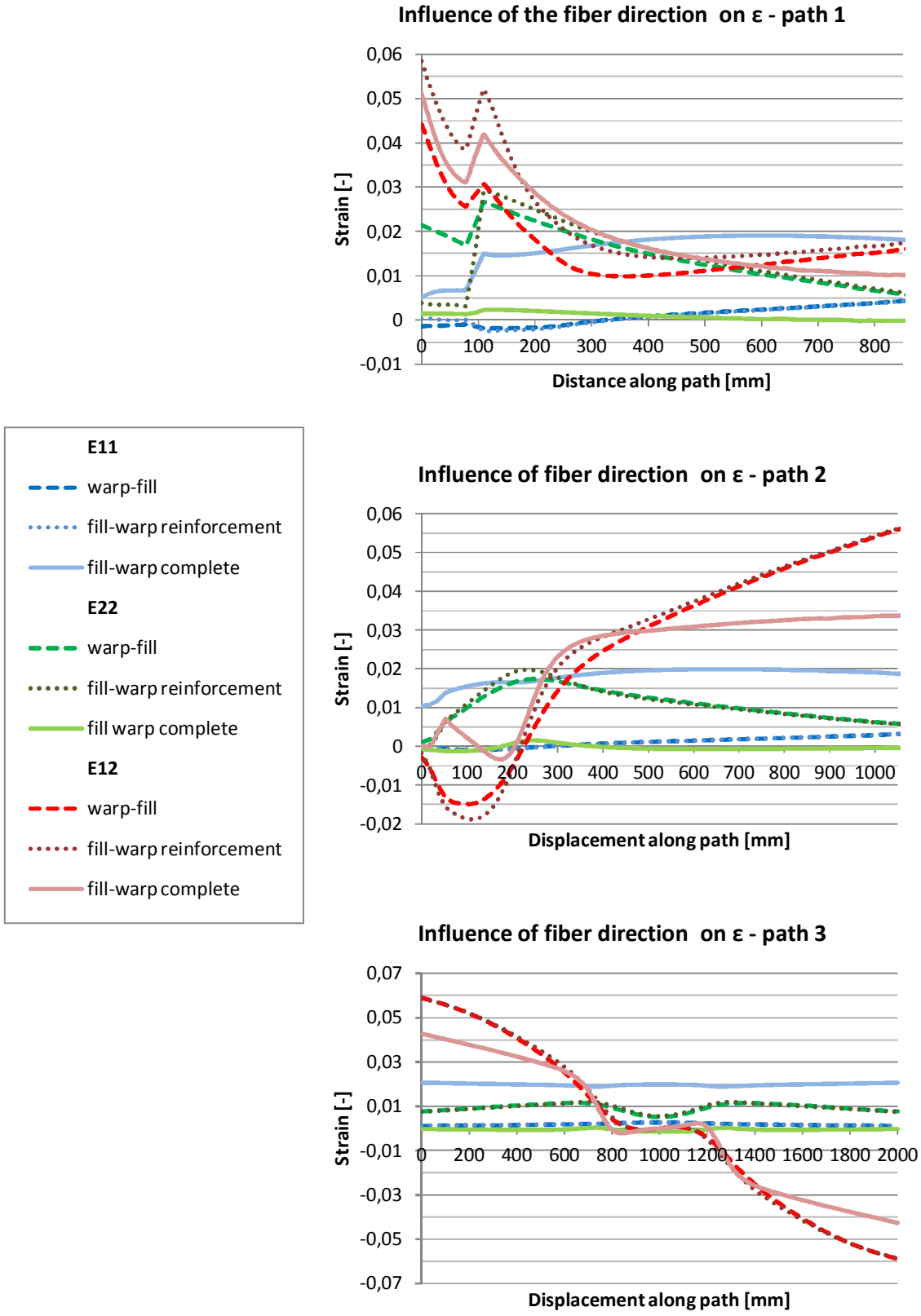

Fig. 111, Fig. 112 and Fig. 113 Influence of the fiber direction on the strain, respectively for path 1, path 2 and path 3

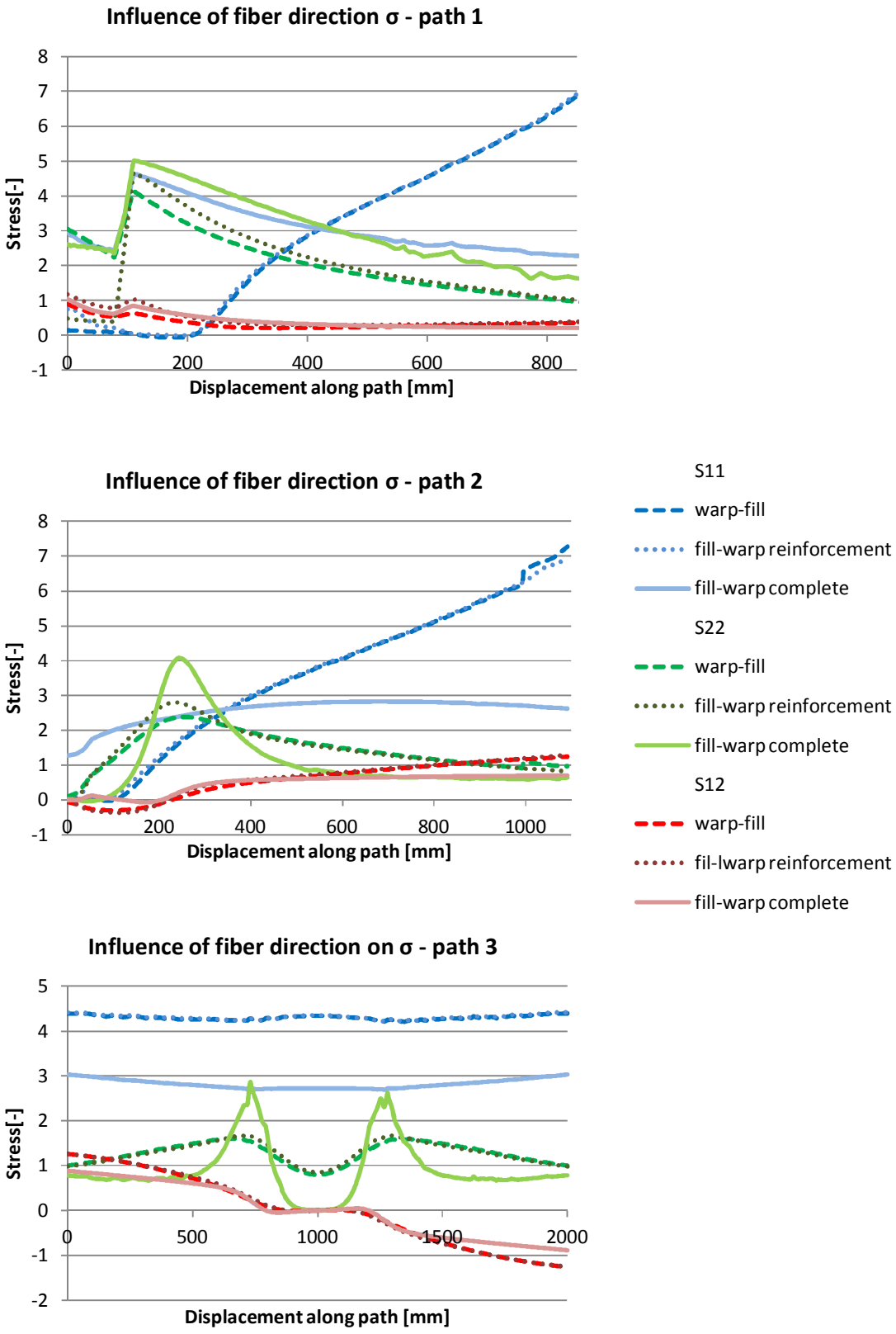

Fig. 114, Fig. 115 and Fig. 116 Influence of the fiber direction on the stress, respectively for path 1, path 2 and path 3

From the graphs can be seen that ε_{11} (blue lines in Fig. 114-116) increases significantly when the orientation of the fibers is completely reversed (full blue line versus dashed blue line). This equals at the same time a more stable stress σ_{11} along the height (path 1) of the triangular membrane, because the much softer fill yarns are replaced by the stiffer warp yarns. An average augmentation factor of 81 is calculated, as shown in Table 11. However, this value is almost only affected by path 2, that increased enormously. If we have a look at Fig.115 however, we can see that it is caused by a local maximum, located underneath the top corner P1. This could also be noted in the contour plots for ε_{22}. The values are locally very high, but in the rest of the membrane they are almost zero.

It could also be noted that changing the fibers to fill-warp in every part of the membrane, has a slightly positive effect on the shear. In the contour plot in Fig. 106. shear strains (red lines) have decreased slightly.

With this knowledge, it is difficult to decide whether it is better to change the yarns to fill-warp direction. The effect on most of the membrane is very good (e.g. $\varepsilon_{22} \approx 0$), but locally very high stresses are measured, causing excessive strains in those areas. This will probably have a negative effect on the fabric after some time.

Fill-warp orientation - reinforcement layer only

	path 1	path 2	path 3	TOTAL
ε_{11}	-0,066	-1,786	-0,005	-0,619
ε_{22}	-0,013	0,013	0,018	0,006
ε_{12}	0,349	-0,091	0,090	0,116
			GLOBAL	-0,166

a

Fill-warp orientation - complete model

	path 1	path 2	path 3	TOTAL
ε_{11}	-0,774	234,875	10,660	81,587
ε_{22}	-0,957	1,059	-1,075	-0,324
ε_{12}	-0,246	0,319	-0,512	-0,146
			GLOBAL	27,039

b

Table 11 Relative augmentation or diminution of the average strain in each directions compared to the original model with warp-fill direction: (a) model with reversed reinforcement layer and (b) model with completely inversed fiber direction.

Fill-warp orientation - reinforcement layer only

	path 1	path 2	path 3	TOTAL
σ_{11}	0,227	0,169	0,003	0,133
σ_{22}	-0,006	-0,020	0,014	-0,004
σ_{12}	0,336	0,082	0,090	0,169
			GLOBAL	0,099

a

Fill-warp orientation - complete model

	path 1	path 2	path 3	TOTAL
σ_{11}	6,019	4,587	-0,344	3,420
σ_{22}	0,499	-0,339	-0,331	-0,057
σ_{12}	-0,193	-0,372	-0,784	-0,449
			GLOBAL	0,971

b

Table 12 Relative augmentation or diminution of the average stress level in each directions compared to the original model with warp-fill direction: (a) model with reversed reinforcement layer and (b) model with completely inversed fiber direction.

On the other hand, the use of a reversed reinforcement layer has a positive influence. The strains in horizontal direction have diminished considerably (62%), while the global strain has diminished with almost 17%. Mainly the diminution of vertical strain and stress in path 1 points out the favorable interaction between the opposite fiber directions of the welded parts at the apex of the membrane. The global stress increases only slightly (9,9%).

5.4.3.2 Conclusion

When the fiber orientation of the membrane as a whole is inversed, globally the strain has decreased, but locally excessive values occur, especially underneath the corners RP1 and RP2 at the top. Hence it is difficult to decide whether this situation is better than vice versa. The assumption at the beginning of this chapter is not easy to confirm. The stress in the membrane exhibits locally very high values (up to 30 MPa).

On the other hand, the change in fiber direction of the reinforcement layers only has a beneficial influence on the membrane as a whole. With the cost of a slight increase in stress due to the interaction between the reversed layer and the original direction of the larger membrane part. The strains in horizontal direction are reduced with 60%. The triangular shaped membrane as a whole has an average total loss of strain of almost 17%.

Chapter 6 | Conclusions and recommendations

"What we call the beginning is often the end. And to make an end is to make a beginning. The end is where we start from."

T. S. Eliot, 1888-1965

6.1 General conlusion

In the perspective of the research on design methods for tensile architecture and in particular reconfigurable and kinematic membrane constructions, this thesis presents a method to simulate an architectural tension membrane coated fabric using finite element method.

A literature study revealed the suitability of membrane elements to represent the structural behavior on an appropriate level. Membrane elements are able to generate stress and strain information of the fabric in an accurate way, without detailed simulation of wrinkles.
The large deformations of coated fabrics under loading are different in each fiber direction, provoked by the severely non-linear elasto-plastic orthotropy of the material. A proper solution method to deal with these highly non-linear deformations is found with the introduction of a viscous force as an artificial damping. Although one must take care in defining the parameters of the damping factor, it is noted that this solution method provides fast and reliable results.

Nevertheless, the simulation results have no meaning without a proper benchmark. Therefore an experiment with a triangular shaped membrane was performed at the Free University in Brussels, loading it only in-plane. By use of the Digital Image Correlation (DIC) technique, the strain patterns for different load levels are recorded, providing enough data to compare with the output of the simulations. During the experiment, large values of strain were observed for both fill and shear direction (range of 1/100), whereas the warp direction only showed strains in the range of 1/1000.
Using the developed non-linear elasto-plastic orthotropic user material as a subroutine, the material behavior of the fabric was mimicked in the simulations for the experiment.

Two approaches for comparison were used to verify the obtained results.
In general, a good correlation was found between the experimental data and the simulation results. The simulated strain patterns are in agreement with the patterns produced by DIC. Moreover, it has been pointed out that the magnitudes of the strain values obtained from the simulation are of the same order with the experiments. The achieved results demonstrate an average deviation with the experimental values between 26% and 50%, depending on the investigated direction. Although these discrepancies are relatively high, they must be interpreted in the perspective of the many factors that can affect the miscorrelation. The most important parameters can be ascribed as:

- The small difference in geometry between the experimental setup and numerical model
- The slightly unequal location of the corresponding paths
- The experimental data is not as stable as the output from the numerical program: varying values and local aberrations due to imperfections cause excessive outliners
- The material model used for the simulations has a only a very small compressive stiffness, resulting in the formation of wrinkles at the slightest pressure force, which was not always established during experiments
- The numerical model is based on biaxial tests with a load ratio 1:1, which is different from the load case in this experiment.

This last problem results in larger deviations as the load is increased, since the load ratio differs with each increment more and more from 1:1.

Finally, the improvements over the more conventional orthotropic and isotropic material models are confirmed. The user material shows an improvement of respectively about 33%% and 66%, requiring only a higher calculation time, but still within a reasonable extent.
The parametric study in the second phase of the project shows that reversing the fibers direction can result in a different deformation of the fabric. In the case of reversing only the fiber directions of the reinforcement layers, the total strains in the membrane have diminished with almost 17% with only a local increment of stress, ascribed to the cooperation of the inversed layers. On the other hand, reversing of the fiber direction in all membrane parts causes lower stresses when the model is viewed in total. Nevertheless, this fiber configuration exhibits local peaks of excessive stress and strain, concentrated underneath the corners of the upper edge. The main reason for this is the reduced interaction between warp and weft fibers.

6.2 Recommendations for future works

Unfortunately, no experimental data is available yet for these situations, but this can be a suggestion to test in the future. The limited time span of this thesis did not allow investigating all possibilities of fiber direction, but this is also something that can be investigated later on. Furthermore, in the presented work the macro-scale coated fabric is approached using membrane elements. Hence the formation of wrinkles remains ambiguous. The elements lack bending stiffness hence the out of plane displacement of the nodes is only influenced by the element shape and the size of the meshing. It would be interesting to use shell elements in order to explore the improvement or deterioration compared to membrane elements.

All these findings prove that the research on the structural behavior of membranes in architecture and the development of their counterpart in numerical simulation is far from finished. Nevertheless, every improvement is a step closer to a more sustainable design method to predict the mechanical behavior. The beautiful and enriching opportunities of tensile architecture must encourage researchers and designers to proceed with investigations and experiments on this complex matter, in order to obtain more accurate predictions of the structure and more economic material use.

Appendix

In this appendix, one can find additional studies that were carried out. However, they are incomplete. Care must be taken in interpreting the results. They are added to this master thesis, because they can give an idea of other possible subjects to investigate. Unfortunately, the limited span of this thesis did not allow to fulfill them.

A. Incorporating gravity

Since we are dealing with lightweight structures, the influence of gravity is of a minor concern and will only have a small influence on the construction. But for reasons of completeness, the gravity load was once added to the model to check if this could slightly ameliorate the results, because the gravity force works in the opposite direction of the applied force.
From the contour plots, almost no difference was noticed for horizontal and shear strain. However, in vertical direction, the stretched area increased significantly. The image can be found in Fig. 117.

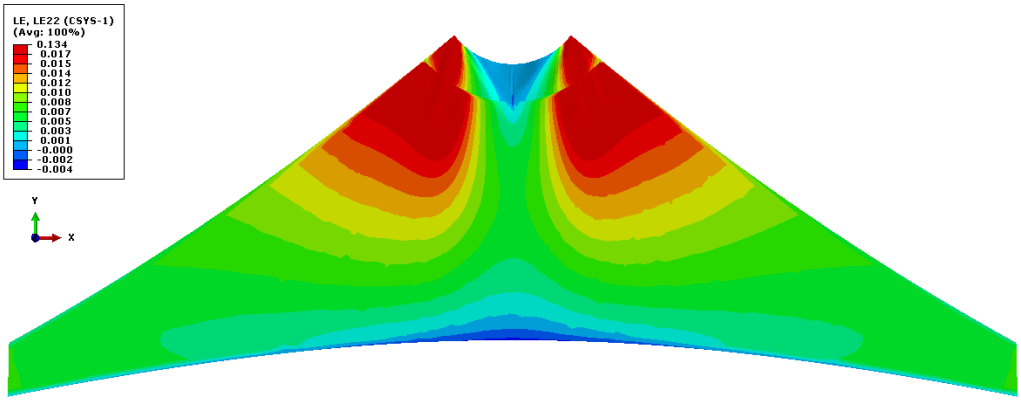

Fig. 117 Contour plot of vertical strains at a top load of L_3 = 7 kN for the model with user material and gravity incorporated [MPa]

This has a negative influence on the comparison with the experimental data. The values for vertical strain were already higher with gravity incorporated, and now, this difference only increases. In the box plot in Fig. 118, the change in deviation is illustrated by the use of path 2. One can see the deviation for the 3 strain directions, at a top load of L_3 = 7 kN, along path 2, and this for the model with gravity. The values from the model without are repeated here to allow comparison.

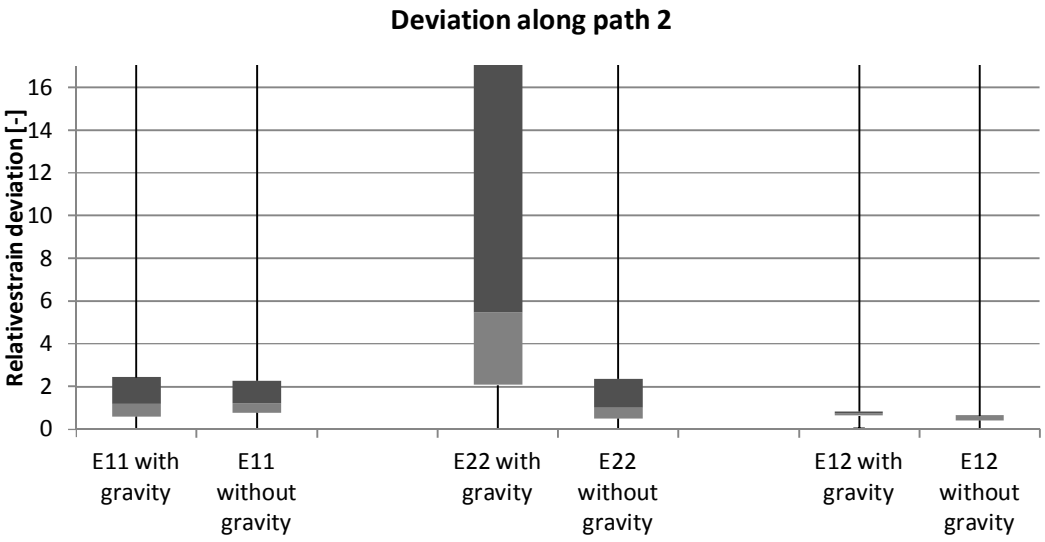

Fig. 118 Change in deviation for the model with and without gravity, at a top load of 7 kN. The strains in all directions are given along path 2.

However, the limited time span of this master thesis did not allow to investigate this issue. This can be a recommendation for future researchers.

B. Kinematic simulation of opening and folding membrane structure

The main topic of this thesis was researching the correlation of an in-plane loaded triangular model. However, the aim of the KFAS project is investigating the behavior of the coated polyester in a retractable system. Since the numerical model is proved sufficient for the in-plane simulation, the transition to the out-of-plane three dimensional modeling can be made. The limited time span of this thesis did not allow to solve this problem completely, but a first onset of a possible strategy is documented in this chapter, after a description of the experimental setup of the problem. However, no details about the topic are known, since the limited time span did not allow to do a good literature review. The simulation that was performed is only based on the knowledge that was gained in the previous simulations of the triangular shaped model in chapter 3.

B. 1 Experimental setup

In 2011, a dome-like structure called 'Contex-T' has been designed and built within an European Union-funded Project. The purpose of this project was to examine the foldability of a retractable system made out of angulated beams and a membrane skin in between (Fig. 119). Simultaneously the stability of the membrane in intermediate configurations was questioned.

a **b**

Fig. 119 (a) concept of the Contex-T project: a dome-like structure with foldable frame and (b) real scale demonstrator of the Contex-T in two intermediate positions

The structure is composed out of 14 identical triangular panels and two boundary panels. The skin is an assembly of flat triangular pieces, welded together into a three dimensional part. The whole is tensioned in a foldable frame using adjustable belts.
To gain more insight in the feasibility of the concept, one unit of the dome was made separately and studied in the AE lab at the VUB in Brussels. This single membrane will be investigated in what follows.

B.2 Geometry and confection

Two membrane panels have been cut from an isosceles triangle with a top angle of 120° and a base length of 6m. The exact geometry is the same as for the two dimensional setup and can be found in the illustration in chapter 3 (Fig. 32). Again, the warp direction of the fibers is aligned with the base border. The two membranes are welded together along the long side. Thus, the unstressed geometry is in this case derived from an unstressed folded state [77].
As it was the case for the triangular shaped membrane in chapter 3, also in the three dimensional (3D) setup, the edges are reinforced by use of belts, and the apex of the membrane is reinforced by a double layer, continuously welded in a similar way as for the reinforcement layer of the first setup.

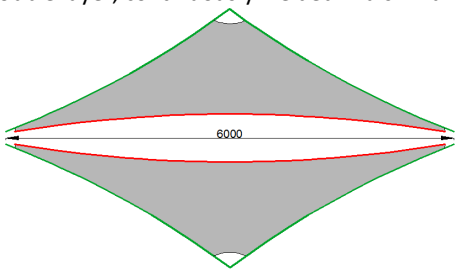

Fig. 120 The geometry of the assembled panels. In green: the place where belts are stitched as reinforcement in red: the welding line

B.3 Setup and loading

The purpose of the 3D-setup was to test if it was possible to obtain intermediate stages between fully opened and fully closed, that are stable and without wrinkles. The initial state of the membrane is closed, and the opining angles of 50° and 90° are achieved by placing a rigid bar between the top corners, as can be seen in Fig. 121.

a b c

Fig. 121 Three examined positions during the 3D-experiment. (a) initial state (b) intermediate state with 50° opening and (c) final state at 90° opening

To achieve these configurations, the model was positioned in place by hanging it from its corner points. The bottom corners were again held fixed during the whole time span of the experiment. However, in this setup an extra belt is laid in the fold of the membrane, allowing to pretension the structure. This belt is not attached to the membrane itself, but connected in the same joints as the bottom corners of the membrane model.

a b

Fig. 122 (a) connection point of reinforcement belts and central belt (b) position of the central belt

After imposing a defined opening angle using the rigid bar, it was tried to tension the membrane in such a way that all wrinkles disappear. This was achieved only by pulling the center of the rigid bar upwardly.
The required force to reach this 'non-wrinkled'-state was recorded by a load cell, positioned in between the hook of the crane and the connection point of the rigid bar (Fig. 123).
For each position, the state without wrinkles required a force of respectively 4,98 kN and 5,38 kN for initial state and 50° opening angle. For 90°-opening the lengths of the top belts had to be adjusted. After abn elongation of these belts, a force of 4 kN was necessary to reach a 'flat' state.

Fig. 123 Global view of the 3D-setup

B.4 Numerical model

As it was already mentioned in the beginning of this section, the research on this model is not complete. Only the first findings are represented here, but the tight time schedule did not allow to document everything with literature studies. What is shown are only own findings and tests, so further researchers are recommended to do first a review of available methods, before proceeding on this topic.

B.4.1 Geometry

The geometry to implement in Abaqus is derived from the geometry of the triangular shaped setup in chapter 3. The same dimensions are used. Only, since we are dealing with a 3D-model, 2 flat membrane triangles are drawn and connected with a curved part in between.

b) By use of the program AutoCAD , a three-dimensional model was created.

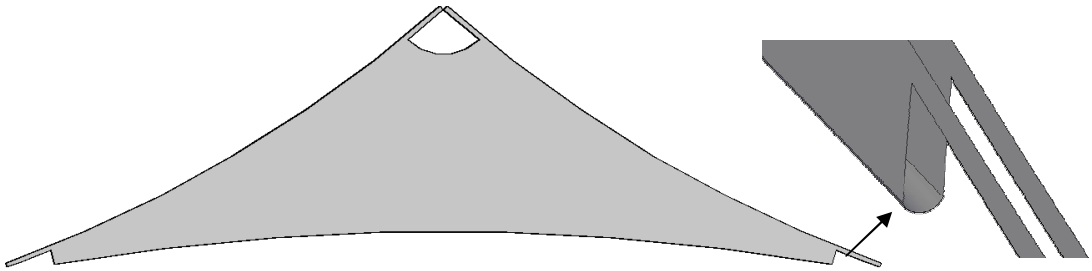

a **b**

Fig. 124 Geometry from AutoCAD, as implemented in Abaqus. (a) overview (b) detail of the curved part in between the two flat panels

B.4.2 Recommendations for contact between belt and membrane

There are several possibilities for the element type of the belt.
For example truss, solid, membrane and shell elements could be effective.
An investigation to the best type to simulate the contact was started, but could not be finished.
- Truss elements proved to be unworthy, because no contact to their outer surface can be assigned. Thus, only contact is made with the central axis, resulting in a line-contact, which is unwanted.
- Solid elements can overcome this issue. One simulation with this element type converged, but very high damping had to be used. However, it is difficult to say if this was due to the element type, because also some mistakes regarding the boundary conditions were made.
This is something that can be investigated further.
- Membranes were also tested, and could be a possible solution.

Because the short time span did not allow to test everything, it is difficult to tell which one will perform better.

What can be said, is that better convergence may be obtained if the welded curve at the bottom side of the membrane is not drawn so round. If the curvature could take more the shape of the belt, e.g. a more flatter curvature, easier contact can be made, and this will reduce the calculation time. A proposal is schematically shown in Fig. 125.

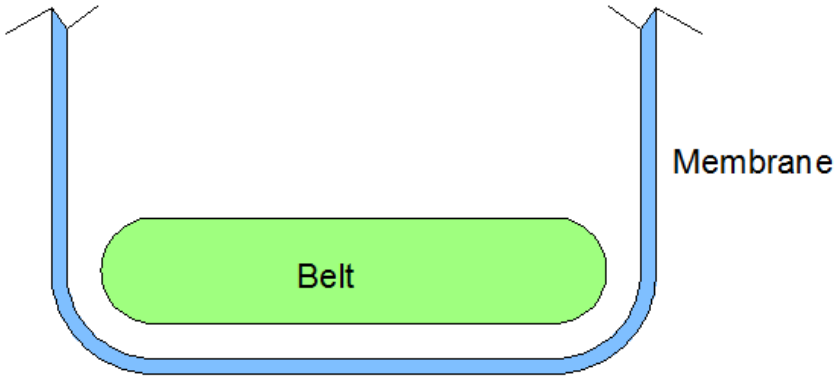

Fig. 125 Proposed geometry to ease contact : section perpendicular through belt and membrane

C Product Sheet T2107

SIOEN COATING
Branch of Sioen Industries

Fabrieksstraat 23, B-8850 Ardooie - Tel +32(0)51 74 09 00 - Fax +32(0)51 74 09 64
sioline@sioen.be - http://www.sioen.com

Technical Data Sheet

T2107

Adhesion / Hechting / Adhérence / Haftung / Adherencia	120 N/5cm	EN ISO 2411 2000
Temperature resistance / Temperatuursbestendigheid / Tenue à la température / Temperatursbeständigkeit / Resistencia a la temperatura	-30/+70 °C	DIN EN 1876/2 1998
Light fastness (Except white and (half-)transparent)	7-8	ISO 105 B02 1988
Lichtechtheid (Uitgezonderd wit en (half-)transparent)		
Tenue à la lumière (Excepté en blanc et (semi-)transparent)		
Lichtechtheit (Ausnahme weiss und (semi-)transparant)		
Resistencia a la luz (Excepto blanco / (semi-)transparente)		
Fire behavior / Brandgedrag / Reaction au feu / Brennverhalten / Fire behavior	M2	NF P 92 507 2004
Fire behavior / Brandgedrag / Réaction au feu / Brennverhalten / Fire behavior	B1	DIN 4102 1981
Reaction to fire / Reactie bij brand / Reaction au feu / Brennverhalten / Reacción al fuego	B-s2,d0	EN 13501-1 2007
Application Tent&TA/ArcMembrane		

"This product may for certain colours contain substances which fall under the Annex XIV of the Reach Regulation 1907/2006/CE. In order to know which colours fall under this annex , you can take contact with the technical department of Sioen Industries. Upon request those substances can be eliminated from the product."

All our technical characteristics are indicative
Rev. 01/11

SIOEN COATING
Branch of Sioen Industries

Fabrieksstraat 23, B-8850 Ardooie - Tel +32(0)51 74 09 00 - Fax +32(0)51 74 09 64
sioline@sioen.be - http://www.sioen.com

Technical Data Sheet

T2107

Fabric / Weefsel / Tissu / Gewebe / Tejido	100 % PES / 1100 dtex	
Weaving style / Binding / Armature / Bindung / Weaving style	P2/2	DIN ISO 9354
Total weight / Gewicht totaal / Poids total / Totalgewicht / Peso total	1050 g/m²	DIN EN ISO 2286/2 1998
Characteristics / Eigenschappen / Caractéristiques / Eigenschaften / Characteristics	ABUV	
Lacquering / Vernis / Lackierung / Lacado	1/1	
Comment / Opmerking / Remarque / Kommentar / Comentario	SIOFLUO	
Embossing / Kalander / Calandre / Lackierung / Embossing	Glossy	
Breaking strength Warp Treksterkte Ketting Résistance rupture Chaîne Höchstzugkraft Kette Resistencia a la rupture Urdimbre	4000 N/5cm	EN ISO 1421/1 1998
Breaking strength Weft Treksterkte Inslag Résistance rupture Trame Höchstzugkraft Schuss Resistencia a la rupture Trama	4000 N/5cm	EN ISO 1421/1 1998
Tear strength Warp Scheurweerstand Ketting Résistance à la déchirure Chaîne Weiterreisskraft Kette Resistencia a la rasgadura Urdimbre	600 N	DIN 53363 2003
Tear strength Weft Scheurweerstand Inslag Résistance à la déchirure Trame Weiterreisskraft Schuss Resistencia a la rasgadura Trama	500 N	DIN 53363 2003

"This product may for certain colours contain substances which fall under the Annex XIV of the Reach Regulation 1907/2006/CE. In order to know which colours fall under this annex , you can take contact with the technical department of Sioen Industries. Upon request those substances can be eliminated from the product."

All our technical characteristics are indicative
Rev. 01/11

D. Product Sheet belts - Load-lok

SPA WEB
Spa Web Limited
Metcalf Drive
Altham
Accrington
Lancs
BB5 5TU
England
Tel: +44 (0)1282 688100
Fax: +44 (0)1282 688105

Product Specification Sheet

Product:	**368/25**
Description:	2000kgs lashing webbing
Material:	Polyester
Weight:	62 gms/mtr + 5 - 5
Width:	25 mm + 2 - 2
Thickness:	2.5 mm + 0.5 - 0.5
Minimum Break Strength:	2,800 Kgs
Average Break Strength:	3,000 Kgs
Elongation at MBS:	13.0%
Elongation @ 500Kgs	3.6%
Elongation @ 1000Kgs	6.0%

Printed 12/03/2013

Contour plots simulation UMAT

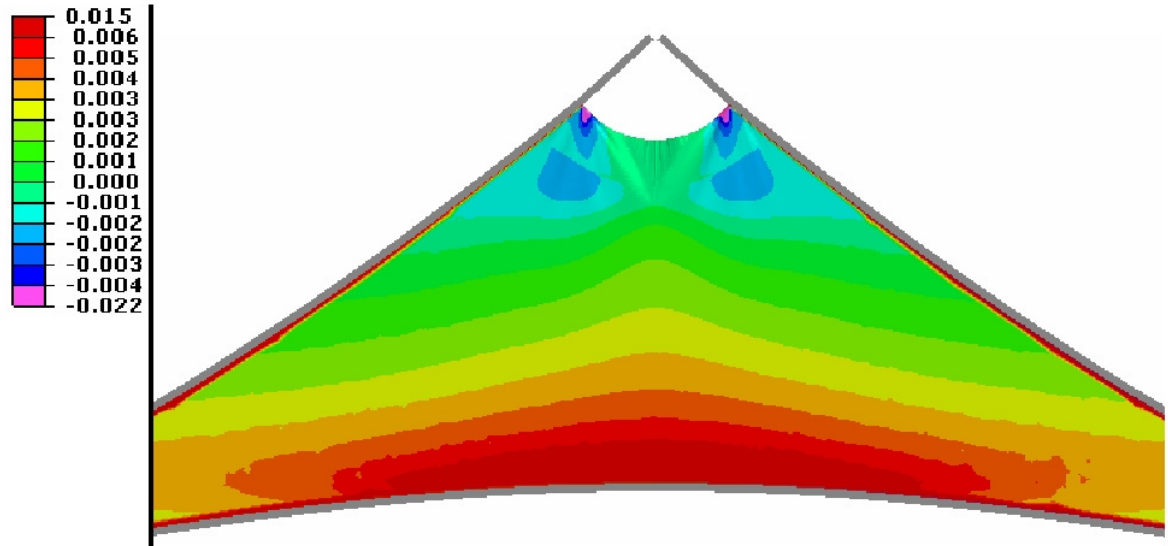

Horizontal strain ε_{11} [-] at top load of L_3 =7 kN

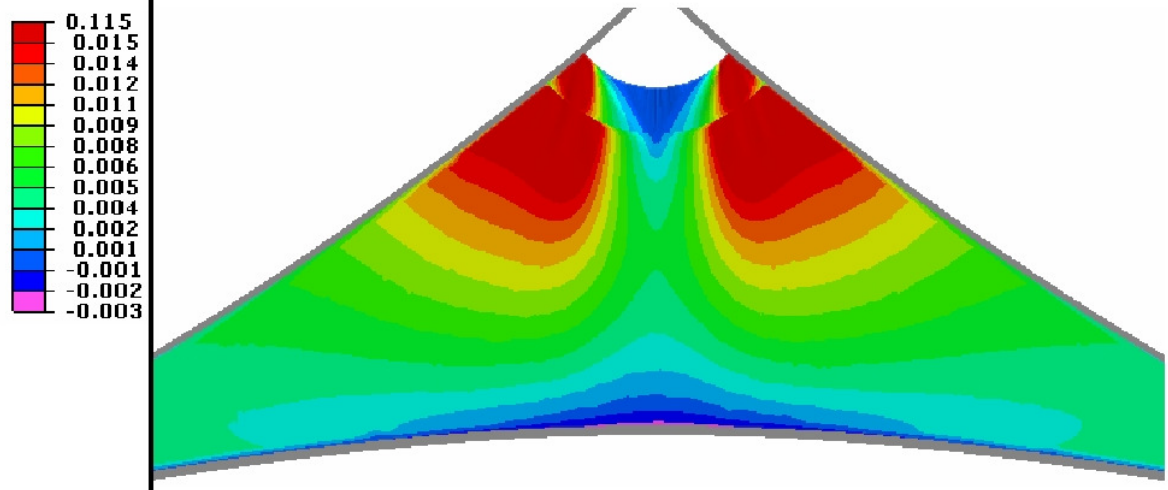

Vertical strain ε_{22} at top load of L_3 =7 kN

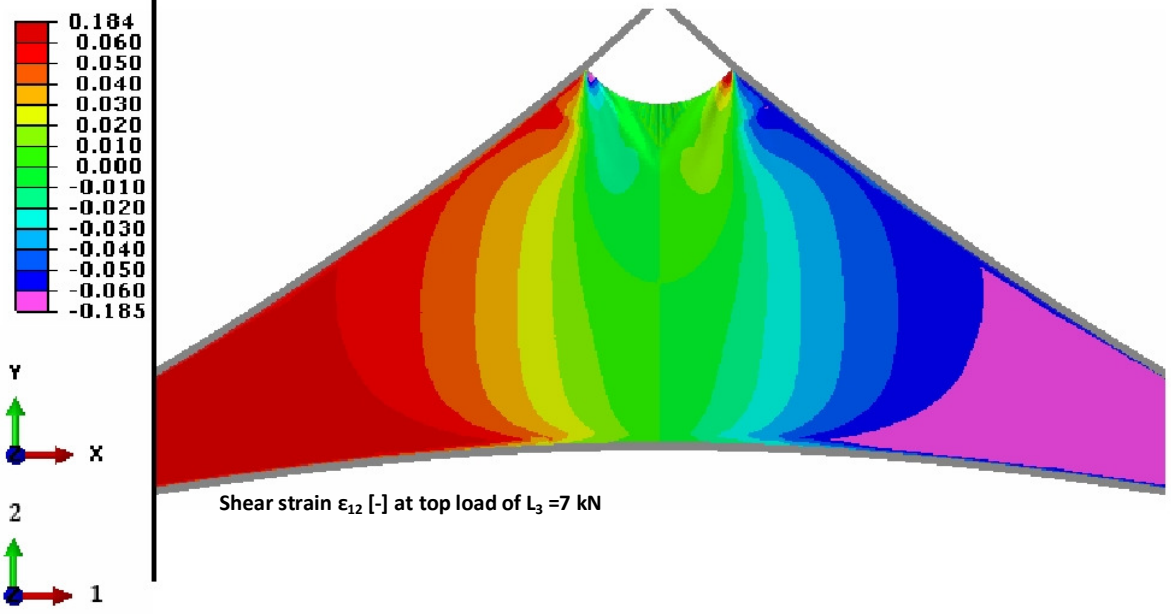

Shear strain ε_{12} [-] at top load of L_3 =7 kN

Contour plots experiment

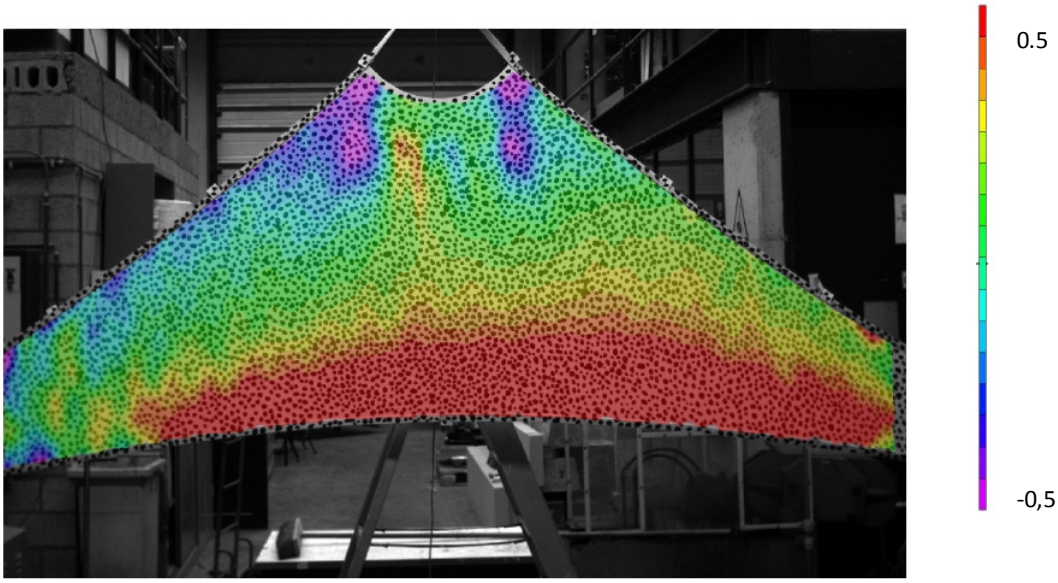

Horizontal strain ε_{11} [%] at top load of L_3 =7 kN

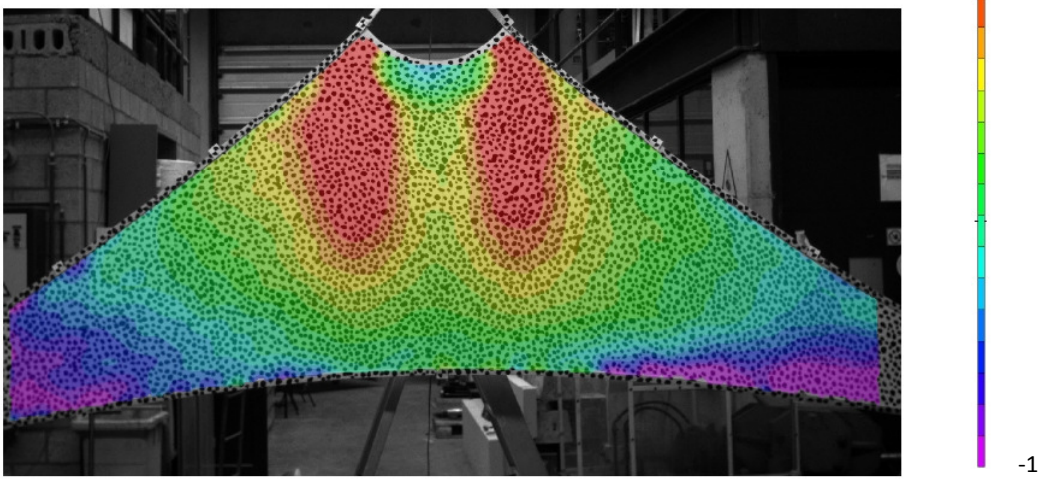

Vertical strain ε_{22} [%]at top load of L_3 =7 kN

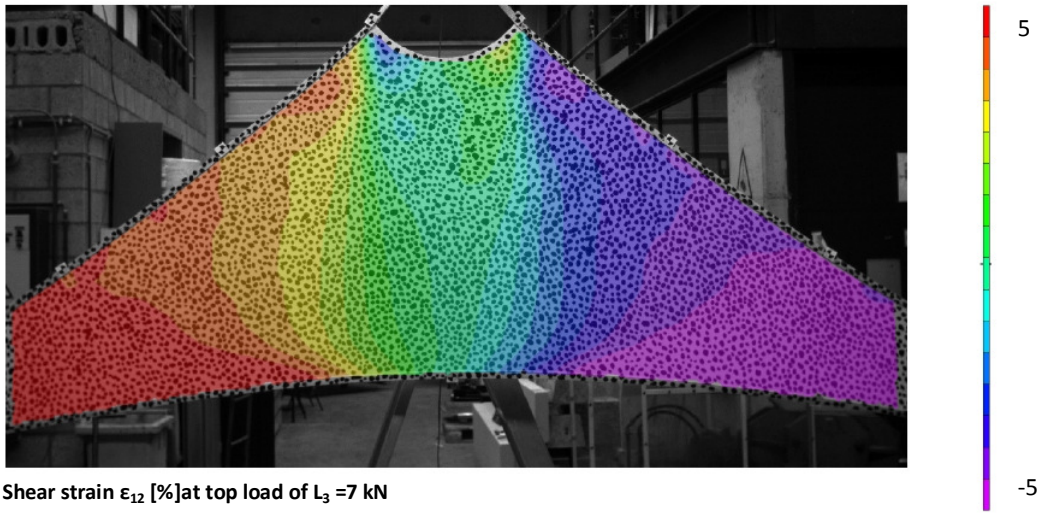

Shear strain ε_{12} [%]at top load of L_3 =7 kN

List of figures

Fig. 1 A tensioned membrane unit folded about 1 axis. (a) The 3 intermediate positions and (b) test setup with opening angle of 50° 3
Fig. 2 Musikpavillon Köln, Frei Otto, 1955 [13] 4
Fig. 3 Eintrittbogen Köln, Frei Otto, 1957 5
Fig. 4 Tanzbrunnen Köln, Frei Otto 5
Fig. 5 Pontiac Silverdome Michigan, Don Davidson [1] 6
Fig. 6 (a) Spreadable process and (b) dipping process [10] 7
Fig. 7 Woven fabric with straight warp and curved fill (a) and the interaction of warp and fill yarns under tension called crimp interchange (b) [16] 8
Fig. 8 Strain in function of stress for fill (a) and warp direction (b) for uniaxial test with increasing load [15] 8
Fig. 9 Strain in function of stress for fill (a) and warp direction (b) for a uniaxial cycle repetition test [15] 9
Fig. 10 Results from biaxial test with different load ratios and cycles: stress-strain curve for fill (a) and warp (b) direction [15] 9
Fig. 11 The landscaping capability of tensile structures [] 10
Fig. 12 Abilene Airport by Fabritec Structures during day (a) and night (b) 10
Fig. 13 Tent of the Glastonbury festival, United Kingdom [] 11
Fig. 14 Foyer of the Masjid Nabawi Mosque in Jerusalem (a) with closed umbrellas and (b) in fully opened configuration in order to provide shading [18] 11
Fig. 15 Opening roof of the bullring in Zaragossa [23] 12
Fig. 16 Mushroom - balloons, Osaka, 1970 [] 12
Fig. 17 Adaptable skin of the Crystalline Towers in Abu Dhabi [] 12
Fig. 18 Experimental approach to shape finding of lightweight structure using soap films [] 13
Fig. 19 Soap-film model for the Munich Olympic Stadium (1972)[] 16
Fig. 20 Approximation of a surface as a cable network [38] 16
Fig. 21 Newton-Raphson method to solve non-linear load-displacement problem[45] 18
Fig. 22 Finding the response of a structure to a load increment ΔP: first iteration 19
Fig. 23 Finding the response of a structure to a load increment ΔP: second iteration 19
Fig. 24 Load parameter control in Riks analysis [45] 21
Fig. 25 Riks algoritm 22
Fig. 26 Benchmark : initial geometry (a) and deformed geometry (b) 22
Fig. 27 Energy balance with damping factor c=0.0002 23
Fig. 28 Deformed state after simulation with too high damping 23
Fig. 29 Energy balance with damping factor c = 2e-8 24
Fig. 30 Comparison of displacement along diagonal axis 25
Fig. 31 (Deformed) Saddle shape with diagonal path in red 25
Fig. 32 Design dimensions of the model, fully symmetric about the dashed line [mm] 28
Fig. 33 (a) Detail of different parts of an anchor point, here at a bottom corner, but analog for top. .. 29
Fig. 34 Naming convention of the model 29
Fig. 35 Connection details of (a) top connection: belts - end clamps - load cell - crane and (b) bottom connection: belts -load cell - turnbuckle fixed structure. 29
Fig. 36 Global view of the triangular shaped test setup just before loading 30
Fig. 37 The slack in the central area after the first load cycle 30
Fig. 38 Comparison of the user material (FEM) with the experimental data from biaxial tests in stress-strain diagrams for warp (a) and fill (b) direction 31
Fig. 39 Assembly of the simplified in-plane triangular shaped model 32
Fig. 40 Schematic illustration of the layup in the simplified model (a) in contrast to the layup in reality (b) 32
Fig. 41 Assembly of the complete numerical model equivalent to the experimental configuration 33
Fig. 42 Load applied on a reference point (a) at a bottom corner (b) at the top). The RP is coupled with the nodes at the end edges of the belts 34

Fig. 43 Two-dimensional element shapes available in Abaqus [], with their integration points in green 35
Fig. 44 Indication of examined point and followed path 35
Fig. 45 Values of the stresses S11 and S22 at point 1 in the membrane for 5 different mesh sizes..... 35
Fig. 46 Computational time of the 5 different meshes in function of their number of elements 36
Fig. 47 Stress S11 along a path running from the upper left membrane corner to the central area for 5 different mesh sizes..... 36
Fig. 48 S22 along a path running from the upper left membrane corner to the central area for 5 different mesh sizes..... 37
Fig. 49 Mesh used in the FEM model..... 37
Fig. 50 Schematic overview of paths along whom the strains are compared (coordinates are in [mm]) 39
Fig. 51 Contour plot simulation for horizontal strain ε_{11} [-] at L_3 =2 kN 40
Fig. 52 Contour plot simulation for horizontal strain ε_{11} [-] at L_3 =4 kN 40
Fig. 53 Contour plot simulation for horizontal strain ε_{11} [-] at L_3 =7 kN 40
Fig. 54 Contour plot experiment for horizontal strain ε_{11} [-] at L_3 =2 kN..... 41
Fig. 55 Contour plot experiment for horizontal strain ε_{11} [-] at L_3 =4 kN..... 41
Fig. 56 Contour plot experiment for horizontal strain ε_{11} [-] at L_3 =7 kN..... 41
Fig. 57 Horizontal stress σ_{11} for a top load of L_3 = 7 kN [MPa]..... 42
Fig. 58, Fig. 59, Fig. 60 Horizontal strain along resp. path 1,2,3 - experiment vs. simulation for L_3 = 2, 4 and 7 kN..... 43
Fig. 61 Relative deviation between experimental and simulated horizontal strain for different load stages (L_3 = 2 kN, 4 kN and 7 kN) for path 1, 2 and 3..... 45
Fig. 62 Contour plot simulation for vertical strain ε_{22} [-] at L_3 =2 kN 46
Fig. 63 Contour plot simulation for vertical strain ε_{22} [-] at L_3 =4 kN 46
Fig. 64 Contour plot simulation for vertical strain ε_{22} [-] at L_3 =7 kN 47
Fig. 65 Contour plot experiment for vertical strain ε_{22} [%] at L_3 =2 kN 47
Fig. 66 Contour plot experiment for vertical strain ε_{22} [%] at L_3 =4 kN 47
Fig. 67 Contour plot experiment for vertical strain ε_{22} [%] at L_3 =7 kN 48
Fig. 68 Vertical stress σ_{22} for a top load of L_3 = 7 kN [MPa]..... 48
Fig. 69 Deformation at the bottom right corner (RP2) at a top load of L_3 = 7 kN. Experimental photo (a) and simulation output (b) 49
Fig. 70, Fig. 71, Fig. 72 Vertical strain along resp. path 1,2,3 - experiment vs. simulation for L_3 = 2, 4 and 7 kN..... 50
Fig. 73 Relative deviation between experimental and simulated vertical strain for different load stages (L_3 = 2 kN, 4 kN and 7 kN) for path 1, 2 and 3 52
Fig. 74 Contour plot simulation for shear strain ε_{12} [-] at L_3 =2 kN 54
Fig. 75 Contour plot simulation for shear strain ε_{12} [-] at L_3 =4 kN 54
Fig. 76 Contour plot simulation for shear strain ε_{12} [-] at L_3 =7 kN 54
Fig. 77 Contour plot experiment for shear strain ε_{12} [%] at L_3 =2 kN 55
Fig. 78 Contour plot experiment for shear strain ε_{12} [%] at L_3 =4 kN 55
Fig. 79 Contour plot experiment for shear strain ε_{12} [%] at L_3 =7 kN 55
Fig. 80 Shear stress σ_{12} for a top load of L_3 = 7 kN [MPa] 56
Fig. 81, Fig. 82, Fig. 83 Horizontal strain along resp. path 1,2,3 - experiment vs. simulation for L_3 =2, 4 and 7 kN..... 57
Fig. 84 Relative deviation between experimental and simulated shear strain for different load stages (L_3 = 2 kN, 4 kN and 7 kN) for path 1, 2 and 3 59
Fig. 85 Contour plot isotropic material for horizontal strain ε_{11} [-] at L_3 =7 kN 64
Fig. 86 Contour plot isotropic material for vertical strain ε_{22} [-] at L_3 =7 kN 64
Fig. 87 Contour plot isotropic material for shear strain ε_{12} [-] at L_3 =7 kN..... 64
Fig. 88 Contour plot linear elastic orthotropic material for horizontal strain ε_{11} [-] at L_3 =7 kN..... 65
Fig. 89 Contour plot linear elastic orthotropic material for vertical strain ε_{22} [-] at L_3 =7 kN..... 65
Fig. 90 Contour plot linear elastic orthotropic material for shear strain ε_{12} [-] at L_3 =7 kN..... 65
Fig. 91, Fig. 92, Fig. 93 Horizontal, vertical and shear strain in comparison to the experimental data for 3 different materials, along path 2 at a top load of L_3 = 7 kN..... 67
Fig. 94 Relative deviation of horizontal, vertical and shear strain from the experimental data for 3 different materials..... 68

Fig. 95, Fig. 96 and Fig. 97 Horizontal, vertical and shear stress in comparison to the experimental data for 3 different materials, along path 2 at a top load of 7 kN 69
Fig. 98 Schematic presentation of the fiber direction for the model with inversed orientation in the reinforcement layers 72
Fig. 99 Weaving process of textile with indication of warp en fill yarns 73
Fig. 100 Schematic presentation of the fiber direction for the model with inversed orientation in all parts 73
Fig. 101 Horizontal strain ε_{11} for model with inversed fiber direction in the reinforcement layer at top load of L3 =7 kN 73
Fig. 102 Horizontal strain ε11 for model with completely inversed fiber direction at a top load of 7 kN 73
Fig. 103 Horizontal strain ε_{11} [-] for model with inversed fiber direction in the reinforcement layer at top load of L_3 =7 kN 74
Fig. 104 Vertical strain ε_{22} [-] for model with inversed fiber direction in the reinforcement layer at top load of L_3 =7 kN 74
Fig. 105 Shear strain ε_{12} [-] for model with inversed fiber direction in the reinforcement layer at top load of L_3 =7 kN 74
Fig. 106 Horizontal strain ε_{11} [-] for model with inversed fiber direction in all membrane parts at top load of L_3 =7 kN 75
Fig. 107 Vertical strain ε_{22} [-] for model with inversed fiber direction in all membrane parts at top load of L_3 =7 kN 75
Fig. 108 Shear strain ε_{12} [-] for model with inversed fiber direction in all membrane parts at top load of L_3 =7 kN 75
Fig. 109 Distribution of vertical stress S22 in the top corner of the membrane with fill-warp orientation in the reinforcement layer (a) in comparison to the original stress distribution with warp-fill orientation (b) 76
Fig. 110 Distribution of vertical stress S22 in the top corner of the membrane with fill-warp orientation in all membrane parts 77
Fig. 111, Fig. 112 and Fig. 113 Influence of the fiber direction on the strain, respectively for path 1, path 2 and path 3 78
Fig. 114, Fig. 115 and Fig. 116 Influence of the fiber direction on the stress, respectively for path 1, path 2 and path 3 79
Fig. 117 Contour plot of vertical strains at a top load of L_3 = 7 kN for the model with user material and gravity incorporated [MPa] 87
Fig. 118 Change in deviation for the model with and without gravity, at a top load of 7 kN. The strains in all directions are given along path 2. 87
Fig. 119 (a) concept of the Contex-T project: a dome-like structure with foldable frame and (b) real scale demonstrator of the Contex-T in two intermediate positions 88
Fig. 120 The geometry of the assembled panels. In green: the place where belts are stitched as reinforcement in red: the welding line 88
Fig. 121 Three examined positions during the 3D-experiment. (a) initial state (b) intermediate state with 50° opening and (c) final state at 90° opening 89
Fig. 122 (a) connection point of reinforcement belts and central belt (b) position of the central belt . 89
Fig. 123 Global view of the 3D-setup 90
Fig. 124 Geometry from AutoCAD, as implemented in Abaqus. (a) overview (b) detail of the curved part in between the two flat panels 90
Fig. 125 Proposed geometry to ease contact : section perpendicular through belt and membrane 91

List of Tables

Table 1 Maximal deviation in Z-direction of the different solution methods with the theoretical formula 26
Table 2 Overview of calculation time for different solution methods 26
Table 3 Material properties of the isotropic belt [] 32
Table 4 Overview of minimum, maximum and average value of horizontal strain along paths 1,2 and 3 at different load stages for L_3 44
Table 5 Overview of minimum, maximum and average value of vertical strain along paths 1,2 and 3 at different load stages for L_3 51
Table 6 Overview of minimum, maximum and average value of shear strain along paths 1,2 and 3 at different load stages for L_3 58
Table 7 Material properties of an isotropic material model based on the results of uniaxial tests 62
Table 8 Material properties of an orthotropic material model based on the results of uniaxial tests .. 62
Table 9 Overview of the calculation time as function of the material model 68
Table 10 Overview of required displacement of RP Top in order to reach a reaction force of 7 kN in function of the material properties 77
Table 11 Relative augmentation or diminution of the average strain in each directions compared to the original model with warp-fill direction: (a) model with reversed reinforcement layer and (b) model with completely inversed fiber direction. 80
Table 12 Relative augmentation or diminution of the average stress level in each directions compared to the original model with warp-fill direction: (a) model with reversed reinforcement layer and (b) model with completely inversed fiber direction. 80

Bibliography

[1]Knippers, J., J. Cremers, et al. (2010). Entwicklung des Membranbaus. Atlas Kunststoffe + Membranen. Detail**:** 15-27.

[2] Chen, S. H., X. Ding, et al. (2008). "Tensile behavior of PVC-coated woven membrane materials under uni- and bi-axial loads." Journal of Applied Polymer Science 107(3): 2038-2044.

[3]Forster, B. and Mollaert. M. (2004). European Design Guide for Tensile Surface Structures, TensiNet.

[4] Kassabian, P. E., Z. You, et al. (1999). "Retractable roof structures." Proceedings of the ICE - Structures and Buildings **134**(1): 45-56.

[5] Mollaert, M. and et al. (2011). Integrated analysis and experimental verification of Kinematic Form Active Structures (KFAS) for architectural applications. Proposal and planning for FWO project.

[6]Corne, E. , TensiNet (2009). "Wimbledon's Centre Court." from http://www.tensinet.com

[7] De Laet, L., (2011). Deployable Tensairity structures - Development, design and analysis, PhD., Vrije Universiteit Brussel (VUB)

[8]Bahamon, A. (2004). The magic of Tents: Transforming Space, Harper Collins.

[9] Mollaert, M., L. D. Laet, et al. (2011). Tensioning a membrane panel in different (un)folding setups. Brussels, Vrije Universiteit Brussel (VUB).

[10] Mollaert, M. (2009). Vorm-actieve constructies. Architecture Department. Brussels, VUB.

[11] Koch, K.-M., K. Habermann, et al. (2004). Membrane structures, Munich, Preston.: 8-41

[12] Shelters, R. S. "Architectural Membrane Materials." Architectural Fabric. from redskyshelters.com.

[13]Drew, P. (1976). Frei Otto Form and Structure, Westview Press.

[14] (19 April 2013). "Fabric Structure." from http://en.wikipedia.org/wiki/Fabric_structure.

[15]Vandenboer, K. (2012). Numerical assessment of material models for coated fabrics in foldable tent structures. Applied Material Sciences. Ghent, University of Ghent.

[16]Bridgens, B., P. D. Gosling, et al. (2003). "Membrane material behavior: concepts, practice and developments." The Structural Engineer **6**.

[17]www.archiexpo.com

[18] www.flickr.com

[19] Nardo, D. (1998). The Roman Colosseum, Lucent Books.

[20] Tadini, E. (1994). Architectura & Natura, Edizioni Gabriele Mazott

[21] Otto, F. and L. Gläser The work of Frei Otto, Museum of Modern Art (New York, N.Y.).

[22] Koch, K.-M., K. J. Habermann, et al. (2004). Membrane structures : innovative building with film and fabric. University of Michigan, Prestel.

[23] Holgate, A. (1997). The Art of Structural Engineering: The Work of Jorg Schlaich and His Team, Axel Menges.

[24] Ishii, K. (1995). Membrane Structures in Japan, SPS Pub. Co.

[25] Del Grosso, A. E. and P. Basso (2010). "Adaptive building skin structures." Smart Materials and Structures **19**(12): 124011.

[26] Golabchi, M. and S. Guest (2009). Morphing multistable textured shells. Proc. IASS Symposium Evolution and Trends in Design, Analysis and Construction of Shell and Spatial Structures, Valencia.

[27]Sofla, A. Y. N., D. M. Elzey, et al. (2009). "Shape morphing hinged truss structures." Smart Materials and Structures **18**(6): 065012.

[28] Rosenberg, D. (2009). Indeterminate architecture: Scissor pair transformable structures. Massachusetts, Massachusetts Institute of Technology.

[29] Kukathasan, S. (2000). Vibration of Prestressed Membrane. Department of Engineering. Cambridge, University of Cambridge.

[30] Johnston, J. D. (2002). " Finite element analysis of wrinkled membrane structures for sunshield applications." American Institute of Aeronautics and Astronautics **1456**.

[31]Meinhold, B. (2010). "Solar-Powered Crystalline Towers Unveiled for Abu Dhabi".from inhabitat.com.

[32] Bach, K., B. Burkhardt, et al. (1988). IL 18, Seifenblasen. Stuttgart, Krämer.

[33]Lewis, W. (2005). "Understanding novel structures through form-finding." Proceedings of ICE- Civil Engineering **158**: 178-185.

[34] Hildebrandt, S. and A. Tromba (1983). Mathematics and Optimal Form. New York, Scientific American Library.

[35] Gosling, P. D., B. N. Bridgens, et al. (2013). "Analysis and design of membrane structures: Results of a round robin exercise." Engineering Structures **48**: 313-328
[36] Bridgens, B. and P. Gosling (2010). Interpretation of results from the MSAJ "Testing Method for Elastic Constants of Membrane Materials". Tensinet Symposium: Tensile Architecture: Connecting Past and Future, GSP. p.49-57
[37]Lewis, W. (1998). "Lightweight tension membranes- an overview." Proceedings ICE - Civil Engineering **126**: 171-181.
[38]Lewis, W. J. (2008). "Computational form-finding methods for fabric structures." Proceedings of the ICE - Engineering and Computational Mechanics **161**(3): 139-149.
[39] nocloudsinthesky.worldpress.com
[40] Wagner, H. (1929). "Flat sheet metal girder with very thin metal web." Zeitschirft für Flugtechnik Motorluftschiffahrt **20**: 200-284.
[41] Mansfield, E. H. (1968). "Tension Field Theory a new approach which shows its duality with inextensional theory." Proceedings 12th Int. Congress Applied Mechanics: 305-320.
[42]Epsteina, M. and M. A. Forcinito (2001). "Anisotropic membrane wrinkling: theory and analysis." International Journal of Solids and Structures **38**(30-31): 5253-5272.
[43]Rimrott, F. P. J. and M. Cvercko (1986). "Wrinkling in thin plates due to in-plane body forces." Inelasticbehavior of plates and shells: 19-48.
[44]Wong, W. Y. and S. Pellegrino (2006). "Wrinkled membranes - Part II: Analytical Models." Journal of Mechanics of Materials and Structures **1**(1): 25-59.
[45]Kuhl, D. (2005). Advanced Finite Element Methods. Bochum, Ruhr University Bochum**:** 189-202
[46]7.1.1 Solving non-linear problems in Abaqus/Standard, in Abaqus 6.12, Abaqus Analysis User's Manual
[47] Zhang, L. G. Y., T. X. (1989). " Modified adaptive dynamic relaxation method and its application to elastic-plastic bending and wrinkling of circular plates" Computers & Structures **33**(2): 609-614.
[48] Brew, J. B., M (1971). "Non-linear structural analysis by dynamic relaxation method." Internal Journal Numerical Methods **3**: 463-483.
[49] Shawi, F. M., AH (1987). "An improved dynamic relaxation method for the analysis of plate bending problems." Computers & Structures **27**: 237-240.
[50] Barnes, M. (1988). "Form finding and analysis of prestressed nets and membranes " Computers & Structures **30**(3): 685-695.
[51] "Calculating the damping factor based on the dissipated energy fraction", 7.1.1 Solving non-linear problems, Abaqus 6.12, Abaqus User's Manual
[52]"The Riks method", 6.2.4 Unstable collapse and postbuckling analysis, Abaqus 6.12, Abaqus Analysis User's Manual
[53] 2.3.2 Modified Riks Method, Abaqus 6.12, Abaqus Theory Manual
[54] Wong, W. Y. and S. Pellegrino (2006). "Wrinkled Membranes- Part III: Numerical Simulations." Journal of mechanics of materials and structures **1**(1): 63-95.
[55]"Using membrane elements in large-displacement implicit analyses", 29.1.1Membrane Elements, Abaqus 6.12, Abaqus Analysis User's Manual
[56]Wang, J. C., Cheng Yan (2012). Finite Element Method in Form-finding Process for Membrane Structures. Project for Finite Element Analysis, Ithaka, Cornell University.
[57]en.wikipedia.org/wiki/Hyperbolic_paraboloid
[58]Houtman, R., H. Werkman. (2004).Chapter 5: Detailing and Connections European Design Guide for Tensile Surface Structures, TensiNet.
[59] Becker, T., K. Slitthof, et al. (2006). Error Estimations of 3D Digital Image Correlation Measurements. Speckles, from Grains to Flowers. Nîmes, France, Dantec Dynamics**:** 6.
[60] Dinh, T. D. (submitted in 2013). "A new Elasto-Plastic Material Model for coated fabric." Ghent, University of Ghent
[61] Load Lok Cargo Lashings, product sheet
[62]12.14 Creating and editing composite layups, Abaqus 6.12, Abaqus Analysis User's Manual
[63] 12.13.10 Creating general shell stiffness sections, Abaqus 6.12, Abaqus/CAE User's Manual
[64] 3.6.2 Axisymmetric shell elements, Abaqus 6.12, Abaqus/CAE Theory Manual
[65]Hughes, T. J. R. and R. L. T. W. Kanoknukulchai "A simple and efficient Finite Element for Plate Bending." International Journal for Numerical Methods in Engineering **11**: 1529-1543

[66]Flores, F. G. and E. Oñate (2011). "Wrinkling and folding analysis of elastic membranes using an enhanced rotation-free thin shell triangular element." Finite Elements in Analysis and Design **47**(9): 982-990.
[67] 28.1.1 Solid (continuum) elements: Choosing between bricks/quadrilaterals and tetrahedra/triangles, Abaqus 6.12, Abaqus Analysis User's Manual
[68] 17.6.1 Verifying your mesh, Abaqus 6.12, Abaqus/CAE User's Manual
[69] 29.1.2 General membrane element library, Abaqus 6.12, Abaqus/CAE User's Manual
[70] Brannon, R. (2000, 27-07-2000). "Define your strain!". from http://www.mech.utah.edu/~brannon/public/strain.pdf.
[71]Bridgens, B. and M. Birchall (2012). "Form and function: The significance of material properties in the design of tensile fabric structures." Engineering Structures **44**: 1-12.
[72]Barnes, M., L. Gründig, et al. (2004). Form-finding, Load Analysis and Patterning. European Design Guide for Tensile Surface Structures. M. Mollaert, Tensinet.
[73] (2013). Hooke's Law. Conversion formulas, Wikipedia, the free encyclopedia.
[74] Gosling, P. D., B. N. Bridgens, et al. (2013). "Analysis and design of membrane structures: Results of a round robin exercise." Engineering Structures **48**: 313-328.
[75]Dinh, T. D. (2013). "A new Elasto-Plastic Material Model for coated fabric.", University of Ghent
[76]Bridgens, B. and M. Birchall (2012). "Form and function: The significance of material properties in the design of tensile fabric structures." Engineering Structures **44**: 1-12.
[77] Mollaert, M., L. D. Laet, et al. (2011). Tensioning a membrane panel in different (un)folding setups. Brussels, Vrije Universiteit Brussel (VUB).